View metadata, citation and similar papers at core.ac.uk

brought to you by CORE

provided by Online Research Database In Technology

Technical University of Denmark

Microchip Electrochromatography

Gústafsson, Ómar; Kutter, Jörg Peter

Publication date:
2008

Document Version
Publisher's PDF, also known as Version of record

Link back to DTU Orbit

Citation (APA):
Gústafsson, Ó., & Kutter, J. P. (2008). Microchip Electrochromatography.

DTU Library
Technical Information Center of Denmark

General rights
Copyright and moral rights for the publications made accessible in the public portal are retained by the authors and/or other copyright owners and it is a condition of accessing publications that users recognise and abide by the legal requirements associated with these rights.

- Users may download and print one copy of any publication from the public portal for the purpose of private study or research.
- You may not further distribute the material or use it for any profit-making activity or commercial gain
- You may freely distribute the URL identifying the publication in the public portal

If you believe that this document breaches copyright please contact us providing details, and we will remove access to the work immediately and investigate your claim.

Microchip Electrochromatography

Ómar Gústafsson

Department of Micro- and Nanotechnology
Technical University of Denmark
Building 345 east
DK-2800 Kongens Lyngby
Denmark

Ph.D. Thesis
April 2008

Supervisor:
Professor Jörg P. Kutter

Preface

This thesis is a partial fulfilment of the requirements for obtaining the Ph.D. degree at the Technical University of Denmark (DTU). The work was carried out at the Department of Micro and Nanotechnology (DTU Nanotech), DTU, from January 2005 to January 2008 in the ChemLabChip group. The Ph.D. project was supervised by Professor Jörg P. Kutter. The Ph.D. study involved a visit to the group of Dr. Stephen C. Jacobson at Indiana University, Bloomington, IN, USA, where I worked with glass to glass bonding that was then utilized for bonding oxidized silicon substrates to glass lids at DTU Nanotech. The Ph.D. study was funded by a DTU stipend.

I would like to thank my supervisor, Professor Jörg P. Kutter for his inspiration and advice, especially when nothing seemed to be going as planned. I would like to thank all the members of the ChemLabChip group at DTU Nanotech for good friendship during my 4 years in the group. I would especially like to thank Klaus Bo Mogensen who fabricated many of the microdevices and showed great patience in helping me with the design and fabrication. I would also like to thank Detlef Snakenborg for his resourcefulness with any problem brought to him. I would like to thank Fredrik Eriksson for the design and fabrication of the oxidized silicon microchip substrates. I would also like to thank Asger Vig Larsen from the Optofluidics group at DTU Nanotech for helping me with nanoimprint lithography and then assisting in troubleshooting when things went wrong.

I would like to thank Stephen C. Jacobson for giving me the opportunity of visiting his group at Indiana University, Bloomington. I would like to thank Yan Liu and Zexi Zhuang from IU for their help in the lab.

I would also like to thank Haukur Gudnason from the BioLabChip at DTU Nanotech for his friendship and all the pointless conversations over a cup of coffee over the past few years.

Finally, I would like to thank my wife Jóhanna for her patience and support and for taking care of our three wonderful daughters Agnes, Ragnhildur and Eyvör while I write these lines.

Abstract

The objective of this thesis is to explore microchip electrochromatography in terms of new integrated functionalities and new substrate materials, with the objective to perform bioanalytical separations. Three different microchips for electrochromatography are presented, each of them featuring a microfluidic network with a standard cross injector and a separation column with solid support structures for a stationary phase.

First, a silicon based microchip for electrochromatography is presented. The microchip features planar, UV-transparent waveguides that are fabricated on the microchip. The waveguides are made of silicon oxynitride that is deposited on the silicon substrate. An octadecylsilane stationary phase is attached to the surface of the microchip and a reversed phase electrochromatography separation of five neutral compounds, utilizing UV-absorbance detection, is demonstrated. A plate height of 5 μm is achieved for a retained analyte.

The second microchip that is presented is also silicon based. All of the structures on the microchip are fabricated in silicon in a single etching step. After the etching, the microchip is oxidized so that the ridge waveguides are oxidized the whole way through. The microchip features planar UV-transparent silicon oxide waveguides, a 1 mm long U-shaped detection cell and fiber couplers to assist with aligning optical fibers to the waveguides. The oxidized silicon microchip has therefore more integrated functionalities than the silicon oxynitride microchip as well as a better limit of detection as much more light is coupled through the oxidized silicon waveguides. A glass wafer is used to seal the microchip. An octylsilane stationary phase is attached to the surface of the microchip and reversed phase electrochromatography is demonstrated by separating three neutral compounds, that are then detected with UV-absorbance. Plate heights ranging from 30-52 μm are achieved in the separation. The high plate heights are due to both fabrication limitations and imperfect design, both of which can at least to some extent be circumvented in future designs.

The final microchip that is presented is a cyclic olefin copolymer (here, Topas) based microchip for electrochromatography. The microchip is fabri-

cated by nanoimprint lithography where an inverted silicon master is pressed into a softened Topas layer that has been spun onto a glass wafer. The microchip is sealed with thin polymer layer that has been spun onto a glass wafer. Reversed phase electrochromatography separation of three fluorescently labeled amines is demonstrated where the underivatized polymer surface is used as a stationary phase. Laser induced fluorescence through the substrate is used for detection as the microchip does not feature waveguides. Plate heights for the separation range from 3.4 μm to 22 μm. Furthermore, experiments on an underivatized Topas capillary are also presented. A cathodic electroosmotic flow is measured in the capillary at pH values ranging from 3-10. A reversed phase electrochromatography separation of three neutral analytes is also demonstrated in the underivatized capillary.

Resume

Formålet med denne afhandling er at undersøge mikrochip elektrokromatografi med hensyn til integration af nye funktionaliteter og substrat materialer til anvendelse indenfor bioanalytiske separationer. Tre forskellige typer mikrochips for elektrokromatografi er blevet undersøgt, hvor hver af dem indeholder et mikrofluid netværk bestående af et kryds for injektioner og en separationskolonne med support strukturer for immobilisering af en stationær fase.

Den første type chip der bliver præsenteret, blev fremstillet på et siliciumsubstrat, som indeholdt elektrisk isolerede kanaler og planare UV transparente bølgeledere. Bølgelederne er fremstillet af siliciumoxynitrid, som er deponeret på en oxideret silicium skive. En octadecylsilan stationær fase er immobiliseret på kanaloverfladen af mikrochippen og en elektrokromatografisk separation af fem neutrale stoffer med UV absorbans detektion, blev vist. En bundhøjde på 5 μm blev opnået for et stof der vekselvirkede med den stationære fase.

Den anden type chip er også baseret på silicium. Alle strukturer er først ætset i substratet i et enkelt ætsetrin. Derefter bliver chippen oxideret for at forme bølgelederne og gøre kanalerne elektrisk isolerede. Chippen indeholder UV transparente bølgeledere, en 1.0 mm lang U-formet detektionscelle og strukturer til at aligne de eksterne optiske fibre til bølgelederne på chippen. De oxiderede chips indeholder derfor flere funktioner end de tidligere chips, samtidig med en forbedret detektionsgrænse, fordi der kan kobles mere lys igennem detektionscellen. Et glas substrat er benyttet til at forsegle chippen. En octylsilane stationær fase blev ligeledes immobiliseret på kanalernes sidevæge og elektrokromatografiske separationer af tre neutrale stoffer blev udført med UV absorbans som detektionsmetode. Bundhøjder var fra 30-52 μm på chippen. Den lave effektivitet skyldes begrænsninger i det benyttede design, som hovedsagligt skulle kunne elimineres i fremtidige designs.

Den sidste type mikrochip er en cyclic olefin copolymer (Topas) baseret mikrochip for elektrokromatografi. Chippen blev fremstillet ved brug af nanoimprint litografi, hvor en inverteret silicium master blev presset mod et Topas lag, der var deponeret på en glas skive. Mikrochippen er forseglet med et tyndt polymerlag, der blev deponeret på en glas skive. Polymeroverfladen kunne benyttes direkte som stationær fase, hvilket blev påvist ved at

foretage en elektrokromatografisk separation af 3 fluoresens mærkte aminer. I dette tilfælde blev fluorescensdetektion benyttet, da chippen ikke indeholder bølgeledere. Bundhøjder er mellem 3.4 og 22 μm. Derudover blev der også foretaget eksperimenter på Topas kapilarrør. Et katodisk elektroosmotisk flow blev målt i kapilarrørene ved pH værdier fra 3 til 10. Det var også muligt at udføre elektrokromatografiske separationer på de ubehandlede Topas kapilarrør.

Contents

Chapter 1

Introduction

In 1979 Terry and co-workers from Stanford University published a paper on a miniaturized gas chromatograph fabricated on a silicon wafer using photolithography [1]. This was the first report of a miniaturized analytical device, later called micro total analysis systems (μ-TAS) or "lab on a chip", but it did not start much excitement right away. It was not until 1990 that silicon based miniaturized analytical systems reemerged with the presentation of an open-tubular liquid chromatograph with an integrated conductometric detector [2]. The field of miniaturized analytical systems expanded very rapidly in the early 1990s with the focus mainly on the basic concepts such as fluidic control, microfabrication, design of individual components, chemical separations and detection [3]. In recent years, the focus of research has shifted towards utilizing the components that have been developed for more complete systems with integrated functionalities and specific applications [4].

There are a number of advantages associated with miniaturizing conventional chemical separation techniques. First of all, the reduced dimensions of the microchip result in reduced sample and reagent consumption and high throughput of analysis, due to short analysis times. Shorter separation channels also result in high electric field strengths at lower voltages as compared to longer capillaries. The fabrication methods utilized offer the possibility of integrating several functionalities onto a single microchip with minimal loss of analytes and resolution in transfer between steps. Fluidic networks for injection right before the separation channel provide a means for rapid valveless injection that minimizes band broadening due to direct transfer of the sample from an injector to the separation column. Similarly, integrated detection right after a separation column also serves to minimize band broadening. Functionalities that have been successfully integrated onto separation microchips include solid phase extraction [5], solvent programming [6], two dimensional separations [7] and filtration [8].

The main disadvantage with downscaling analytical methods is that the

limit of detection is reduced due to the small detection volume, while the length of the separation channel potentially limits the separation efficiency.

The aim of this project was to work on miniaturized capillary electrochromatography, especially related to applications in biochemical separations such as proteins, peptides and biogenic amines. Although none of the work presented ultimately demonstrated separation of these biochemicals, the detection methods used, both UV-absorbance and laser induced fluorescence (LIF) of fluorescently labeled amines, are both well suited for the detection of these biochemicals. Instead more focus was put on using simpler analytes to demonstrate the chromatographic interaction in these initial steps of development and the more complex biochemical separations can be developed at later stages with more optimized microsystems that should yield better separation efficiencies.

The following sections are intended to familiarize the reader with concepts that are dealt with in microchip electrochromatography. Section 1.1 presents capillary electrochromatography (CEC), electroosmotic flow, the separation principles in CEC and the application of CEC in microsystems. Section 1.2 deals with detection in separation microsystems, with special emphasis on optical detection using UV-absorbance and LIF as those methods are used in the research presented in the following chapters. Sections 1.3 introduces the substrates used in this work; glass, silicon and polymers and their relevant microfabrication techniques. In chapters 2, 3 and 4 different designs of electrochromatography microchips will be presented and chromatographic separations on them demonstrated. In each of these chapters the limitations of each design is discussed, how these designs can be improved further and how the separation efficiency can be improved. Chapter 5 contains some general conclusions of the project.

1.1 Capillary electrochromatography

CEC is a chemical separation method that can be viewed as a hybrid between capillary electrophoresis (CE) and high performance liquid chromatography (HPLC). In HPLC the mobile phase is driven by external pressure, while in CEC the transport of the mobile phase is performed by exploiting electroosmotic flow (EOF) that is induced by an electric field, just as in CE. The main separation principle in CEC is the same as in HPLC, where a liquid mobile phase is pumped past a stationary phase. Chemicals that interact with the stationary phase will be retained by the stationary phase, resulting in separation of differently retained chemicals. CEC also has a secondary separation mechanism due to the electric field that is necessary to drive the EOF. In an electric field charged analytes will have an electrophoretic mobility relative to the bulk liquid The electrophoretic mobility is dependant on the charge and the size of the ion [9]. The principles of CEC

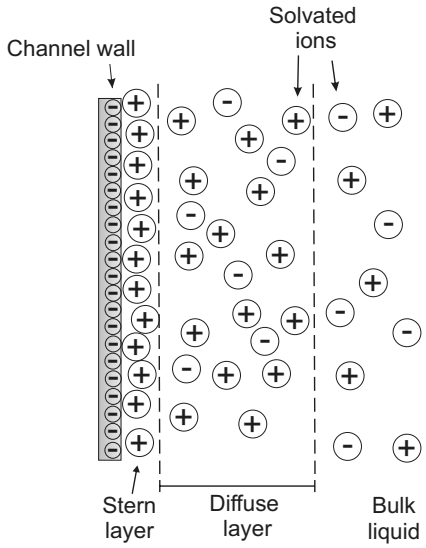

Figure 1.1: Schematic of excess charge distribution close to a channel wall. The negative charges on the wall is due to dissociation of groups on the substrate surface. Some of the positive charges in the solution are adsorbed to the negative surface, forming the Stern layer. The remaining excess of mobile positive charges form the diffuse layer. The bulk liquid has no net charge as positive and negative ions cancel each other out.

are introduced in the following subsections, first electroosmotic flow, then liquid chromatography and finally the application of CEC in microchips is presented.

1.1.1 Electroosmotic flow

EOF is the bulk flow in a capillary or a microchannel that arises from applying an electric field in the axial direction. EOF originates at a surface that is charged due to dissociation of surface groups. The surface is most frequently negatively charged, commonly due to dissociation of silanol groups (-SiOH). Positive ions in the solution are drawn to the negatively charged surface by electrostatic forces, while solvated negative ions are pushed away from the surface. Close to the surface, positive ions form a strongly bound immobile layer called the Stern layer. Outside the Stern layer is a layer with an excess of mobile positive ions that is called a diffuse layer. Figure 1.1 shows a schematic of a negatively charged surface and solvated ions close to the surface. The whole system maintains electroneutrality with the excess positive ions in the Stern and diffuse layers canceling out the negative charge on the substrate wall.

The thickness of the diffuse layer δ can be expressed by:

$$\delta = \left(\frac{\varepsilon k T}{N_A e^2 \sum_i z_i^2 c_i} \right)^{1/2} \tag{1.1}$$

where ε is the permittivity of the liquid, k is the Boltzmann constant, T is the temperature, N_A is Avogadro's number, e is the elementary charge, i is the index for different ions in the solution, z is the valence and c is the concentration of the ions [10]. The thickness of the double layer decreases with increasing buffer concentrations and typically measures a few nanometers for common buffer concentrations at room temperature [9]. The electrostatic potential across the diffuse layer is called the ζ-potential. The ζ-potential can be approximated for low potentials by:

$$\zeta \cong \frac{\delta \sigma}{\varepsilon} \tag{1.2}$$

where σ is the surface charge density.
When a voltage is applied parallel to the channel surface the excess mobile positive charges in the diffuse layer are pulled toward the cathode. The fluid layers adjacent to the diffuse layer are dragged along through viscous forces. This results in a constant velocity throughout the bulk solution in the channel giving a flat flow profile in the bulk liquid. Figure 1.2 shows a schematic of EOF in a capillary, and shows that the flow velocity drops to zero at the surface. The flow velocity is constant outside the diffuse layer. As mentioned before, the typical thickness of the diffuse layer is a few nanometers, but the width of a microchannel is usually much larger; on the order of micrometers. Therefore the electroosmotic flow in channels that have dimensions larger than a micrometer can be viewed as having a constant flat flow profile throughout the channel.

The mobility of the electroosmotic flow can be expressed theoretically by the Smoluchowski equation

$$\mu_{eo} = \frac{\varepsilon \zeta}{\eta} \tag{1.3}$$

where η is the viscosity of the solution. By combining Equations 1.1, 1.2 and 1.3 we get an approximation for the electroosmotic mobility at low zeta potentials

$$\mu = \frac{\sigma}{\eta} \left(\frac{\varepsilon k T}{N_A e^2 \sum_i z_i^2 c_i} \right)^{1/2} \tag{1.4}$$

Equation 1.4 tells us that the electroosmotic mobility is dependant on the surface charge density, the viscosity, the dielectric constant, the ionic strength of the buffer and the temperature. Glass surfaces that are common

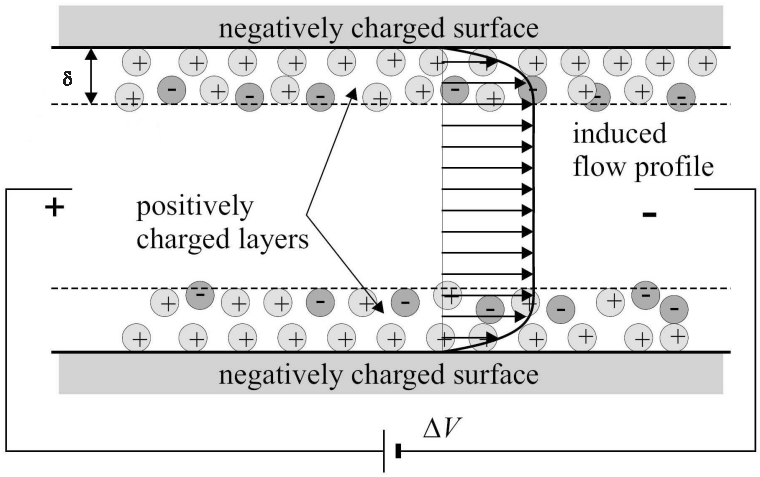

Figure 1.2: EOF in a microchannel. The positively charged diffuse layer is pulled toward the cathode, dragging along the bulk solution through viscous forces. Figure adapted from [11].

in CE have silanol groups on the surface. The dissociation of silanol is pH dependant and therefore the surface charge density of the glass surface is pH dependant. This is supported by the fact that the EOF measured on glass surfaces drops at low pH values [12].
The EOF is usually measured by adding a neutral marker that migrates with the bulk liquid and measuring the arrival time of the marker at the detector. Another way of measuring the EOF is to monitor the current change as buffers with different ionic strength replace one another in the channel [13].

1.1.2 Chromatography

Chromatography is a chemical separation technique that is based on differential distribution of solutes between two phases, which move at different speeds with respect to each other. Most frequently, one of the phases is stationary, while the other is mobile and moves by or through the stationary phase. Solutes that distribute differentially between the two phases will have different apparent velocities through the stationary phase column and thus be separated. Chromatography can be divided into many categories based on both the physical states of the two phases as well as the mechanism of interactions that can be exploited to get differential transport. In this work I solely used liquid chromatography (LC) where the mobile phase is a liquid, but it is also possible to have a mobile phase that is a gas or a supercritical fluid. In liquid chromatography the solute interacts with both the stationary and the mobile phase. Liquid chromatography can divided into several different groups based on the type of interaction that is utilized. In adsorption chromatography the solute adsorbs to the surface of the stationary

phase. In partition chromatography the solute dissolves in a layer of liquid stationary phase that is bonded to support structures (e.g. porous particles in conventional HPLC). Other forms of liquid chromatography include ion exchange chromatography, molecular exclusion chromatography and affinity chromatography and will not be presented further here [14].

The most common form of chromatography, and the one used in this project, is reversed phase (RP) chromatography. Reversed phase chromatography is a chromatography method where the stationary phase consists of hydrophobic groups, frequently alkylsilanes such as octadecylsilane or octylsilane and the mobile phase is aqueous.

While the mechanism of interaction determines the type of chromatography, there are several different ways to realize the stationary phase in a chromatography system. The simplest realization is open tubular (OT) chromatography where the stationary phase is attached to the surface of a narrow tube or a capillary, forming a thin layer of a stationary phase. A drawback of the open tubular chromatography columns is that volume of the stationary phase (V_s) is low compared to the volume of the mobile phase (V_m). The ratio between V_m and V_s in a chromatography column is called the phase ratio, β. β is defined as

$$\beta = \frac{V_m}{V_s} \tag{1.5}$$

A low β is feasible for a chromatography column. The most common way to reduce β is to increase V_s by using packed columns. These columns are filled with particles, usually a few micrometer in diameter, that are confined in the column by retaining frits and coated with the stationary phase. The packed particles drastically increase the pressure needed to pump liquid through the separation column. Monolithic or continuous beds are another type of support for a stationary phase. These are created in situ by polymerization, resulting in a macroporous polymer monolith that contains covalently linked $0.1-0.4\ \mu m$ particles [15]. The polymer monoliths have higher porosity than the packed beads, resulting in a lower pressure needed to achieve the same flow rate. The stationary phase functionality of the polymer monolith is controlled by the monomer composition in the polymerization reaction [16, 17]. Another alternative for stationary phase supports are microfabricated support structures in the separation column that the stationary phase is then attached to. This type of stationary phase supports is unique for microfabricated separation columns as they rely on the same manufacturing procedures as the microchips and were first realized in 1998 by He et al [18, 19]. Structures based on these designs are utilized in this project and are described further in Section 1.1.3.

Several physical parameters are needed to explain how chromatography works and to determine the quality of a chemical separation. First of all the analyte distribution between the phases is described by the distribution

coefficient K:

$$K = \frac{c_s}{c_m} \tag{1.6}$$

where c_s is the concentration in the stationary phase and c_m is the concentration in the mobile phase. K describes the concentration ratios at equilibrium between the two phases, while the ratio of the amount of analyte in each of the two phases is expressed by the retention factor k, obtained by multiplying K with the inverse phase ratio:

$$k = K\frac{V_s}{V_m} \tag{1.7}$$

In chromatography k gives a measure of how much time an analyte spends in the stationary phase relative to the mobile phase. The retention factor can also be determined from experimental values obtained from the chromatogram:

$$k = \frac{t_r - t_m}{t_m} \tag{1.8}$$

where t_r is the retention time of a retained analyte and t_m is the retention time for an unretained analyte. Using Equation 1.8 the retention factor for each analyte can be determined experimentally if the retention time of an unretained analyte is known. The retention ratio R is the fraction of solute in the mobile phase and is only dependant on the retention factor:

$$R = \frac{1}{1+k} \tag{1.9}$$

R can be used to determine the velocity of a retained analyte zone u_R:

$$u_R = Ru_0 \tag{1.10}$$

where u_0 is the mobile phase velocity.

Separation efficiency

Separation efficiencies are usually reported in plate heights or plate numbers. A plate number (N) can be viewed as how many liquid-liquid extraction steps would be needed to achieve an observed separation. The plate height H can be viewed as an index of how much a sample zone (peak) broadens during its transport through a separation system and is defined as:

$$H = \frac{\sigma^2}{X} \tag{1.11}$$

where σ^2 is the variance of the Gaussian peak profile and X is the separation distance. A small plate height indicates a sharp peak. To describe a chromatography system more completely the van Deemter formalism is used

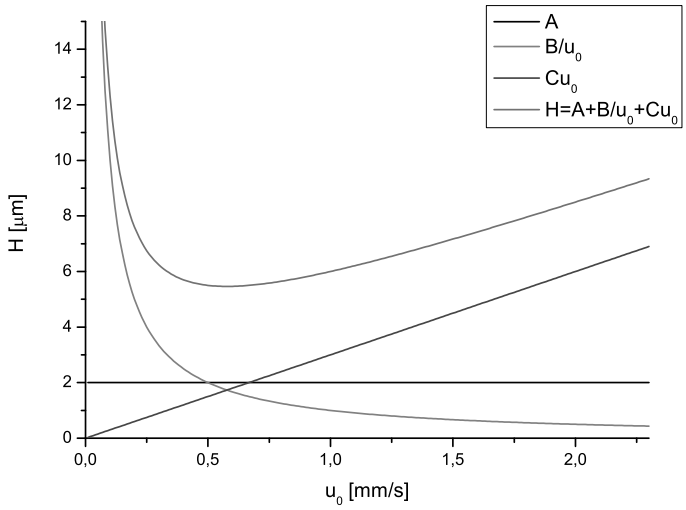

Figure 1.3: Van deemter plot of plate height (H) versus linear velocity (u_0). The individual components of the Van deemter equation are plotted separately as well as the combined plate height. The constants are arbitrarily set to: A=2, B=1 and C=3.

to describe how the plate height for a specific analyte changes as a function of the mobile phase flow rate u_0

$$H = A + \frac{B}{u_0} + Cu_0 \tag{1.12}$$

where A, B and C are constants that vary depending on column designs, different stationary phases, mobile phase composition and analytes. Figure 1.3 shows how each of the three terms of the van Deemter equation changes with respect to flow rate and the combined effect on the plate height.

The A-term is a collection of constant contributions to the plate height. In a packed column there are multiple flow paths available for the liquid and these may be of slightly different lengths, resulting in a constant band broadening contribution for that specific column. The multiple flow paths available through a column are therefore one contribution to the A-term. Inhomogeneous packing of the particles in the column will also contribute in the A-term. Constant band broadening sources such as the injection plug length and the detector path length are also included in the A-term. To minimize the A-term for a chromatography column a very uniform packing is required. Furthermore the injection and detection volume should be monitored to make sure that they do not contribute significantly to the total plate height.

The B/u_0-term is called the longitudinal diffusion term and B is given

by

$$B = 2D_m \tag{1.13}$$

where D_m is the diffusion coefficient of the solute in the mobile phase. The B/u_0-term causes a sharp rise in the plate height at low flow rates. This is due to the fact that the sample zone spends more time in the separation column and thus gets more time to broaden by diffusion. Although it is possible to reduce the B/u_0-term of the plate height by changing temperature and the mobile phase to reduce the diffusion coefficient of the analytes it is usually not considered feasible [20]. The only practical means to reduce the effects of the B/u_0-term is to run the separation at sufficient flow velocities.

The Cu_0-term is the contribution of mass transfer to the plate height and comes from the finite time needed for the solute to equilibrate between the mobile and the stationary phase. The mass transfer can be split up into two parts $C = C_s + C_m$ where C_s is the rate of mass transfer through the stationary phase and C_m is the mass transfer through the mobile phase. The expressions for C_s and C_m in open microchannels for partitioning chromatography are:

$$C_s = \frac{k}{(1+k)^2}\frac{2d_s^2}{3D_s} \tag{1.14}$$

$$C_m = \frac{1+6k+11k^2}{96(1+k)^2}\frac{d_m^2}{D_m} \tag{1.15}$$

where k is the retention factor, d_s is the thickness of the stationary phase film, D_s is the diffusion coefficient of the solute in the stationary phase, d_m is the the shortest dimension within the separation microchannel (i.e. depth of the microchannel for wide and shallow channels) and D_m is the diffusion coefficient of the solute in the mobile phase [9].

The mass transfer term is linearly dependant on flow rate and therefore it becomes important in increasing the plate height at high flow rates. To reduce the effect of the Cu_0-term both C_s and C_m can be reduced. This can be done by changing the thickness of the stationary phase d_s and the channel dimensions d_m as these factors are both squared. The stationary phase is frequently a monolayer of alkylsilanes, covalently bonded to the surface, so the thickness of the stationary phase film is the length of the molecule and can not be reduced further. Reduction of the channel dimensions is therefore the most suitable option to reduce the effects of the Cu_0-term on the plate height.

For adsorption chromatography the mobile phase term is the same but since the analytes are adsorbed to a surface instead of migrating into a stationary phase the corresponding C-term, C_{ads}, is different from C_s. The expression for C_{ads} is:

$$C_{ads} = \frac{2k}{(1+k)^2 k_d} \tag{1.16}$$

where k_d is the rate constant of analyte desorption [21].

Plate number N is the number of plate heights H per separation length L

$$N = \frac{L}{H} \tag{1.17}$$

N is dimensionless and is usually referred to as plates. N can be obtained experimentally by rewriting Equation 1.17 in the form

$$N = \frac{16t_r^2}{w^2} = \frac{5.545t_r^2}{w_{1/2}^2} \tag{1.18}$$

where t_r is the retention time of the peak, w is the width of the peak at the base and $w_{1/2}$ is the width of the peak at half height. The width of the peak at half height is frequently used because it can be hard to determine the baseline width if the baseline is fluctuating. The width of the peak at half height for Gaussian peaks is related to the standard deviation $w_{1/2} = 2.35\sigma$, see Figure 1.4.

Resolution

The objective of a separation is to resolve a mixture of compounds into individual peaks. Resolution R_s is used to determine how well two adjacent peaks are resolved and is defined:

$$R_s = \frac{L_2 - L_1}{2(\sigma_1 + \sigma_2)} \tag{1.19}$$

where L_1 and L_2 are the separation distances for the two components and σ_1 and σ_2 are the standard deviations of the two peaks. To experimentally determine the resolution of two peaks in chromatography it is most common to use the retention time of the peaks instead of the the separation distance and the peak width instead of the standard deviation. The peak width w is defined as $w = 4\sigma$

$$R_s = \frac{2(t_2 - t_1)}{w_1 + w_2} = 0.589\frac{\Delta t}{(w_{1/2-1} + w_{1/2-2})/2} \tag{1.20}$$

t_1 and t_2 are the retention times for each of the peaks, and $\Delta t = (t_2 - t_1)$. w_1 and w_2 are the widths of the two peaks at the base. $w_{1/2-1}$ and $w_{1/2-2}$ are the peak widths at half the peak heights. Figure 1.4 shows a schematic of two gaussian peaks with baseline resolution (defined as $R_s = 1.5$). All relevant factors for determination of resolution are marked on the figure. The resolution of two adjacent peaks can be related to the plate number and the retention factors of the two peaks

$$R_s = \frac{\sqrt{N}}{4}(\frac{\alpha - 1}{\alpha})(\frac{k_2}{1 + k_2}) \tag{1.21}$$

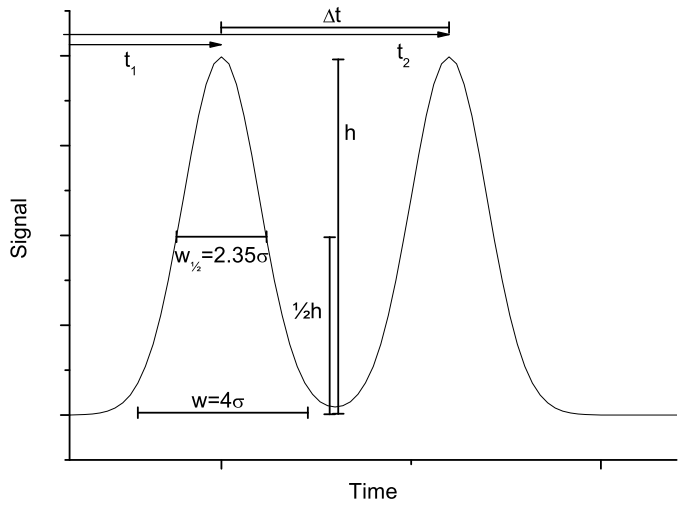

Figure 1.4: Two Gaussian peaks with a resolution of 1.5. Relevant widths, heights and retention times for the calculation of resolution (R_s) are marked on the image.

where $\alpha = k_2/k_1$ is called selectivity. k_1 is the retention factor for the less retained compound and k_2 for the more retained compound. From Equation 1.21 we can see that by increasing the plate number of closely spaced peaks the resolution is increased. This can be viewed as reducing the width of the peaks to achieve better resolution.

1.1.3 Microchip Electrochromatography

While pressure driven chromatography systems are dominant in more traditional formats, there are still relatively few reported examples of pressure driven liquid chromatography on microchips [16, 22, 23]. There are several advantages with using pressure driven flow instead of electroosmotic flow, most notably better flow velocity control. The problem with electroosmotic flow is that the flow velocity is dependant upon the properties of the mobile phase, such as pH, electrolyte concentration, wall surface material, adsorption of molecules to the surface, composition of sample matrix and the amount of organic modifier in the mobile phase. Pressure driven flow also offers a greater freedom in using different solvents while electrically driven flow is reliant on a solvent that will cause dissociation of surface groups in the column. Finally pressure driven flow does not interfere with electrical detection methods. Given these advantages it seems a bit odd that pressure driven flow is not more popular for microchip separations. This is largely due to limitations with applying high pressure to microchips, as problems

with mechanical sealing for interfacing external pumps with microchips limit the maximum allowable inlet pressure to $10-30$ bar, an order of magnitude lower than what is frequently used for traditional HPLC. On-chip pumps are even more limited as they have been shown to deliver pressures up to 4.5 bar [24]. Furthermore, the fact that pressure driven flow is dependant on the channel dimensions makes the separation efficiency extremely sensitive to small deviations in the channel dimensions, explaining the lack of successful open-tubular on-chip pressure driven liquid chromatography separations reported [15].

Electroosmotic flow on the other hand is very easily applied in microfluidic systems and needs no pumps, valves or moving parts; only electrodes that are connected to a high voltage power supply and placed at the inlet and outlet fluidic reservoirs. This simple application of an electric field to generate bulk flow is one of the major advantages of CEC compared with HPLC [25]. Because the electroosmotic flow is generated on the surfaces inside the channels there are no problems associated with increased back-pressure from smaller channels as in the case of pressure driven flow. Another advantage of using electroosmotic flow is that the linear flow velocity in a separation column is not affected by the channel dimensions. This means that very small channel dimensions, which minimize mass transfer contributions to the plate height, can be employed without increasing the necessary voltage while in HPLC a higher pressure is required to maintain the flow velocity [26].

The first electrochromatography separation on a microchip was presented by Jacobson et al in 1994 and involved functionalizing the surface of an open channel glass microchip with an octadecylsilane (C18) for a reversed phase separation of neutral analytes [27]. To lower the phase ratio and get higher retention factors compared to the open channel microchips, several methods have been realized as mentioned above. We have chosen to use the design proposed by He et al in 1998, where the chromatography column consists of a microfabricated array of pillars, which are used as support structures for a stationary phase [19]. These structures are not only intended to increase the surface area of the separation column, but also to increase the homogeneity of the separation column, as the size, shape and position of the pillars can be controlled very precisely down to the sub-micron range [28]. A homogenous separation column leads to a reduction in the A-term of the van Deemter equation, as the flow paths through the column are more homogenous than those in packed beds [29]. Figure 1.5 shows an example of an array of hexagonal pillars. The pillar rows are staggered so that each row is offset be half the period of the pillars, resulting in mixing nodes between the rows. The presence of the mixing nodes is important as the trans-channel mixing nodes compensate for surface heterogeneity that causes band broadening [30].

Substantial simulation work has been presented on fluidic flows in or-

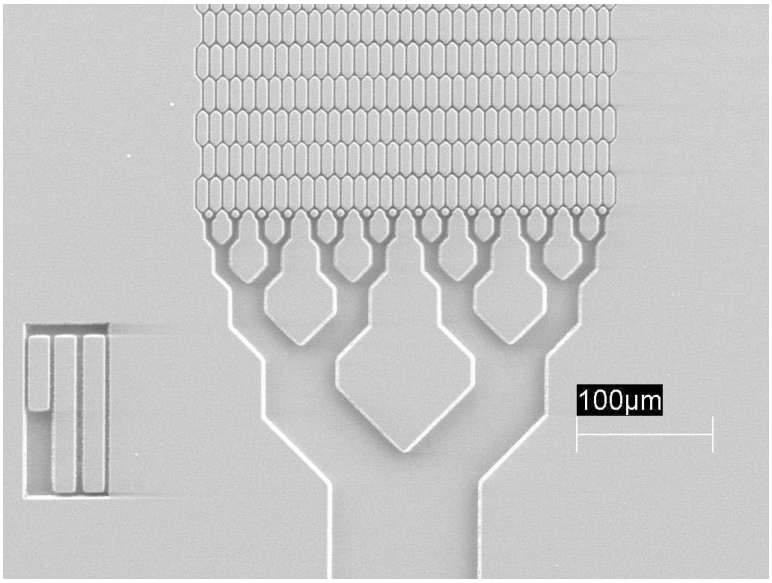

Figure 1.5: Microfabricated separation column with an array of pillars. The pillars are elongated hexagons and the channel between the pillars is 2.5 μm wide. A binary splitting structure distributes flow from the main channel evenly over the entire separation column. Each channel splits up into two channels that are half the width of the original one, keeping the cross sectional area of the channels constant.

dered pillar arrays. The results have shown that lower plate heights can be achieved in ordered pillar arrays than in packed beds and that the plate heights are similar to those for monolithic columns [31]. A recent review has compiled the data from various simulation work on ordered pillar arrays and published a set of design rules regarding size and shape of pillars, external porosity and various other factors that affect the separation performance of the chromatography column [32].

The main disadvantage with micromachined solid support structures is the fact that they are solid. Even though they decrease the phase ratio of the column compared to open channel chromatography, the phase ratio of the micromachined columns are still well above that of the columns packed with porous particles and the monolithic columns. One suggestion to decrease the phase ratio for the micromachined support structures by making porous pillars instead of solid ones using, e.g., "black silicon" [33].

One important aspect of all microchip separation methods is the introduction of analytes into the separation channel. Macroscopic systems usually introduce the sample by some mechanical means, for example by using a rotary injection valve with a sample loop as in HPLC or by physically moving a capillary to a sample vial and aspirating a small sample plug as in CE. Very few microsystems on the other hand use mechanical injections, but instead rely on controlling fluid movement in the system. The separation system needs to be capable of reproducibly injecting small well defined plugs of sample into the separation column. When using electrically driven flow on microchips it is most common to use valveless injection schemes where a four way channel intersection or a cross is used to inject a sample plug into the separation channel. The currents in the microchannels and the resulting fluid flow can be predicted based on the resistance of the channels and by using Kirchhoff's rules [34]. Based on these simple principles it is possible to change the voltages that are applied to different channels to control the fluid movement within the microchip. There are mainly two different injection schemes that are used for microchips with electrically driven flow. The first one is called gated injection and is shown schematically in Figure 1.6.

Gated injection is based on three separate steps, pre-injection, injection and run, and by changing the applied voltage it is possible to switch between these different steps very fast. In the pre-injection step the sample is continuously pumped from a sample reservoir (S) into a waste reservoir (SW) through the injection cross while the mobile phase (M) is continuously pumped into the separation channel (W) and (SW) to prevent leakage of sample into the separation column. In the separation step the voltages are set so that the sample (S) flows into the separation column (W) and there is no flow in the two side channels (SW) and (M). The run step has the same settings as the pre-injection step so that fresh mobile phase (M) flows into the separation column (W) that now contains a defined sample plug. The amount of sample that is injected can easily be varied by changing

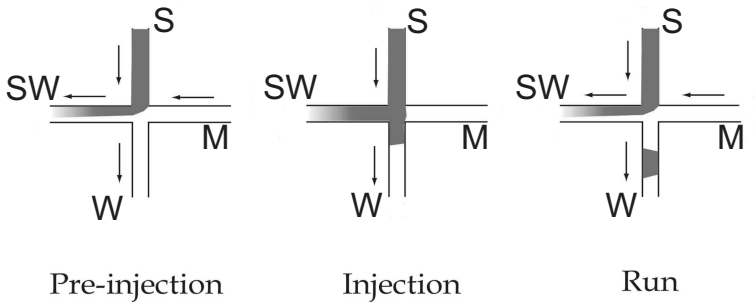

Figure 1.6: Gated injection. During pre injection sample (S) flows into sample waste (SW) and mobile phase (M) flows into the separation column (W) and (SW) to prevent leakage of sample into the separation column. In the injection step the sample (S) flows into the separation column (W) while both (SW) and (M) have no flow. In the run step the settings are the same as in pre injection where (M) flows into the separation column (W) and (SW) that now has a sample plug and (S) flows into (SW). Figure adapted from [35]

the time of the injection step, thereby changing the length of the plug. The main drawback of the gated injection is that there is an electrophoretic bias in the injection, that is species with different electrophoretic mobilities are not injected in equal amounts [36].

The second type of injection scheme is called pinched injection and is depicted in Figure 1.7. Pinched injection is based on two steps: load and separation. In the load position the sample (S) flows across the injection cross towards a waste (SW) reservoir. There is also flow of mobile phase from both the top (M) and the bottom (W) reservoirs to the waste reservoir (SW). The sample stream (S) is "pinched" between the two mobile phase streams, (M) and (W). In the run settings, mobile phase flows from (M) into the separation column (W) and a small flow into the side channels (S) and (SW) pushes the sample away to prevent leakage into the channel. The size of the sample plug can be controlled by the amount of pinching by (M) and (W) but the upper limit of the plug size is the width of the channels. This size limitation can be a drawback for dilute samples , but larger plugs can be injected by offsetting the two side channels (S) and (SW) for a variation of the pinched injection, sometimes referred to as a double-T injection. The length of the injection plug in a double-T injection is controlled by the length of the offset between the channels. Pinched injections do not have an electrophoretic bias in the injection as long as the load step is allowed to proceed for a sufficiently long time [36].

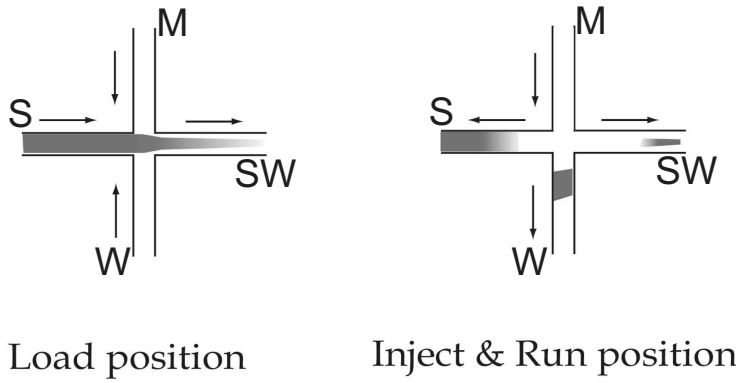

Figure 1.7: Pinched injection. In the load step the injection cross is loaded with sample from the sample reservoir (S) that flows towards sample waste (SW). At the same time mobile phase flow from both (M) and (W) pinch the sample to control the size of the sample plug. In the run step the mobile phase flows from (M) into the separation column (W). A small flow from (M) toward (S) and (SW) prevents leakage into the separation column. Adapted from [35]

1.2 Detection in separation microchips

The goal of this section is to present the detection principles used in my work with a special emphasis on microchip applications. The microchips that are presented in this thesis utilize UV-absorbance detection presented in Section 1.2.1 and laser induced fluorescence presented in Section 1.2.2. A vast number of other detection methods have been realized on microchips. Other microchip detection methods are not presented here but a nice overview of those methods can be found in reviews on the subject [37, 38].

1.2.1 Absorbance

Absorbance detection is the most widely used detection method in macroscopic chromatographic and electrophoretic separation systems [39]. This is largely due to the fact that absorbance detection in the visible and ultra violet range can be used to detect a large number of molecules that possess natural absorbance at these wavelengths. By using direct detection of molecules, disadvantages associated with derivatization, such as added sample preparation complexity and altered physical and chemical behavior of the analytes can be avoided. Absorbance detection in the UV range is especially interesting for the detection of organic compounds and biological compounds such as proteins, peptides and low molecular weight metabolites, as these frequently have no absorbance in the visible range but possess chemical groups that absorb light in the UV range. Despite the wide range

of applications for absorbance based detection systems only a relatively few microchip separation systems utilizing absorbance detection have been reported. The absence of microchip applications can largely be explained by looking at Beer's law that defines absorbance A as:

$$A = -logT = \varepsilon bc \tag{1.22}$$

where A is the absorbance, T is the transmittance through a sample, ε is the molar absorptivity, b is the optical path length through the sample and c is the concentration of the sample. This shows that the absorbance is linearly dependant on the concentration of the analyte and this correlation makes the quantification of analytes based on their absorbance relatively straightforward. The problem associated with absorbance detection in microchips is that the absorbance is linearly dependant on the optical path length b. Most microchips using absorbance measurements rely on bulk optics where the optical path is perpendicular to the plane of the microchip [40]. That means that the depth of the microchannel is probed and due to the fabrication techniques utilized the channel depths are usually less than 30 μm [39], while the width can be much larger. The limited optical path length results in a poor limit of detection. To increase the path length and thereby the limit of detection planar waveguides have been utilized. Planar waveguides are in essence optical fibers that are microfabricated in the microchip substrate and guide light by total internal reflection. Microfabrication allows for the integration of waveguides that are perfectly aligned with a microchannel for the delivery and collection of light at nearly any desired location on the microchip. This not only makes it possible to probe the width of the microchannel instead of the depth, but also makes even larger path length detection cells (U-shaped or Z-shaped) available by having turns in the microchannels that are coupled to the waveguides. Figure 1.8 shows a microfabricated 750 μm long Z-shaped detection cell.

When using UV-absorbance for detection additional demands are put to the microchip substrate material as they (or some parts of the microchip) need to be UV-transparent. In Section 1.3 the properties of different substrates that are frequently used for microsystems are presented.

In previous work from my group, Nickolaj Jakob Petersen and Klaus Bo Mogensen have presented two different approaches of making UV-transparent waveguides for absorbance detection in electrophoretic microsystems [28, 41–43].

In my work, I have used these two types of UV-transparent waveguides and incorporated them into microchips for electrochromatography separations. In Chapter 2, I present an electrochromatography microchip with UV-transparent waveguides made from silicon oxynitride. In Chapter 3, I present an electrochromatography microchip with UV-transparent waveguides that are made from oxidized silicon and have superior optical properties to the oxynitride waveguides and very low propagation loss.

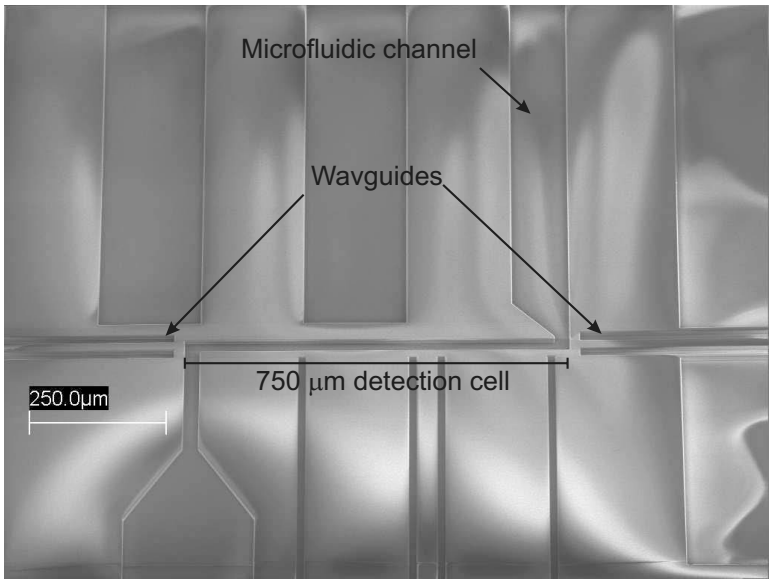

Figure 1.8: A 750 μm long Z-shaped detection cell for absorbance measurements. Waveguides extend from both directions to deliver/collect light to and from the cell. In this detection cell the channel width is reduced to increase the flow velocity through the detection cell to minimize the band broadening effects of the detection cell.

1.2.2 Fluorescence

Fluorescence is the emission of light that occurs when molecules that have been excited by photons return to their ground states and emit photons in the process. Although all molecules that absorb light have the potential to fluoresce, only a small fraction of molecules actually do. This is because generally molecules decay from the excited state by radiationless transitions that are faster than the fluorescence decay. The wavelength of the emitted light is generally longer than the wavelength of the absorbed light as some energy is lost due to radiationless relaxation (heat) before light is emitted as the molecule drops down to the ground state. The emission intensity I at low concentrations can be described by:

$$I = kP_0c \tag{1.23}$$

where P_0 is irradiance of the excitation light, c is the concentration of the fluorescing analyte and k is a constant that depends on the quantum efficiency of the analyte, molar absorbance and other factors. As with absorbance, the fluorescent signal is linearly dependant on the concentration of the analyte. The important difference between absorbance and fluorescence is that the fluorescence intensity is also linearly dependant on the intensity of the excitation light, whereas the absorbance is independent of the intensity of

the excitation light. This makes it possible to get higher sensitivity for a sample by increasing the incident light intensity. Due to this the limit of detection in fluorescence is typically one to three orders of magnitude lower than what is typically seen for absorbance measurements [14].

The problem with using fluorescence for detection is, as mentioned earlier, that very few compounds intrinsically fluoresce and therefore analytes need to be labeled with fluorescent tags before analysis. Despite this drawback, fluorescence is the most important optical detection method utilized in microchips. Laser induced fluorescence (LIF), is the most commonly used method, where a laser is used to achieve monochromatic, high intensity excitation light that can be focused onto a micron sized detection area. The popularity of fluorescence detection in microchips is mainly based on that it can more easily be adapted to low concentration/low volume microsystems than absorbance and can achieve a very low limit of detection [39].

In Chapter 4, I present a polymer electrochromatography microchip that utilized LIF detection on a commercial microchip detection system.

1.3 Substrates for electrochromatography

When choosing a substrate for an electrochromatography microchip there are several aspects that need to be considered. First of all, the substrate must show a significant EOF. Secondly, it must be possible to introduce a stationary phase onto the substrate. The substrate must also be chemically resistant to the organic solvents used in electrochromatography as well as the analytes. For optical detection the substrate needs to be transparent at the desired wavelengths or at least have parts that are transparent, e.g. transparent waveguides or transparent lids. The substrate also needs to be electrically insulating as otherwise the current will simply short circuit through the substrate instead of being conducted through the microfluidic channels. The final consideration is which microfabrication methods can be used for the substrate, as the choice of available methods is governed by the different material properties for the substrates. In the following subsections I will present the properties of three groups of commonly used microchip substrates, glass, silicon and polymers.

1.3.1 Glass

Glass is the most common type of substrate material used for microchip fabrication because it can be structured using well developed microfabrication methods, has suitable chemical and optical properties, has well established surface modification chemistries and is electrically insulating [44]. Standard photolithography is used to define structures on the surface. Microchannels are usually made by wet chemical etching with hydrofluoric acid (HF) that results in an isotropic etch. The sidewalls of channels made with an isotropic

wet chemical etch are semicircular and that severely limits the fabrication of more complex structures such as solid pillar arrays. Pillar arrays have been made in quartz (silicon dioxide) wafers using deep reactive ion etching (DRIE) where a stream of plasma etches the substrate vertically, allowing construction of more complex structures [18]. Quartz wafers are expensive but as they are UV transparent they can be used for detection in the UV range. Borosilicate glass (Pyrex® or Borofloat®) is more commonly used as it is relatively inexpensive but has the disadvantage that it is not UV transparent. Glass substrates are not suitable for waveguide fabrication as the light can leak into the substrate instead of being guided through the waveguide. Glass substrates are frequently used as lids for silicon substrates as it can be an advantage to have a transparent lid so the microchannels can be visually inspected. The lids can be bonded to silicon substrates either by anodic or thermal fusion bonding. The EOF on both borosilicate and quartz substrates is well documented and they have a similar electroosmotic mobility at pH values above 7. Below a pH value of 7 the electroosmotic mobility for quartz drops off much faster than that of borosilicate glass [45]. The microchips presented in Chapters 2 and 3 have lids that are made from a borosilicate glass.

1.3.2 Silicon

Most clean-room microfabrication processes were originally developed for silicon by the microelectronics industry but are also quite applicable for the fabrication of microfluidic systems. Deep reactive ion etching can be utilized on silicon substrates to achieve very high aspect ratio structures for chromatography pillar arrays [28]. Silicon is not optically transparent and therefore silicon microchips frequently have a glass lid to facilitate optical detection. Optical components such as waveguides, LEDs and photodiodes can be fabricated on the silicon substrate through well established processes and therefore integrated with the microfluidic channels for simplified detection compared to bulk optics. The main problem with using silicon for electrochromatography systems is that silicon is a semiconductor and therefore can not withstand high voltages without electrical breaktdown [46]. Thermally grown silicon dioxide layers on top of the silicon substrate can be used to achieve sufficient electrical insulation. A 13 μm thick silicon dioxide layer has been shown to withstand a potential of over 10 kV [47]. The good thermal conductivity of the silicon has also been demonstrated to have a positive effect on heat removal from a silicon based separation device, thereby minimizing the effects of Joule heating on the separation efficiency [48]. Surface modification procedures for glass can be utilized on oxidized silicon as the oxidized silicon has silanol (Si-OH) groups for derivitization on the surface just like glass surfaces. The silanol groups are also important for the electroosmotic flow in the microchannels. The microchips

presented in Chapters 2 and 3 are both based on silicon and have a thermally grown layer of silicon dioxide to electrically insulate the fluidic network from the silicon.

1.3.3 Polymers

Polymers have been hailed as a good alternative to the traditional glass and silicon substrates for commercial microfluidic devices [49]. One of the main driving factors is that the cost of producing polymer microsystems is only a fraction of the cost of their glass or silicon counterparts. Microfabrication in polymers offers a wide variety of different techniques. Direct microfabrication techniques such as micromilling [50] and laser ablation [49] are suitable for prototyping with low resolution but are not suitable for high volume fabrication as the processes are sequential and therefore rather time consuming. Parallel microfabrication techniques based on replicating an inverted master are more suitable for high volume fabrication and can yield micron sized features [51]. Commonly used parallel microfabrication techniques include injection molding [52], nanoimprint lithography [51], hot embossing [53] and casting [54]. The resolution that can be achieved in these methods is based on the resolution of the fabrication technique used for fabricating the inverted master, most commonly photolithography. The wide range of available plastic material makes it possible to choose material properties that are suitable for the desired application. Poly(methylmethacrylate) (PMMA) is a widely used thermoplastic in microsystems, but as it has poor chemical resistance to solvents such as methanol and acetonitrile it is not suitable for an electrochromatography system [49]. Polycarbonate as well suffers from poor chemical resistance to solvents [49]. Poly(dimethylsiloxane) (PDMS) is a silicone based polymer that has been used for making electrochromatography microchips [54–56]. PDMS is suitable for casting where a prepolymer solution and a curing agent are mixed and the polymerization solution is subsequently poured over an inverted master of the microchip. The main problem with using PDMS for electrochromatography is that it is known to absorb chemicals, especially hydrophobic chemicals and organic solvents, into the hydrophobic polymer matrix and swell in the process [57]. Several methods to reduce the absorption of chemicals into the PDMS matrix have been published, including blocking the surface with polyelectrolyte multilayers [56] and filling the PDMS matrix with small particles of transition metal oxides [58, 59]. PDMS is also frequently used as a lid to seal glass or silicon microfluidic systems as it is easy to bond the elastic polymer to even relatively rough surfaces [28]. Cyclic olefin copolymer (COC, brand names: Topas, Zeonor, Zeonex) is a thermoplastic that has many properties that are required of a substrate for electrochromatography. Topas is chemically resistant to acids, bases and polar solvents [60] and is optically transparent even below 300 nm making UV-absorbance measurements possible [61]. Topas

microsystems can be made in large volumes utilizing high throughput fabrication techniques such as injection molding and nanoimprint lithography. The Topas polymer is naturally hydrophobic but surface modifications by photografting to introduce different surface functionalities, such as a more stable EOF, have been demonstrated [62, 63].

In Chapter 4, I present a Topas electrochromatography microchip that is fabricate by nanoimprint lithography, where an inverted silicon master is pressed into a softened Topas substrate.

Chapter 2

Silicon Oxynitride Microchips

The following material was presented in an talk entitled "The effect of interpillar distances in ordered pillar arrays on separation efficiency in microchip capillary electrochromatography" at the Gordon-Kenan Graduate Research Seminar on Analytical Chemistry in Roscoff, France, June 10-12, 2005.

2.1 Introduction

In this chapter an electrochromatography microchip with integrated waveguides for in-plane absorbance detection is presented. The UV-transparent waveguides are made from silicon oxynitride and their fabrication and performance has been previously reported by my group for a capillary electrophoresis microchip [41–43]. The waveguides allow for label-free detection of many organic compounds by UV absorbance measurements across the microfluidic channels. Microfabricated solid support structures as proposed by He et al [18,19] are utilized to increase the volume of the stationary phase in the separation column and to achieve homogenous flow patterns throughout the separation column. The microfluidic network and the waveguides need to be fabricated in separate steps resulting in a fabrication process involving several photolithography masks that need to be aligned precisely with the substrate.

2.2 Experimental

2.2.1 Reagents

N-octadecyltrimethoxysilane was obtained from ABCR (Karlsruhe, Germany). Toluene, methanol, acetone, acetophenone, propiophenone, butyrophenone, valerophenone and hexanophenone were obtained from Sigma-

Aldrich (Schnelldorf, Germany). Sodium tetraborate decahydrate was obtained from Riedel-de Haën (Schnelldorf, Germany).

2.2.2 Microchip layout

Figure 2.1 shows the design of the microchip. The fluidic part of the chip has a standard cross injector setup. The main channels are 120 μm wide and 9 μm deep. The separation column is based on the design proposed by Regnier and co-workers, where the main channel divides several times leading into an array of hexagonal pillars, see Figure 1.5. The separation column is 2.8 cm long. The channel widths between the pillars are 2.5 μm after the fabrication. The channel width between the pillars can be decreased further by depositing tetraethoxy silane (TEOS-glass) on the surface of the pillars using chemical vapor deposition. In some of the following experiments a 0.5 μm and 0.75 μm layer of TEOS glass has been deposited on the surface resulting in channel widths in the separation column of 1.5 and 1.0 μm. There are 32 pillars in each row. A 750 μm long Z-shaped detection cell with planar waveguides for absorbance detection is placed shortly after the separation column. Furthermore another set of waveguides that allows for absorbance detection across the 120 μm wide channel are placed between the separation column and the detection cell. The waveguides are 6 μm high and 24 μm wide. The waveguides have turns on them so that the optical fibers that connect to the waveguides are offset to avoid the collection of stray light directly across the chip. Optical fibers that are aligned with the waveguides with the help of an alignment stage and a microscope are glued to the edge of the chip.

2.2.3 Microchip fabrication and preparation

The microfabrication is described in detail in the Ph.D. thesis of Klaus Bo Mogensen [64]. The microchips are fabricated in 4 inch silicon wafers that are 525 μm thick. Figure 2.2 shows a schematic of the cross section of the chip. First the silicon substrate was thermally oxidized (wet oxidation) for 21 days in order to grow a 10-15 μm layer of silicon dioxide to electrically insulate the channel network from the silicon substrate. A 6 μm thick layer of silicon oxynitride (SiO_xN_y) was deposited onto the wafer using plasma enhanced chemical vapor deposition (PECVD). The silicon oxynitride is UV transparent and serves as the core of the waveguide. The waveguide network was then etched by reactive ion etching using poly silicon as an etch mask. Undoped silica was deposited by PECVD for waveguide cladding. The microfluidic channels were etched using reactive ion etching with poly silicon as an etch mask. The channels were etched through the cladding and the waveguide core and into the insulating silicon dioxide layer, which also acts as a bottom cladding for the waveguide. Finally a 500 μm thick

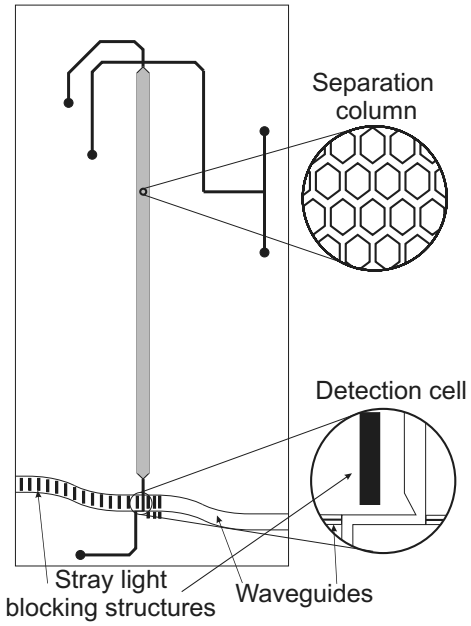

Figure 2.1: Design of the CEC microchip with silicon oxynitride waveguides. Thick lines represent channels. The pillars are elongated hexagons with mixing nodes between rows. UV-absorbance can be measured over the 120 μm wide channel or the Z-shaped detection cell after the separation column. Blocking structures minimize stray light from being collected by the receiving optical fiber. Glass reservoirs are glued to the microchip lid over at the end points of the channels.

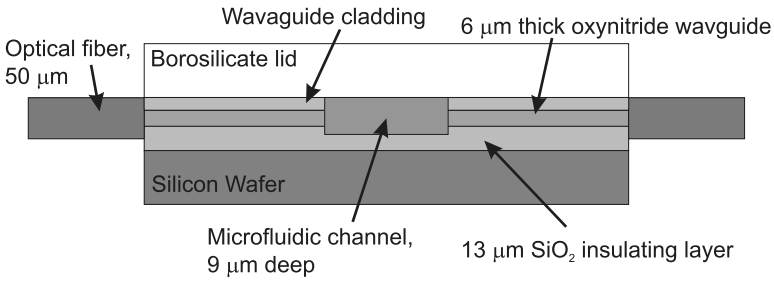

Figure 2.2: Cross section of the microchip. The optical fiber is aligned with the 6 μm thick silicon oxynitride layer. The dimensions on the figure are not to scale.

borofloat glass lid was anodically bonded to the microchip. Access holes were etched through the glass lid with hydrofluoric acid before the bonding.

After fabrication a stationary phase was covalently bonded to the channel surfaces in the microchip. The coating procedure was adapted from method described by Kutter et al. [6] where the microchip is filled with a mixture of 10% (w/w) n-octadecyltrimethoxysilane and 0.01% n-butylamine in dried toluene. The microchip was placed in a vessel with saturated toluene atmosphere and the reaction allowed to proceed overnight at room temperature. The chip was then rinsed thoroughly with toluene followed by rinse with methanol and then the chip was finally dried. Glass reservoirs were glued to the chip and the optical fiber aligned with the waveguides and glued to the chip. The chip was conditioned with a 10 mM tetraborate mobile phase containing 10-40% methanol before operation.

2.2.4 Experimental setup

The experimental setup is depicted in Figure 2.3. A 100 W mercury lamp (L.O.T. Oriel GmbH, Darmstad, Germany), equipped with a 254 nm bandpass filter (254S25-50, L.O.T. Oriel GmbH) was used. The lamp includes focusing optics for coupling light into optical fibers. UV-transparent pure-silica optical fibers with a 50 μm core and a 70 μm outer diameter (FVP050055065, Polymicro Technologies, Phoenix, AZ, USA) were used to couple light from the lamp to the microchip and then from the microchip to a photomultiplier tube (model no. 77348, Oriel Instruments, Stratford, CT, USA) that was used for detection. The optical fibers were aligned with the waveguides and then permanently glued to the side of the microchip. A UV-transparent, UV curing adhesive (Epotek 09146, Epoxy Technology, Billerica, MA, USA) was used to fasten the optical fibers to the chip. To secure the fibers completely another UV-curing adhesive (NOA 63, Norland Precuts Inc., North Brunswick, NJ, USA) was utilized. An amplifier (SR750, Stanford Research Systems, Sunnyvale, CA, USA) converted the PMT signal from current to voltage. The amplifier also incorporated a low pass filter, which was set to 10 Hz in all measurements. The data was collected at 50 Hz through an analog to digital board (SS420, Beckman Instruments, Fullerton, CA, USA). The data was acquired using Gold Nouveau software (Beckman Instruments) An in-house written Lab VIEW 6i (National Instruments, Austin, TX, USA) software controlled an in-house built power supply that could deliver voltages up to 4 kV to the fluidic reservoirs on the microchip to control the electrokinetic transport in the channels. The flow was controlled by applying different voltages to the fluidic reservoirs on the chip, and the resulting flow was proportional to the current in the channel. Fast switching of the voltages allowed injections of well defined plugs of sample into the separation channel.

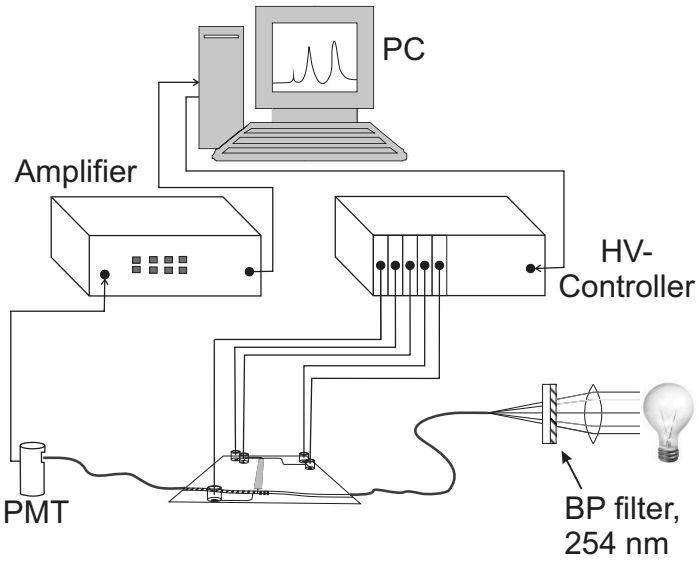

Figure 2.3: Experimental setup for CEC measurements on a microchip with UV-transparent silicon oxynitride waveguides. 254 nm light from a mercury lamp is focused into an optical fiber. The optical fiber is glued to a microchip and the light is coupled into a planar waveguide that carries the light to a detection region. Another waveguide collects the light and carries it to an optical fiber that is coupled to a PMT. The PMT is connected to an amplifier and current/voltage converter. The output of the amplifier is collected on a computer. A computer also controls the electrokinetic flow in the microchip by controlling the voltages that are applied through a high voltage power supply.

2.2.5 Microchip CEC operation

To determine the voltage settings needed for a microchip CEC run a procedure described by Nickolaj J. Petersen [47] was used where the resistances of the channel segments are determined. All channels and reservoirs are filled with mobile phase. Platinum electrodes are put into two reservoirs at a time, one of them is connected to the high-voltage power supply and the other one is connected to ground through an amperometer. The resistance between each set of reservoirs is determined by measuring the current between the reservoirs for 5 different voltages (100-500 V). The resistance is found from the slope when plotting the applied voltage U, as a function of the monitored current, I. A more detailed description for the determination of injection voltages and formulas for calculation of the resistances and voltages for each channel segment is given in Appendix B. Frequently the calculated potentials would lead to a slight leakage of sample into the separation column so the voltages would need to be manually fine tuned to get reproducible injections.

In the following experiments gated injection is used where the reservoir at the end of the separation channel is grounded through an amperometer. The current in the microchip is a good indicator of problems since instabilities in the current are usually caused by bubbles or other disturbances in the separation column. All samples were diluted in the same mobile phase as the one used in the separations. This was done to keep the conductivity of the sample plug nearly identical to the mobile phase as that greatly simplified predicting the flow patterns during operation.

As the output of a PMT is actually a measure of the transmitted light and not the absorbance, the signal needed to be converted into absorbance units. The absorbance is related to the transmission of light as described in Equation 1.22. In order to determine the transmission through a sample, a value for 100% transmittance through the detection cell, P_0, needs to be determined. I chose to use the average light intensity for the first 3 seconds of each run as P_0. The absorbance is then determined by:

$$A = -logT = -log\Big(\frac{P}{P_0}\Big) = -log\Big(\frac{PMT\ signal}{average\ PMT\ signal_{first\ 3\ seconds}}\Big) \tag{2.1}$$

In all of the following experiments absorbance detection across the 120 μm microchannel was used. The reason for not using the longer pathlength detection cell was that previous results on the same design of microchips showed that a comparable limit of detection was achieved when using the shorter 120 μm detection path as the longer detection cell [41]. This is due to the fact that a large portion of the light that enters the long detection cell is lost due to spreading while more light is coupled into the collection waveguide over the shorter pathlength. Larger waveguides as presented in Chapter 3 are able to transmit much more light through the chip and there-

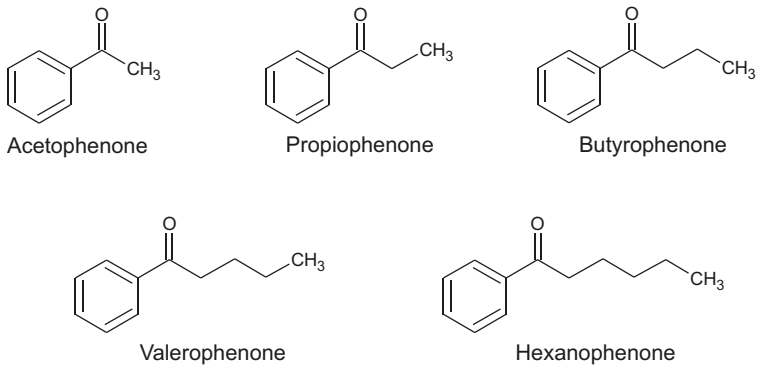

Figure 2.4: Chemical structures of the alkylphenones used for analysis. Acetophenone, propiophenone, butyrophenone, valerophenone and hexanophenone.

fore get a better limit of detection. The detection cell also turned out to be prone to clogging with small particles and while the the flow through the channel was not disrupted the particles could completely block the light going through the detection cell.

2.3 Results and discussions

To verify reversed phase chromatographic retention on the microchip, five uncharged alkylphenones were separated. Figure 2.4 shows the chemical structure of the five analytes; acetophenone, propiophenone, butyrophenone, valerophenone and hexanophenone. The analytes are phenones with different length alkyl chains, ranging from a single methyl group for acetophenone to a pentyl chain for hexanophenone. The hydrophobicity of the analytes increases as the length of the carbon chain increases, acetophenone being the least hydrophobic and quite easily soluble in water while hexanophenone is the most hydrophobic and only very slightly soluble in water. The sample solution that is prepared contains an organic modifier such as methanol or acetonitrile to ensure sufficient solubility of all the analytes. All the analytes have a similar molar absorptivity at 254 nm so the components can have a similar concentration for detection.

A mixture of all 5 alkylphenones was separated on a microchip where the channel widths in the separation column had been reduced to 2.0 μm with TEOS glass deposition before attaching the octadecyl stationary phase to the channel surface. Absorbance at 254 nm was measured across the 120 μm wide channel, approximately 2 mm after the pillar region. Figure 2.5 shows a chromatogram of a typical separation on the microchip with 25% methanol in the mobile phase at an electric field strength of 620 V/cm. All

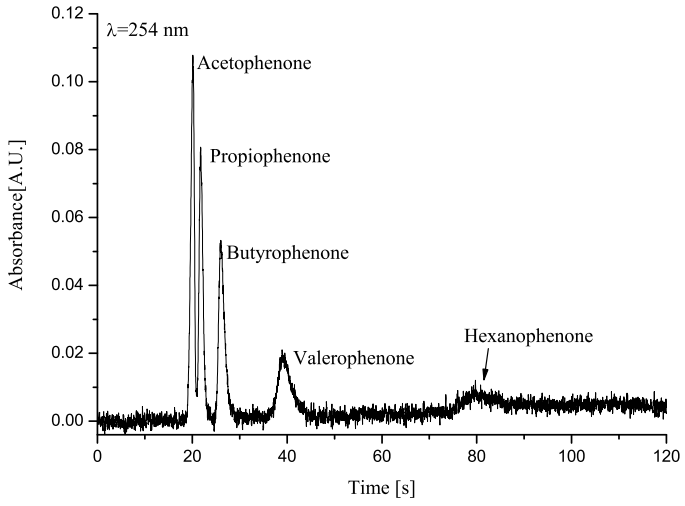

Figure 2.5: Microchip electrochromatography separation of 5 alkylphenones: acetophenone (0.6 mg/mL), propiophenone (0.7 mg/mL), butyrophenone (0.8 mg/mL), valerophenone (1.0 mg/mL) and hexanophenone (1.0 mg/mL). Mobile phase: 10 mM tetraborate buffer at pH 9.2 and 25% methanol. Octadecyl stationary phase. Field strength 620 V/cm. Gated injection, 0.2 s injection. Absorbance detection at 254 nm. Sampling rate 50 Hz.

of the injected components can be identified from the chromatogram, but the first two are not quite baseline separated. All of the components in Figure 2.5 are retained, when compared to a run with acetone that is unretained. The retention factors are: acetophenone 0.17, propiophenone 0.26, butyrophenone 0.51, valerophenone 1.3 and hexanophenone 3.6. The plate heights for the analytes are: acetophenone 9.0 μm, propiophenone 8.4 μm, butyrophenone 12.1 μm, valerophenone 19.8 μm and hexanophenone 32 μm. These plate heights are rather high for microchip CEC so it should be possible to improve the plate heights by optimizing the separation. To improve the plate heights new microchips with smaller interpillar distances were prepared. The organic modifier in the stationary phase was also changed from methanol to acetonitrile to achieve higher linear velocities at the same electric field strength. This was done because the electroosmotic mobility in a mobile phase containing acetonitrile is higher than for a mobile phase containing the same concentration of methanol due to a lower ε_r/η-ratio (see Equation 1.4) for methanol containing mobile phases [65].

The two new microchips had 1.5 μm and 1.0 μm interpillar distances and both were prepared by depositing TEOS glass on the microchip surfaces before bonding. The decreased interpillar distance should reduce the Cu_0-term of the van Deemter equation as C_m is dependant on the channel dimensions squared (Equation 1.15). Two of the retained alkylphenones, propiophenone and butyrophenone, were chosen to make van Deemter plots to characterize the separation columns and find the optimum linear velocity and the lowest achievable plate heights. To make the van Deemter plots the linear velocity in the separation columns needs to be determined. This was done by injecting a sample plug with an unretained and uncharged analyte, acetone in this case, into the separation column and measuring the arrival time at the detector. The mobile phase velocity u_0 is simply the length of the column (2.8 cm) divided by the arrival time of acetone at the detector. The linear velocity for each of the chips was then determined for different electric field strengths. Figure 2.6 shows a plot of the linear velocity as a function of the electric field strength in a separation column with 1.5 μm interpillar distance.

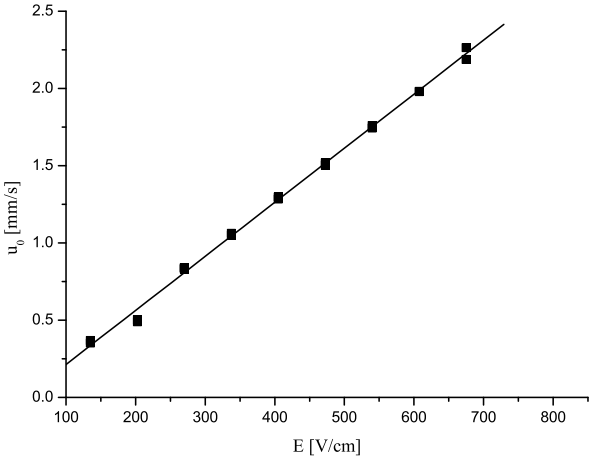

Figure 2.6: Linear velocity u_0 as a function of the electric field strength in an electrochromatography microchip with 1.5 μm interpillar distance. Acetone is used as an EOF marker to determine the dead volume of the separation column. Mobile phase: 10 mM tetraborate pH 9.2 and 25% acetonitrile

The velocity u_0 is linearly dependent on the electric field strength E: $u_0 = E\mu_{eo}$. The slope of the graph is then the value of the electroosmotic mobility μ_{eo}, $3.5 \cdot 10^{-4}\ cm^2\ V^{-1}\ s^{-1}$. The value is comparable to what is expected for glass or silicon microchannels [12].

Measurements of the plate height of propiophenone and butyrophenone on the two different microchips were carried out using 25% acetonitrile in the mobile phase and both of the chips having an octadecyl stationary phase. The analyte mixture was injected three times at each voltage setting. The resulting van Deemter plots are shown together in Figure 2.7.

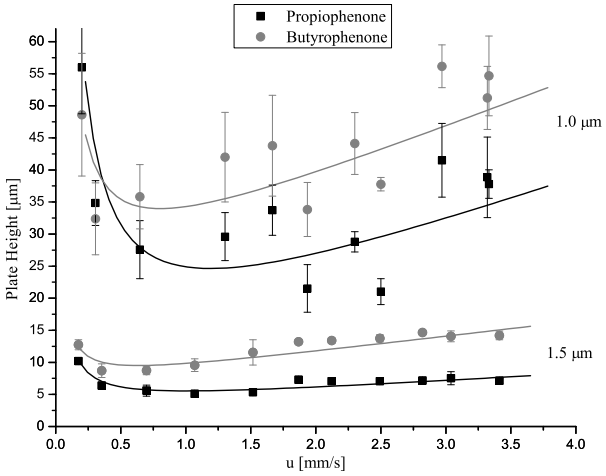

Figure 2.7: Van Deemter plots for propiophenone and butyrophenone for two different microchips, with 1.0 μm interpillar distance and 1.5 μm interpillar distance. All measurements are made in a mobile phase containing 10 mM tetraborate at pH 9.2 and 25% acetonitrile. Error bars show one standard deviation for measurements in data point. Octadecyl stationary phase.

It is clear from the van Deemter plots that the reduction of the channel widths in the separation column has the opposite effect to what was expected. The microchip with 1.5 μm interpillar distance had minimum plate heights of 5.0 μm and 8.7 μm for propiophenone and butyrophenone, respectively, which is acceptable for microchip electrochromatography. The microchip with 1.0 μm interpillar distance, on the other hand, had minimum plate heights of 21 μm and 32 μm for propiophenone and butyrophenone, respectively. This unexpected increase in the plate heights may be explained by two possible reasons.

First of all, when TEOS deposition is used to reduce the channel widths the total cross sectional area becomes smaller in the separation column than in the regular channels. This is explained in Figure 2.8 where the cross sections of a regular channel and the separation column are compared before and after deposition of 0.75 μm TEOS. The reason for the smaller cross sectional area is that in the conformal TEOS deposition, a glass layer is deposited on all surfaces. In the separation column there is simply more surface to deposit glass on than in the regular channel due to the pillars in the separation column. In the separation column a 0.75 μm thick glass layer will be deposited on both sidewalls of 32 2.5 μm wide channels, resulting in 48 μm reduction of the combined width of the column. The regular channels only have two sidewalls so the total width reduction of the regular channels will only be 1.5 μm with the same deposition.

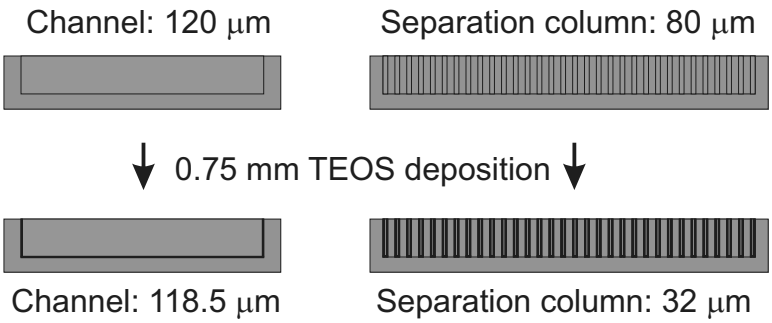

Figure 2.8: The effect of channel width reduction with TEOS glass deposition. A regular microchannel with a width of 120 μm compared with a separation column consisting of 32 channels, each of them 2.5 μm wide. The effects of a 0.75 μm TEOS glass deposition are shown.

Because of the different cross sectional area in the different channel segments, the mobile phase that is flowing into the separation column from a regular channel needs to increase the linear velocity to keep the volumetric flow rate a constant and maintain the continuity condition. The mobile phase therefore needs to accelerate on the boundary between the two channel segments and a pressure gradient forms [66]. The parabolic flow profile due to the pressure gradient will be superimposed on the flat electroosmotic flow profile and will therefore deform the sample plug and lead to band broadening. This effect should increase as the channel widths in the separation column get smaller because the acceleration is greater.

The other source of band broadening arises from the attachment of a stationary phase to the microchip surfaces. A guest student in our labs noticed that when operating microchips with channel dimensions in the separation column below or around 1 μm, aggregates seemed to form and clog the separation column. A SEM image of the aggregates in the separation column confirmed this observation (see Figure 2.9). These aggregates are thought to be made out of polymerized stationary phase molecules that form when the channels are coated with the stationary phase. Due to their size, the aggregates get stuck in the pillar array, and can cause partial clogging of the separation column. The resulting flow irregularities around the clogged channels will then lead to band broadening. Previously the student had observed that channels below 2.5 μm start to clog with aggregates when using an octadecyl stationary phase, while an octyl stationary phase could easily be used down to about 1 μm channels. If the aggregates are causing the observed band broadening it is consistent with the fact that more band broadening is observed for smaller channel widths as these would clog more easily. It is not quite clear why these aggregates form but one explanation could be that water that has been physisorbed onto the microchannel surface catalyzes polymerization of the monomers that form the stationary

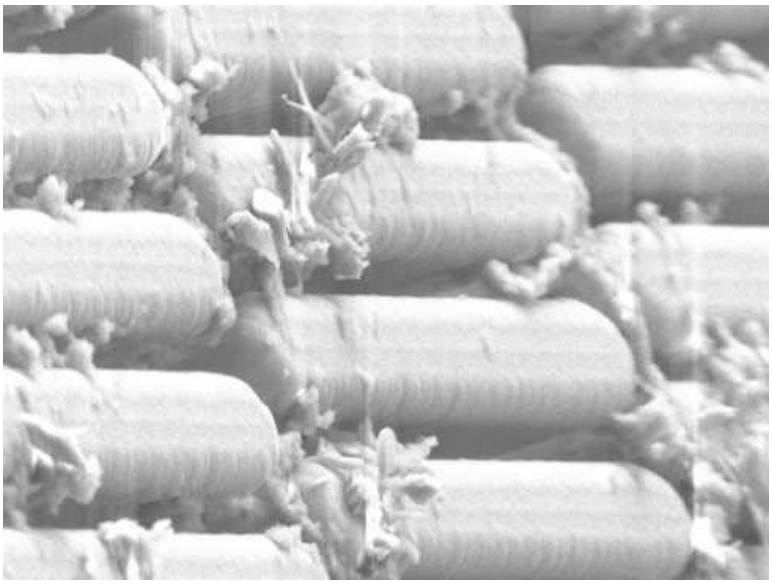

Figure 2.9: SEM image of aggregates in a separation column with 1 μm interpillar distance after coating with an octyl stationary phase. Image courtesy of Wim De Malsche.

phase. The increased surface area in the pillar array would then lead to more water being physisorbed and a higher chance of polymerization resulting in aggregates.

The lifetime of the microchips used in this study was quite short, only 1-2 days and after that it got impossible to achieve sharp peaks through the separation column due to clogging. This is especially inconvenient as a long time is needed to prepare each chip, coat the channels with a stationary phase and then align and glue optical fibers for detection.

2.4 Conclusions and outlook

In this chapter, microchips with integrated silicon oxynitride waveguides for UV-absorbance detection and solid support structures for a stationary phase were presented. Reversed phase electrochromatography separation of 5 neutral alkylphenones was demonstrated on the microchips coated with an octadecyl stationary phase. Plate heights of 5.0 μm and 8.7 μm were obtained for propiophenone and butyrophenone, respectively, on a microchip with 1.5 μm interpillar spacing. Experiments with varying the interpillar distances in the microchips resulted in an unexpected rise in the plate height as the interpillar distance was decreased. This was attributed to the formation of a pressure gradient at the boundary between the regular channels and the separation column that deformed the sample plug as well as the formation of aggregates of stationary phase particles that clog the small channels in

the separation column.

To keep the cross sectional area a constant throughout the microchip a new mask would need to be designed for every interpillar distance tested. This was not pursued in the current project as the focus was directed towards a more integrated microchip where shorter time is needed to prepare each microchip, especially with regards to alignment of optical fibers through fiber couplers.

To avoid the formation of stationary phase aggregates it is more suitable to use an octyl stationary phase as these seem to form smaller particles and not be as problematic with clogging unless in sub-micron channels. It would be advisable in the future to do some more detailed experiments to find a suitable coating procedure for the microchips with pillar arrays as their fabrication and preparation is very time consuming so a longer life time of the microchips would be desirable.

Chapter 3

Oxidized Silicon Microchips

The major part of this chapter is based on images and text from a research article entitled "Electrochromatography chip with integrated waveguides for UV absorbance detection", submitted to the Journal of Micromechanics and Microengineering. Here, the article has been expanded to include more details and images in order to give a more in-depth view of the work and to explain some concepts in more detail.

3.1 Introduction

Capillary electrochromatography (CEC) is a chemical separation technique that is a hybrid between high performance liquid chromatography (HPLC) and capillary electrophoresis (CE). Originally, CEC was performed using materials developed for liquid chromatography, i.e., a stationary phase made by tightly packing functionalized particles into a separation column [67]. Microchip CEC possesses several advantages compared to traditional CEC. The smaller physical dimensions make microchips more suitable for portable separation units than the bulky benchtop machines used in conventional CEC. Integrated on-chip fluidic networks in microdevices offer reduced contribution of non-diffusional band broadening sources, such as from injectors, connectors, transfer tubing and detectors, making higher separation efficiencies possible [68]. The short separation length on microchips results in fast separations and high electric field strengths at relatively low voltages. The small dimensions of the chip also reduce the reagent consumption and thereby the operating costs [9, 69]. Despite all this, the adaptation of CEC to miniaturized formats was not straightforward. In particular, problems with packing particles or beads uniformly inside a capillary or a microfluidic channel led to the development of several alternatives for making a homogenous stationary phase [70]. Some of the first on-chip electrochromatography studies utilized an open channel approach where the stationary phase is covalently bonded to the surface of a shallow channel, thus cir-

cumventing the packing issue altogether [27]. In-situ polymerized porous monolithic chromatographic columns have also been shown to be useful in CEC microchips. Monolithic columns are contiguous units of macroporous material. The porous network in the column gives a high surface area, and the surface functionalities can be customized to fit a specific separation by the choice of monomers that are then polymerized to form the monolithic column [71]. High efficiency microchip separations have been presented on both silica- and organic polymer-based monoliths [16, 72, 73]. Regnier and co-workers suggested and demonstrated the use of microfabricated support structures inside the separation column to increase the surface-to-volume ratio and thus the loading capacity of the stationary phase [18, 19, 54]. These types of separation columns consist of a highly regular array of pillars with narrow channels between them. The size, shape and positions of the pillars can be controlled very precisely in the photolithographic processes employed during the fabrication of the microchips.

A microfabricated chromatography column with support structures for the stationary phase has several advantages. It is possible to fabricate structures that are inherently much more regular than what is achievable using traditionally packed beds. These structures can be optimized to provide close to ideal flow patterns thus enabling higher separation efficiencies by reducing the A-term of the van Deemter equation [26, 74]. The increased separation efficiencies of perfectly uniform micromachined pillars compared to packed beds have been demonstrated both in simulations and experiments [29, 75].

Most microchip separation techniques reported use laser induced fluorescence (LIF) detection because of its high selectivity and sensitivity. The drawback of using LIF is that most analytes do not possess native fluorescence, thus requiring a labeling step before detection. UV-absorbance detection is much more common in conventional electrophoresis and liquid chromatography due to its direct applicability to a wide range of analytes. In microchips, optical measurements are usually performed using free-space optics where the excitation is perpendicular to the plane of the chip. Because of the fabrication methods utilized the channels are relatively shallow (tens of micrometers) compared to their width, limiting the path length to the depth of the channel. This is a drawback for absorbance measurements as the signal is proportional to the detection length, which results in a higher limit of detection for shorter path lengths [39]. My research group has previously reported longer pathlength detection cells consisting of microfabricated in-plane waveguides aligned with U- or Z-shaped detection cells with pathlengths up to one millimeter [28, 41, 43]. Using a U-shaped detection cell and UV-transparent waveguides a limit of detection of 20 μM for paracetamol using UV-absorbance at 254 nm was demonstrated [28].

Previously, my research group fabricated capillary electrophoresis microchips featuring a similar design as presented here, but sealed with PDMS

lids [28]. The reason for using a PDMS lid in the previous work was that, due to the elasticity of PDMS, bonding to the processed surface was straightforward while the refractive index of PDMS still made it a suitable cladding material for the silicon dioxide waveguide. There are, however, several problems with regards to using PDMS lids for electrochromatography microchips. Absorption of chemicals is always an issue as hydrophobic compounds tend to migrate into the PDMS matrix and cannot be eluted again. Attempts to reduce the absorption using different modifications of the PDMS material [55, 58, 76] did not provide the desired effect for our chips. Furthermore, the attachment of a stationary phase to the silicon dioxide surface is performed using toluene as solvent, which makes PDMS swell severely, resulting in the delaminating of the PDMS lid from the chip. Clearly, the optimum lid for the electrochromatography microchip would be made of glass. However, the bonding of such a lid to the processed silicon dioxide surface of the wafer is challenging, but became possible by adapting a procedure originally developed for glass to glass thermal bonding by Jacobson et al [36].

In this chapter the first microchip for electrochromatography with integrated waveguides for in-plane absorbance detection is presented. This makes the device the most complete microfabricated chromatography chip utilizing optical detection to date in terms of integrated functionalities. The waveguides are furthermore made from silicon dioxide which makes them UV-transparent [28], facilitating label-free, sensitive detection of many organic compounds by UV absorbance measurements. This type of waveguide has the lowest propagation loss in the UV range presented to date [28]. The whole microchip, including microfluidic channels, optical network and fiber couplers, is fabricated in a single etching step, resulting in a very simple and robust fabrication procedure.

3.2 Experimental

3.2.1 Reagents

N-octyldimethylchlorosilane and toluene were obtained from Sigma-Aldrich (Bornem, Belgium). Acetonitrile, acetophenone, valerophenone, hexanophenone, thiourea, ammonium hydroxide and hydrogen peroxide were obtained from Sigma-Aldrich (Schnelldorf, Germany). Sodium tetraborate decahydrate was obtained from Riedel-de Haën (Schnelldorf, Germany).

3.2.2 Microchip layout

A single-mask approach where all fluidic and optical components are fabricated in the same layer is utilized to make the chip as simple and robust as possible. However, this has the consequence that the possible channel depths have a lower limit given by the outer diameter of the optical fiber

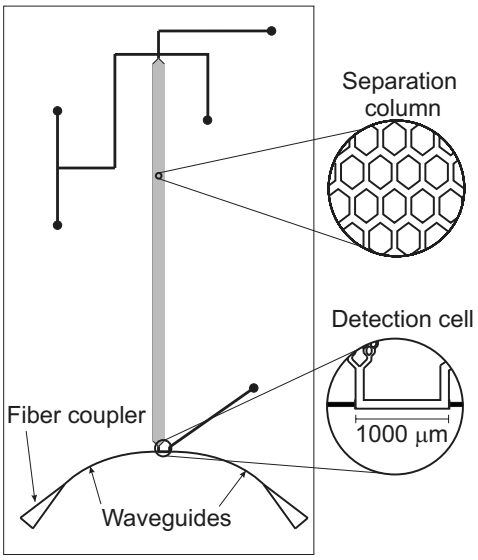

Figure 3.1: Design of the electrochromatography microchip. Bold lines represent fluidic channels and waveguides. The separation column is 33 mm long and contains an array of hexagonal pillars with 4 μm wide channels between them. A U-shaped detection cell that is 1 mm in length is positioned after the separation column. Microfabricated fiber couplers assist with aligning optical fibers to the planar waveguides on the chip. Reservoirs are placed at the endpoints of the fluidic channels.

used, which should be easily insertable in the fiber couplers channel. The optical fiber that was used had a diameter of 70 μm, which made a channel depth of around 100 μm reasonable.

Figure 3.1 shows the design of the microchip. The fluidic part of the chip has a standard cross injector setup. The main channels are 64 μm wide and 99 μm deep. The separation column is based on the design proposed by Regnier and co-workers [19] where the main channel divides several times leading into an array of hexagonal pillars (see Figure 1.5). The pillars have a width of 16 μm after oxidation while the space between the pillars is designed to be 4 μm wide. In this initial design, relatively wide pillars were chosen to ensure that they would withstand the deep etching step and still be sufficiently robust. There are 30 pillars in each row. A 1 mm long U-shaped detection cell is placed directly after the separation column. On-chip waveguides are aligned with the detection cell to couple light to and from the detection cell, facilitating absorbance detection. The waveguides feature a 20^{o} bend to avoid the collection of stray light [28]. Fiber couplers are fabricated on the chip to allow for insertion of optical fibers with up to 70 μm in outer diameter. The fiber couplers are tapered channels that guide the optical fibers towards the end facets of the waveguides, ensuring

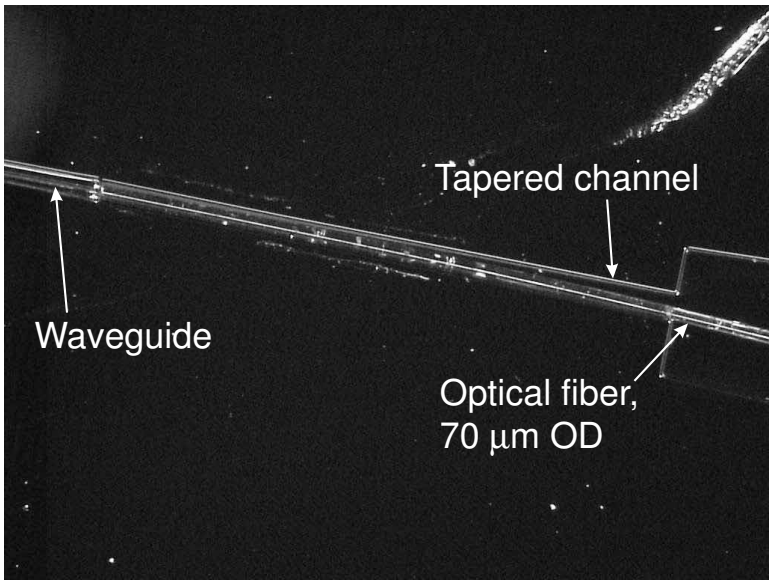

Figure 3.2: Photograph of an optical fiber in the microchip fiber coupler. Optical fiber extends from right, into the tapered channel and is aligned with the end facet of the waveguide. A 22 μm wide waveguide extends from the facet and to the left. The waveguide has air as cladding on either side

perfect alignment between the optical fiber and the waveguide, without the use of an alignment stage and a microscope (see Figure 3.2). The optical fibers were inserted manually into the fiber couplers and held in place using adhesive tape. This option was chosen over a more permanent solution using epoxy-based glues, since it offered more experimental flexibility.

3.2.3 Microchip fabrication and preparation

The microchip was fabricated from 4 inch diameter silicon wafers with a thickness of 525 μmusing deep-reactive ion etching. The majority of the fabrication process was previously described by Mogensen et al [28]. All structures were made in a single etching step and etched to a depth of 99 μm. After the etching, the silicon substrate was thermally oxidized using wet oxidation for 21 days, resulting in a silicon dioxide thickness of 13-15 μm. The reason for the thick oxide layer was twofold: first, to ensure that the microfluidic channels were electrically insulated from the underlying silicon wafer for applied voltages up to 10 kV [43], and second, to completely oxidize the waveguide ridge structures in order to make UV transparent ridge waveguides (see ref. [28] for more details).

The oxidized silicon substrate with the microchannel network was sealed with a borofloat glass lid. The bonding procedure was adapted from a glass

to glass fusion bonding method described by Jacobson et al [36]. Prior to bonding, access holes were sandblasted through a 500 μm thick borofloat glass lid. The glass lid and substrate were hydrolyzed in a dilute mixture of ammonium hydroxide, hydrogen peroxide, and water (2:1:2) at 75 °C for 30 min. Following sonication in ultrapure water for 10 min, the substrate and lid were brought into contact while still wet. The assembly was dried at 90 °C for 2 h to remove excess moisture between the two layers and permanently annealed at 550 °C for 10 h. Glass reservoirs were then glued on top of the lid.

For reversed phase electrochromatographic separations, hydrophobic octyl silanes were covalently attached to all surfaces in the microchannels as described by De Malsche et al [22]. The microchip was completely filled with the coating solution, 15% n-octyldimethylchlorosilane in toluene. The reaction was allowed to proceed overnight at room temperature. After coating, the chip was rinsed with toluene for 30 min, followed by methanol for 30 min, and finally filled with the desired mobile phase.

3.2.4 Experimental setup

A 100 W mercury lamp (L.O.T. Oriel, Stratford, CT, USA), equipped with a 254 nm bandpass filter was used. The lamp includes focusing optics for coupling light into optical fibers. A UV-transparent pure-silica optical fiber with a 50 μm core and a 70 μm outer diameter (FVP050055065, Polymicro Technologies, Phoenix, AZ, USA) was used to couple light from the lamp to the microchip and then from the microchip to a photomultiplier tube (H5784-06, Hamamatsu, Japan). For noise reduction a lock-in amplifier (SR830, Stanford Research, Sunnyvale, CA, USA) was used. An optical chopper connected to a controller (SR 540, Stanford Research, Sunnyvale, CA, USA) chopped the incident light at 430 Hz and the lock-in amplifier filtered away all other frequencies. The time constant of the lock-in amplifier was 100 ms. Data acquisition was performed at 50 Hz using an in-house written Lab VIEW 6i (National Instruments, Austin, TX, USA) software. The same software controlled an in-house built power supply that could deliver voltages up to 4 kV to the fluidic reservoirs on the microchip to control the electrokinetic transport in the channels. The flow was controlled by applying different voltages to the fluidic reservoirs on the chip, and the resulting flow was proportional to the current in the channel. Fast switching of the voltages allowed injections of well defined plugs of sample into the separation channel.

3.2.5 Microchip CEC operation

To determine the required voltage settings the same procedure as describe in subsection 2.2.5 was applied.

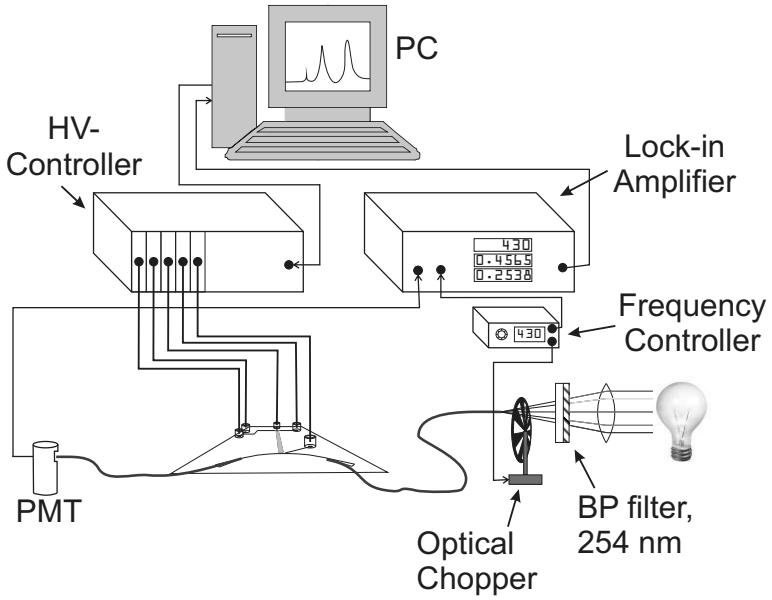

Figure 3.3: Experimental setup for microchip electrochromatography measurements using UV-absorbance detection. Light from a mercury lamp with a 254 nm bandpass (BP) filter is focused into an optical fiber through an optical chopper operated at 430 Hz. Light is coupled to and from a detection region with waveguides that are aligned with the optical fibers with on-chip fiber couplers. The collecting optical fiber is connected to a PMT. The PMT is connected to an lock-in amplifier that also controls the chopping frequency. The output of the amplifier is collected on a computer. A computer also controls the electrokinetic flow in the microchip by controlling the voltages that are applied through a high voltage power supply.

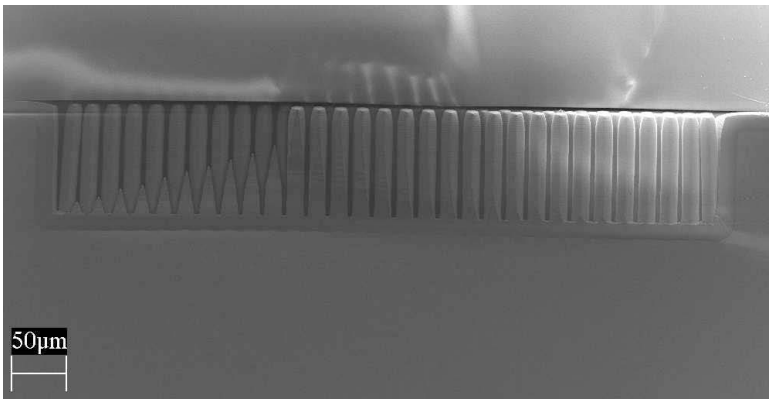

Figure 3.4: SEM image of the microchip. Cross section of the separation column with a glass lid. The pillars shown are 99 μm high and the width of the channels between the pillars is 3.7 μm. An approximately 15 μm thick silicon dioxide layer is present around the edges of the fluidic channel.

The gated injection scheme was utilized in all of the following experiments with the waste reservoir at the end of the separation column grounded through an amperometer to monitor current instabilities in the microchip.

All samples were diluted in the same mobile phase as the one used in the separations to keep the conductivityduring the separation constant. As the output of a PMT is actually a measure of the transmitted light and not the absorbance, the signal needed to be converted into absorbance units as described in Subsection 2.2.5.

In all of the following experiments UV-absorbance detection across the 1 mm detection cell is used. The detection cell on the current microchip was not as prone to clogging as the detection cell on the microchip presented in Chapter 2 because the channel width did not change in the detection cell. Much more light is also transmitted through the detection cell on the current microchip than on the microchip presented in Chapter 2. This is due to both the different materials of the waveguides and the different sizes of the waveguides. The cross sections of the waveguides are 6 μm by 24 μm for the oxynitride waveguides, but 99 μm by 22 μm for the silicon dioxide waveguides used in this chapter.

3.3 Results and discussions

3.3.1 Microfabrication

After fabrication, the channels in the separation column were measured and had a depth of 99 μm and a width of 3.7 μm between the pillars. Figure 3.4 shows a SEM image of the cross section of the separation column. Regular

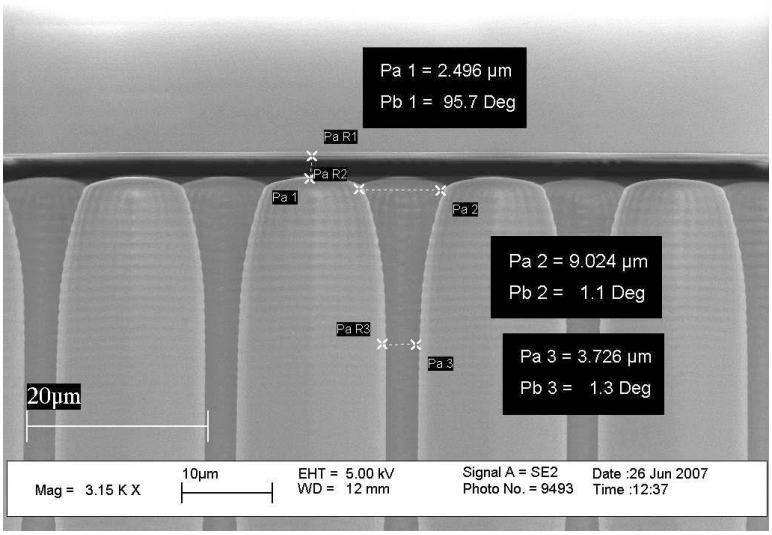

Figure 3.5: SEM image of a bonded chromatography column. Closeup of the top region. The gap from the top of the pillars to the glass lid is 2.5 μm. The channel width increases from 3.7 μm to 9.0 μm in the top 16 μm of the pillars.

channels on the microchip (i.e., outside the pillar array area) are 64 μm wide. The pillars are slightly rounded at the top after the oxidation step. As a result, the channels widen from 3.7 μm to 9 μm in the top 16 μm of the pillars. Figure 3.5 shows a close up of the of the top of the pillars where the widening of the pillars is clearly visible.

Another consequence of the oxidation is that the pillars are not bonded to the glass lid, as evidenced in Figure 3.5. This is because the volume expansion of the pillars is mostly lateral, while on the flat, unstructured chip surface the volume expansion is solely upwards. The spacing between the pillar tops and the top glass plate was measured to 2.5 μm. This value is less than the channel widths in the separation column so the spacing should not have detrimental effects on the mass transfer characteristics (C_m term of the van Deemter formalism) of the separation column, as the diffusion distance from the pillar tops to the lid is shorter than the diffusion distance in the channels between the pillars [77]. However, the spacing might increase the contribution to the A-term of the van Deemter equation as the separation column is not as homogenous as it would be with the lid completely bonded to the pillars.

The yield for adequately bonded chips was 80%. Figure 3.6 shows a photograph of a well bonded chip where the channel region is completely bonded but some non bonded regions are visible on the edge of the microchip. The 20% failure rate of the bonding is due to the relatively high surface

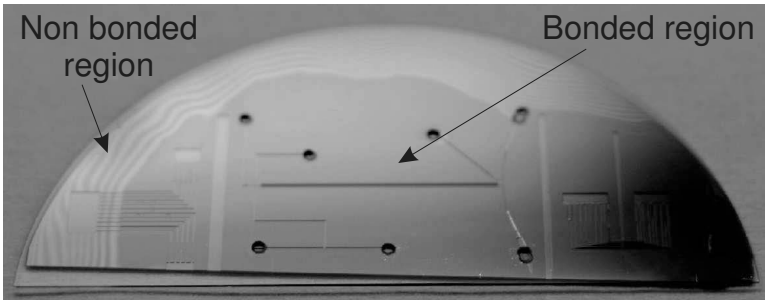

Figure 3.6: Photograph of a bonded microchip. The light region at the top edge of the chip is not bonded while the rest of the chip (darker region) is bonded. The region with the microfluidic channels is completely bonded so this microchip would be considered adequately bonded.

roughness of the oxidized surface, as compared to polished wafers. The root mean square surface roughness (R_q) of the oxidized silicon substrate was measured to be 0.4 nm using an atomic force microscope (AFM). Generally, a surface roughness of less than 0.5 nm is considered essential for good bonding [78, 79].

The waveguides are 22 μm wide and 99 μm deep and are completely oxidized [28]. Figure 3.7 shows an SEM image of the waveguides and the detection cell on the chip. The waveguides have the same spacing to the top of the glass lid as the pillars in the separation column. Air is therefore the cladding both on the top and sides of the waveguides, and the refractive index of the lid is not important for the waveguide function. However, there is no cladding at the bottom of the waveguide, which is why light can leak out into the oxidized silicon here. However, the amount of light lost through the bottom part of the waveguide has been shown not to add significantly to the propagation loss, which was previously measured to 0.8 dB/cm at 254 nm, while the coupling loss across the detection cell was 8 dB [28].

3.3.2 Microchip CEC separation

Thiourea was injected into the column to verify proper fluidic control in the microsystem and to optimize the injection settings using the high voltage power supply. Thiourea is uncharged and does not have affinity towards the stationary phase; consequently, it can be used as a marker to determine the electroosmotic mobility. This was done by measuring the arrival time of thiourea at the detector and using the length of the separation column to calculate the velocity of the sample plug. The velocity of the sample plug was then plotted as a function of the electric field strength, which was varied from 344 V/cm down to 153 V/cm. The electroosmotic mobility was then determined from the slope and was $4.52 \cdot 10^{-4}\ cm^2\ V^{-1}\ s^{-1}$ in 10 mM

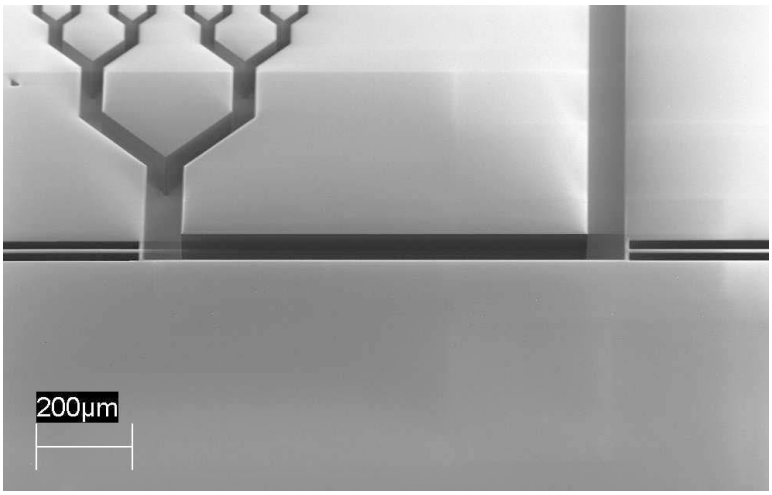

Figure 3.7: A SEM image with a tilted view of the 1 mm long U-shaped detection cell. The 22 μm wide waveguides extend from both sides of the detection cell.

tetraborate buffer at pH 9.2 with 10% acetonitrile as the mobile phase.

To verify successful surface modification and the presence of a stationary phase in the separation column, three neutral compounds were chosen for analysis: acetophenone, valerophenone and hexanophenone (see chemical structures in Figure 2.4). All three analytes have a similar molar absorptivity at 254 nm and their hydrophobicity increases as the length of their alkyl chains increases from one carbon for acetophenone to four carbons for valerophenone and five carbons for hexanophenone. Because the analytes do not carry any charge, they cannot be separated by electrophoresis. The interactions of the analytes with the octylsilane stationary phase, however, are different, resulting in different retention times and separation. Figure 3.8a-c shows separations of the three analytes with 50%, 30% and 10% acetonitrile in the mobile phase, respectively. In Figure 3.8a all the analytes co-elute as the high content of acetonitrile in the mobile phase decreases any interaction of the analytes with the stationary phase to a level where no separation is observed. In Figure 3.8b there is separation of the three analytes, but they are not baseline resolved. The final separation, Figure 3.8c, shows the three analytes all baseline resolved with 10% acetonitrile in the mobile phase. The last eluting peak is very broad compared to the other peaks because of the higher retention factor of the analyte and the resulting longer transit time through the system, allowing more time for longitudinal diffusion in the column. The first eluting peak, acetophenone, is not retained by the stationary phase (similarly to thiourea), and thus, the elution time of the first peak gives a measure of the electroosmotic mobility, allowing the retention factors, k, for the retained analytes to be calculated. All three

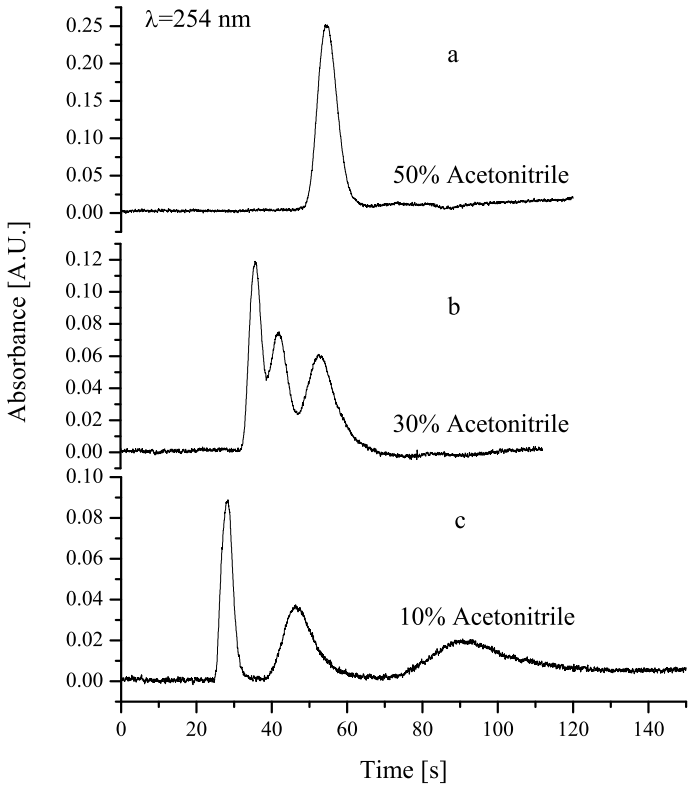

Figure 3.8: Microchip separation of acetophenone (100 $\mu g/mL$), valerophenone (200 $\mu g/mL$) and hexanophenone (300 $\mu g/mL$) with decreasing amounts of organic modifier in the mobile phase. (a) 50% acetonitrile, 10 mM tetraborate pH 9.2 mobile phase. (b) 30% acetonitrile, 10 mM tetraborate pH 9.2 mobile phase. (c) 10% acetonitrile, 10 mM tetraborate pH 9.2 mobile phase. Absorbance detection at 254 nm. E=306 V/cm. 1 s gated injection. Sampling frequency 50 Hz.

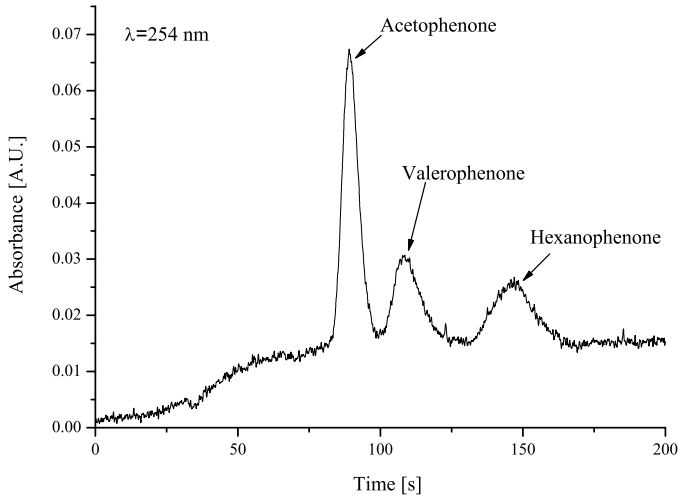

Figure 3.9: Optimized microchip separation of acetophenone (100 $\mu g/mL$), valerophenone (200 $\mu g/mL$) and hexanophenone (300 $\mu g/mL$). 30% acetonitrile, 10 mM tetraborate pH 9.2 mobile phase. Absorbance detection at 254 nm. E= 153 V/cm. 1 s gated injection. Sampling frequency 50 Hz. Plate heights are 30, 43 and 52 μm, respectively.

runs are performed using electric field strength of 306 V/cm in the separation column. However, the elution time for the unretained peak increases as the acetonitrile concentration increases. This is because the increased acetonitrile concentration in the mobile phase lowers the viscosity, dielectric constant in the mobile phase, and ζ-potential at the wall-mobile phase interface [80]. Combined, these effects reduce the electroosmotic mobility. The retention factors, k, for the retained analytes in the chromatograms in Figures 3.8a-c are as follows: for valerophenone: 0.18, and 0.63 for 30% and 10% acetonitrile, respectively; for hexanophenone: 0.48 and 2.20 for 30% and 10% acetonitrile, respectively. None of the analytes showed any retention when using mobile phase containing 50% acetonitrile.

The separation was further optimized at 30% acetonitrile concentration by altering the electric field strength in order to reduce the plate heights in the separation column. Figure 3.9 shows a chromatogram of an optimized separation. The electric field strength in the separation column is 153 V/cm for this separation. The plate heights in the separation are 30 μm for acetophenone, 42 μm for valerophenone and 53 μm for hexanophenone. These plate heights are rather high compared to what can be expected from microchip electrochromatography. There are two main contributions that increase the plate heights. First, the sample plug deforms because of a pres-

sure gradient on the boundary between the regular channels and the separation column. The pressure gradient arises because the total cross sectional area of the channels is larger in the separation column than in the regular channels [66]. To maintain the continuity condition and have a constant volumetric flow rate through the channels, the linear velocity at the open channel/column boundary has to change at both the inlet and the outlet of the column, leading to a pressure gradient that superimposes a parabolic flow profile on top of the flat electroosmotic flow profile, deforming the sample plug and leading to band broadening. This is not the consequence of an a priori incorrect design, but a result of the volume expansion caused by the oxidation step. This can be improved in future designs by optimizing the column design so that the cross-sectional area is more uniform throughout the channel network after the oxidation step.

The second contribution to band broadening is the non-uniformity of the channel widths in the separation column. As mentioned before, the channels between the pillars widen at the top, from 3.7 μm to 9.0 μm, and this leads to increased diffusion distances for analytes at the top of the channels. The increased diffusion distance will increase the C-term of the van Deemter equation as the C-term is proportional to the square of the channel width. The fact that a decrease in the linear velocity results in a reduction of the plate height also hints towards the possibility that we are in the region of the van Deemter plot where the C-term has a larger influence, i.e., at linear velocities larger than the optimal velocity. The difference in channel widths arises because of volume expansion of the pillars during thermal oxidation. The volume expansion is mostly lateral, but on the top there is vertical volume expansion. Oxidation from the top of the pillar proceeds until it reaches a region that is already oxidized from the sides. Therefore, the region near the edges of the pillars stops the vertical volume expansion relatively quickly, but the region in the middle continues until the pillar is oxidized all the way through. Since the oxide takes up more volume than the original silicon, this will result in varying channel widths over the height of the channels. The length of the top part of the pillars affected by this rounding is same as the width of the pillar, both of these being 16 μm in this case.

The present design was a compromise between conservative pillar dimensions to ensure durability, separation performance and ease of operation. It is intended to address these limitations in future designs of the microchip to increase the separation efficiency in the column by reducing the width of the pillars. This will stop the vertical volume expansion earlier, leading to a smaller region with widened channels due to rounding at the pillar tops. The widening itself will be reduced as well. The decreased pillar dimensions will furthermore reduce the spacing between the pillars and the lid as the vertical volume expansion under the pillars will be more complete with narrower pillars. Unfortunately, the current fabrication approach cannot

overcome these detrimental effects completely.

3.3.3 Additional considerations

The main problem with the operation of the microchips presented in this chapter is that it proved hard to get consistent injections of sample into the separation column. This problem presented itself with leakage of analyte into the separation column during pre-injection mode. This occurred around 5 min after applying high voltage to the microchip. Similar anomalies were described by Crabtree et al [81] in 2001. They attributed the problem to pressure effects such as siphoning due to difference in liquid levels in the reservoirs but mainly to flow driven by Laplace pressure that is generated at meniscus interfaces, in this case the liquid-air meniscus in the fluidic reservoirs.

The average velocity of the flow generated by siphoning in a 64 μm by 100 μm channel that is 2 cm long is approximately 0.1 mm/s for every mm of height difference between the reservoirs. When compared to the flow velocities in the separation column of around 1 mm/s this can be quite significant if the height difference is a couple of mm and could therefore interfere with the injections.

The volume in each of the reservoirs is the same (75 μL) at the start of each run and therefore the meniscus should have a similar contact angle with the glass surface in the reservoir and the opposing Laplace pressures from each of the reservoirs should cancel each other out. The volume in the reservoirs will change during runs due to the bulk flow in the chip. For a linear flow velocity of 1 mm/s the volumetric flow rate is approximately 6 nL/s. That means that in 300 seconds, nearly 2 μL of mobile phase will have gone from one reservoir to another. The volume change in the reservoir will also change the shape of the meniscus as the meniscus profile does not translate up and down the reservoir like in a capillary [81]. The differently shape menisci will lead to different Laplace pressures in the reservoirs and thus to pressure induced flow in the microchannels. Evaporation from the reservoirs will also change the volume, but the evaporation should be close to identical for all the reservoirs. The electrodes that dip into the reservoirs will also affect the shape of the menisci, depending on where they penetrate the meniscus.

This microchip is much more sensitive to pressure effects than microchips with shallow channels as the linear velocity of the pressure induced flow increases drastically as the channel dimensions are increased. As the depth of the microchannels is set by the diameter of the optical fiber it is not possible to make shallower channels to reduce the effects of pressure anomalies. The channels could be made narrower to increase the hydrodynamic resistance and thereby reduce the linear velocity induced by the pressure difference. Another possibility would be to have pillars in parts of the channels close

to the inlets. The pillars would serve both to increase the hydrodynamic resistance in the channel segment to prevent pressurized flow, but would also serve as particle filters to prevent particles in the solutions from clogging the separation column.

3.4 Conclusions and outlook

In this chapter, I have demonstrated the fabrication and operation of a silicon-based microchip for electrochromatography. The microchip has a standard cross injector and a separation column with microfabricated solid support structures for the stationary phase. UV- transparent waveguides are used to couple light through a 1 mm U-shaped detection cell, and integrated fiber couplers assist with alignment of optical fibers to the waveguides. The microchip was fabricated in a single etch step and then thermally oxidized to achieve electrical insulation of the channels and UV-transparency of the waveguides. A glass lid was thermally bonded to the substrate for sealing. It can be problematic to bond a glass lid to processed silicon wafers but the procedure we adapted from glass to glass bonding proved reliable and had an acceptable success rate. An octylsilane stationary phase was covalently attached to the silanol groups on the surfaces in the microchip.

Electrochromatography separations were performed on the chip where three neutral compounds were baseline separated and detected using UV-absorbance at 254 nm. An optimized separation of the compounds resulted in plate heights of 30-52 μm. Although these plate heights are an order of magnitude larger than what might be expected for microchip electrochromatography, it is likely that improved designs will reduce the plate heights. This can be achieved by optimizing the inlet/outlet structures to prevent a pressure gradient from forming and also by reducing the width of the pillars to achieve a more uniform channel width in the separation column after oxidation.

The optical part of the microchip is quite robust and both the waveguides, fiber couplers and detection cell have relatively few problems associated with them and could therefore be used unaltered in future designs. The main issues regarding new designs based on this microchip will therefore be to optimize the fluidic part of the chip. As mentioned before the inlet/outlet structures need to be optimized and could possibly be replaced by using different injection schemes, for example using pressurized injection schemes that are decoupled from the mobile phase flow as described by De Malsche et al [22]. The design must also try to minimize pressure driven flow in the channels, either by reducing the channel width or by introducing pillars in some channel segments to increase the flow resistance. However, the current project did not involve any further work on this microchip design.

Chapter 4

Polymer Microchips

The major part of this chapter is based on images and text from a research article entitled "Underivatized cyclic olefin copolymer as substrate material and stationary phase for capillary and microchip electrochromatography", submitted to Electrophoresis. Here, the article has been expanded to include more details and images in order to give a more in-depth view of the work and to explain some aspects of the work more thoroughly.

Furthermore, parts of this work were presented on a poster entitled "Nanoimprinted polymer microchips with solid support structures for capillary electrochromatography" presented at LabAutomation in Palm Springs, USA on January 28-31 2007, and on a poster entitled "Microchip Electrochromatography using Native Topas as the Stationary Phase" presented at Microscale BioSeparations in Berlin, Germany on March 11-13 2008.

4.1 Introduction

Capillary electrochromatography (CEC) is considered to be a hybrid between high performance liquid chromatography (HPLC) and capillary electrophoresis (CE). CEC utilizes the partitioning of solutes between a stationary and a mobile phase, just as in HPLC, while the flow (electroosmotic flow, EOF) is generated by an electric field, as in CE [26]. CEC was originally performed in packed columns, similar to those used for HPLC, where the stationary phase is derivatized onto small particles that are packed into fused silica capillaries. Problems with making homogenously packed beds inside a capillary or a microfluidic channel led to the development of several alternatives for preparing a homogenous stationary phase [25]. Some of the first microchip electrochromatography work focused on using an open channel approach where the stationary phase is covalently bonded to the surface of a shallow microfluidic channel, thus completely avoiding the problems associated with packing a homogenous bed altogether [27]. Porous polymer monolithic columns for electrochromatography have also been utilized

both in microchips and in capillaries [16, 73]. Monolithic columns are essentially a contiguous unit of macroporous material. The porous material is polymerized in-situ and the stationary phase functionality is introduced together with the monomers that form the monolith [82]. The porous network yields a very high surface area and the surface functionalities can be tailored to fit a specific separation problem by the appropriate choice of monomers and additives in the preparation cocktail. In 1998, Regnier and co-workers presented an alternative to the porous polymer monolith chromatography columns for microchips [19] that yields similar separation efficiencies [31]. Their design is based on microfabricating a highly ordered array of pillars separated by narrow channels. The pillars serve as support structures for a stationary phase and their size, shape and position can be controlled very precisely in the photolithography processes employed for fabrication.

There are several advantages with using microfabricated chromatography columns with solid support structures. The fabricated structures are inherently more regular than what is achievable with traditionally packed beds and their structure can be optimized to achieve close to ideal flow patterns thus reducing the effects of the A-term of the van Deemter formalism and resulting in higher separation efficiencies [26, 74]. Both simulations and experiments have confirmed that higher efficiencies can be achieved in ordered pillar array columns than in traditionally packed bed columns [29, 83].

Miniaturization has led to an increased interest in new materials for analytical devices. Polymers are an especially interesting group of substrates as they offer a wide variety of material properties and functionalities. One of the advantages that polymers have over the more traditional microchip substrates, such as glass and silicon, is that their microfabrication methods are very well suited both for rapid prototyping such as micromilling [50] and low cost mass production such as nanoimprint lithography [51] and injection molding [49, 53]. The possibility to mass produce microsystems in polymers makes inexpensive disposable analytical devices a feasible option.

One of the concerns with using polymers for CE and CEC are the relatively unknown surface properties of the polymers. The EOF is dependant on surface charges and while many polymers have no chemical moieties that are immediately expected to carry a charge [84], a significant EOF has been measured for a variety of common substrates for polymer microchips, such as poly(dimethylsiloxane) (PDMS) [85], poly(methylmethacrylate) (PMMA) [86], SU-8 [12] and cyclic olefin polymers (here: Zeonor) [84]. Several groups have reported on surface modifications for polymers that can be used to control the surface properties (including charge density), both to regulate EOF and to introduce other functionalities such as a retarding stationary phase [59, 62, 87]. The drawback of chemically modifying the polymer surface is that it increases the complexity of the fabrication process and can, in some cases, cause permanent clogging of small channels due to uncontrolled polymerization in the bulk liquid [76].

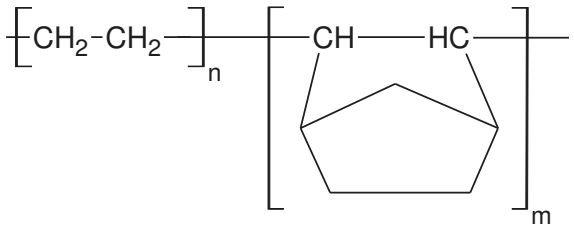

Figure 4.1: The chemical structure of Topas, a cyclic-olefin copolymer

Cyclic olefin copolymer (COC) is a relatively new class of thermoplastic polymers based on cyclic olefin monomers and ethene, see Figure 4.1. Due to the bulky cyclic olefin units, COCs generally have a high glass transition temperature, are optically clear and show low moisture absorption [88]. Several types of COCs are commercially available from different vendors under brand names such as Topas, Apel, Arton, Zeonor and Zeonex. Topas is a COC with many promising features for applications with microfabricated analytical devices. As it is a thermoplastic, it can be used in high throughput fabrication methods such as nanoimprint lithography and injection molding. Furthermore, Topas is chemically resistant to many organic solvents that are commonly used as additives in the mobile phase in CEC [60]. Finally, it is optically transparent into the UV range, making absorbance detection below 300 nm possible [61].

In this chapter, the use of unmodified Topas for reversed phase electrochromatography separations is presented, both in a capillary and on an imprinted microchip. This is possible by directly utilizing the hydrophobic surface of the polymer as a stationary phase for reversed phase separations. First, the use of a commercially available underivatized Topas capillary for open tubular CEC is presented. Then the fabrication of nanoimprinted microchips with solid support structures in the separation channel is described and a reversed phase separation in the underivatized microchip channels is demonstrated.

4.2 Experimental

4.2.1 Reagents

Acetonitrile, toluene, acetophenone, valerophenone, hexanophenone, thiourea, sodium carbonate, N,N-dimethylformamide, butylamine, hexylamine, octylamine, ethanolamine and Trizma base were obtained from Sigma-Aldrich (Schnelldorf, Germany). Sodium tetraborate decahydrate was obtained from Riedel-de Haën (Schnelldorf, Germany). Citric acid, acetic acid and hydrochloric acid were obtained from Merck (Darm-

stadt,Germany). Atto 532 N-hydroxysuccinimide (NHS) ester, 2-(N-morpholino)ethanesulfonic acid (MES), sodium dihydrogen phosphate and sodium hydroxide were obtained from Fluka (Schnelldorf, Germany). mrI T85-5.0 thermoplastic polymer was obtained from micro resist technology (Berlin, Germany). Topas 9506 was obtained from Ticona (Frankfurt, Germany).

4.2.2 Instrumentation

Experiments on capillaries were performed in a P/ACE-MDQ capillary electrophoresis system (Beckman Instruments Inc., Fullerton, CA, USA), using UV absorbance detection at 254 nm. Topas 8007 capillaries (ID/OD = 25/360 μm) were obtained from Paradigm Optics (Vancouver, WA, USA). The capillary was cut into 31 cm long pieces using a razor blade and inserted into a standard P/ACE capillary cartridge. Absorbance detection was performed through the capillary 21 cm downstream from the injection point. Microchip CEC measurements were carried out on a Microfluidic Tool Kit (Micralyne Inc., Alberta, Canada) with a 532 nm Nd-YAG laser module for laser induced fluorescence detection.

4.2.3 Microchip layout

Figure 4.2 shows the layout of the electrochromatography microchip. The microchip has a standard cross injector design. The separation column is based on a design first published by He et al. [19], where the column consists of an array of hexagonal pillars and repeated binary splitting structures at the inlet of the column to uniformly distribute the sample from a single inlet over the entire column width. The total cross sectional area of the channels in the inlet is kept constant by splitting each channel into two channels, each half as wide as the original channel. The separation column is 1.5 cm long. Each row of pillars in the separation column consists of 64 pillars that are 4 μm wide, 8 μm long and the channel between two adjacent pillars is 2 μm wide. Regular channels on the chip are 128 μm wide. All the channels on the microchip are 5 μm deep.

4.2.4 Microchip fabrication and preparation

Imprinting master fabrication

The imprinting master contains a negative pattern of the channel layout, so that after pressing the master into a softened polymer, the desired microfluidic structures remain in the polymer. Figure 4.3 shows a schematic of the fabrication process. The master was fabricated on a 4 inch silicon wafer with a thickness of 525 μm. The pattern from the mask was transferred to the wafer using UV-photolithography. Deep reactive ion etching

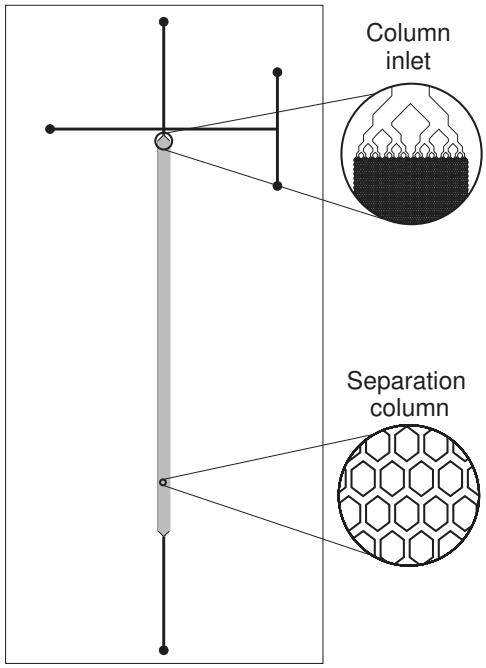

Figure 4.2: Electrochromatography microchip design. All lines represent microfluidic channels and the circles represent access holes in the microchip. Cylindrical glass reservoirs are glued on top of the access holes. The microchip has a standard cross injector and a side-T for solvent programming. All regular channels are 128 μm wide and 5 μm deep. A binary splitting structure distributes the flow from the main channel evenly over the whole column. The separation column is 1.5 cm long and consists of rows of hexagonal pillars with approximately 2 μm channels between the columns.

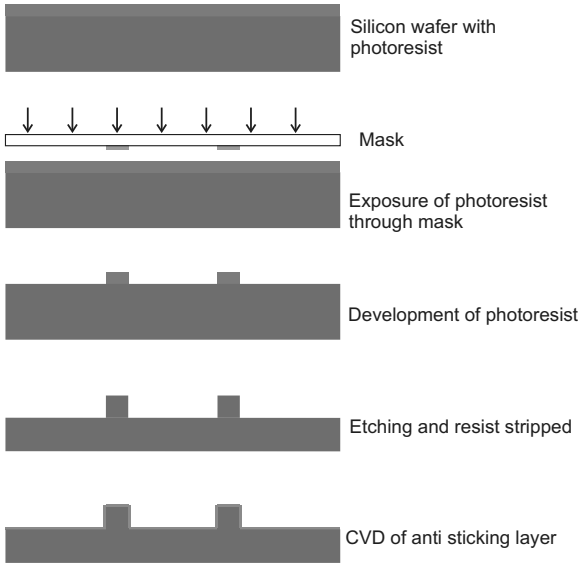

Figure 4.3: Schematic of the fabrication process for the imprint master. First, a layer of photoresist is spun onto the silicon substrate. UV-photolithography is used to transfer the pattern from a mask to the photoresist. The resist is then developed, removing all photoresist that was exposed to the UV-light. Deep reactive ion etching is used to etch all parts of the wafer not protected by the photoresist. The remaining photoresist is then removed and an anti sticking coating is covalently linked to the wafer surface using chemical vapor deposition (CVD).

was performed in an inductively coupled plasma etcher (Surface Technology Systems, Newport, UK) using the Bosch process, which consists of alternating etching and passivation steps. It was necessary to optimize the etching process to prevent a negative slope on the sidewalls, as that would result in structures on the master that are wider at the bottom than at the top, and, consequently, could cause problems with the release of the imprinted polymer structures from the master. We used an etching/passivation ratio of 1.18 that resulted in a positive slope on the sidewall of less than four degrees and, most importantly, facilitated an easy separation of the master from the imprinted chips. The total etching time was 128 seconds. After etching, the photoresist was stripped off in an acetone bath. Finally, an anti-sticking layer was applied to the surface of the master to further facilitate the release of the microchips after imprinting. The application of the anti-sticking layer was performed by chemical vapor deposition (CVD) in a MVD 100 Molecular Vapor Deposition System (Applied Microstructures Inc., San Jose, CA, USA). In the CVD, the stamp was first treated with oxygen plasma to remove any residual organic material off the surface. Then, 1H,1H,2H,2H-perfluorodecyltrichlorosilane reacted with the silanol groups on the stamp surface, forming a monolayer of fluorocarbon chains, which are covalently attached to the surface.

Microchip fabrication

The imprinting process was adapted from a process described by Bilenberg et al. [51]. Figure 4.4 shows a schematic of the imprinting process and subsequent processing steps. The imprinting substrate was prepared by spin coating mrI T85-5.0, dissolved Topas 8007, onto a 4 inch borofloat glass wafer, resulting in a seven μm thick layer of polymer on the wafer. The inverted silicon master and the polymer substrate were brought together and imprinted at 190°C with a force of 10 kN for 10 minutes in an EVG 520HE nanoimprinter (EV Group, St. Florian, Austria). Two flexible 0.5 mm graphite sheets were placed on either side of the two wafers to ensure homogenous imprinting. After cooling to 60°C the imprint force was released and the stamp and the substrate were manually separated. The substrate was then laminated with an adhesive film and a CO_2-laser was used to burn holes through the film at the end of the microfluidic channels. Access holes were subsequently powder blasted through the glass substrate, using the adhesive film as a mask. The adhesive film was finally removed and the wafer rinsed thoroughly with water. A 4 inch borosilicate wafer spin-coated with a 300 nm thick layer of Topas 9506 was used to seal the microchip. The substrate and the lid were brought together, heated to 70°C and a force of 10 kN was applied for 10 minutes using an EVG 520HE nanoimprinter. This bonding procedure does not require a plasma treatment [89] and hence does not affect the surface properties of the substrate material. The procedure

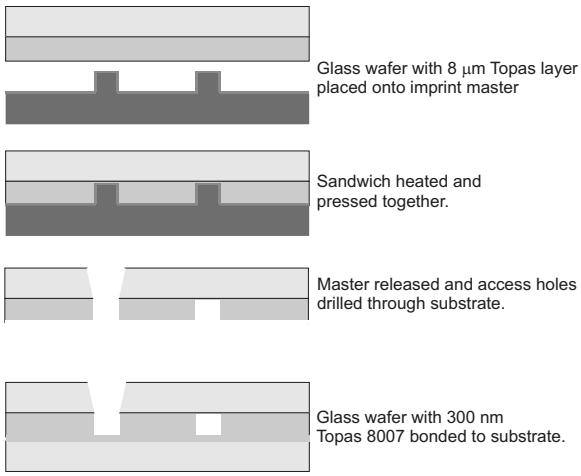

Figure 4.4: Schematic of the fabrication process for the polymer microchip. A 8 μm thick layer of Topas 8007 is spin coated onto a borosilicate wafer. The polymer substrate and the imprint master are then brought together, the sandwich is heated to 190°C and pressed together. After cooling the imprinted substrate is separated from the master and access holes are sandblasted through the substrate. The substrate is finally sealed with a borosilicate wafer with a 300 nm thick layer of Topas 9506. The substrate and the lid are pressed together and heated to 70°C for bonding

for the imprinting is described in more detail in Appendix D.

4.2.5 Experimental setup

A commercial system, the Microfluidic Tool Kit, was used for microchip operation and detection. The experimental setup is shown schematically in Figure 4.5. Detection is achieved using an inverted epi-fluorescence setup. A 4 mW frequency doubled Nd-YAG laser with a wavelength of 532 nm is used for excitation. The laser beam goes through a dichroic beamsplitter and a microsocpe objective with 40 fold magnification and a numerical aperture of 0.55 that focuses the beam onto a 10-20 μm diameter spot in the microchannel. The emitted light is collected by the same microscope objective and reflected by the dichroic mirror through 2 filters, one longpass filter and one bandpass filter. Both filters are designed to filter the intense laser light away from the relatively weak fluorescence signal. Only approximately $6 \cdot 10^{-7}$% of the laser light will be transmitted through the two filters while the major part of the fluorescent signal collected by the microscope objective will be transmitted through the two filters. A PMT is used to measure the fluorescence intensity. The output from the PMT is collected by the Microfluidic Toolkit module that is connected to a computer. The module also serves as a high voltage power supply. Software supplied with

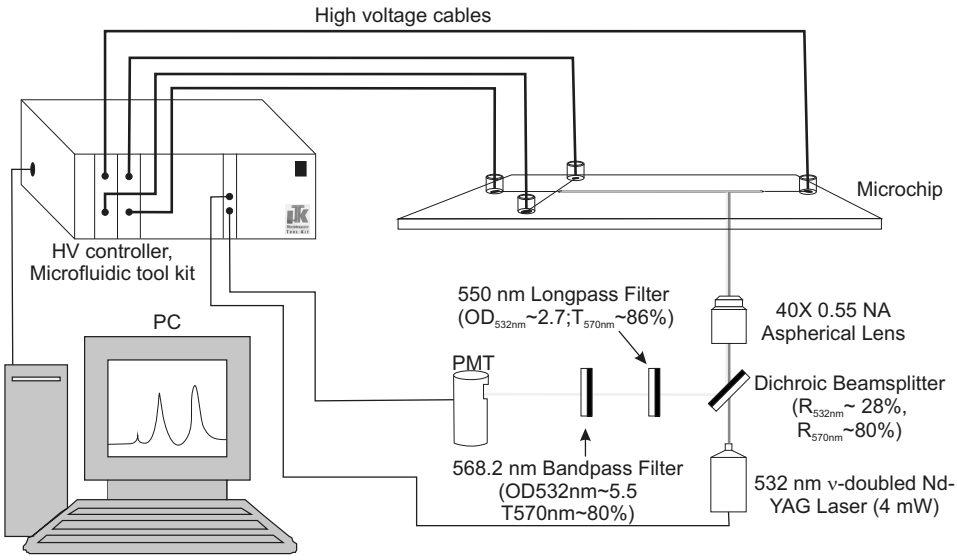

Figure 4.5: Epi-fluorescent setup for microchip LIF measurements using a Microfluidic Toolkit. A Nd-YAG laser with a wavelength of 532 nm is used for excitation (green line). The laser beam is focused onto the microchip and the emitted light is collected by the same microscope objective (yellow lines). The excitation light is filtered from the fluorescent light by one longpass filter and one bandpass filter. The fluorescent signal is measured by a PMT. The Microfluidic Toolkit module also supplies the voltages that are applied to the reservoirs. A PC is used to control the system and to record data.

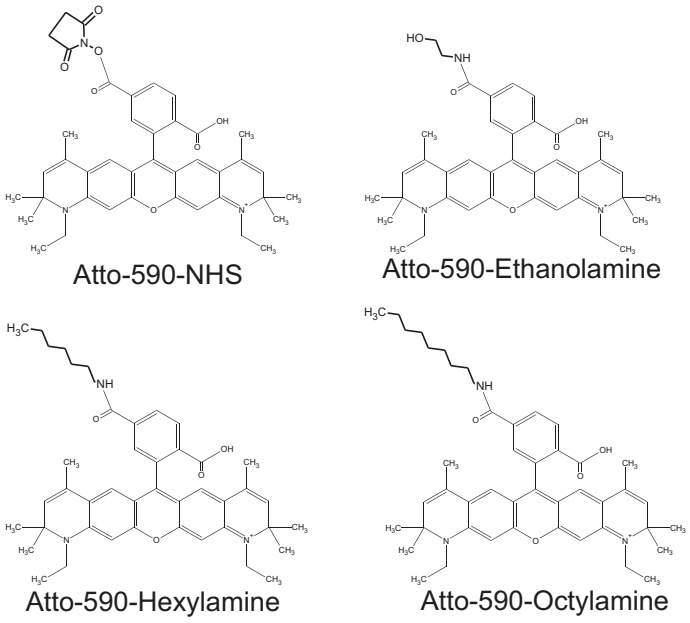

Figure 4.6: Chemical structure of Atto-590-NHS and Atto-590 labeled ehtanolamine, hexylamine and octylamine. (The structures for Atto-532 are not yet publicly available due to patent issues.)

the system is used to control the applied voltages, laser and PMT settings as well as for collecting data.

4.2.6 Fluorescent labeling of amines

To detect analytes on the microchip it is necessary for the fluorophore to have good excitation overlap with the laser wavelength of 532 nm. To prove the separation characteristics of the native surface, the analytes should furthermore preferably not be separated by electrophoresis, only by reversed phase chromatography. The Atto-532 fluorophore with an N-hydroxysuccinimide (NHS)-ester for coupling to amines was chosen. The NHS-ester is very reactive towards amines where the NHS serves as a good leaving group to facilitate the formation of an amide bond between a carboxylic group and the amine. Four amines, ethanolamine, butylamine, hexylamine and octylamine, were labeled. The hydrophobicity of the amines increases as the length of the alkyl chain increases. Figure 4.6 shows the structure of 3 Atto-590 labeled amines and an Atto-590-NHS reactive label. Atto-590 and Atto-532 are both rhodamine based dyes and therefore similar in structure but the structure of Atto-532 is not yet publicly available due to patent issues. The labeling reaction was performed by mixing 1.0-2.5 mM amine

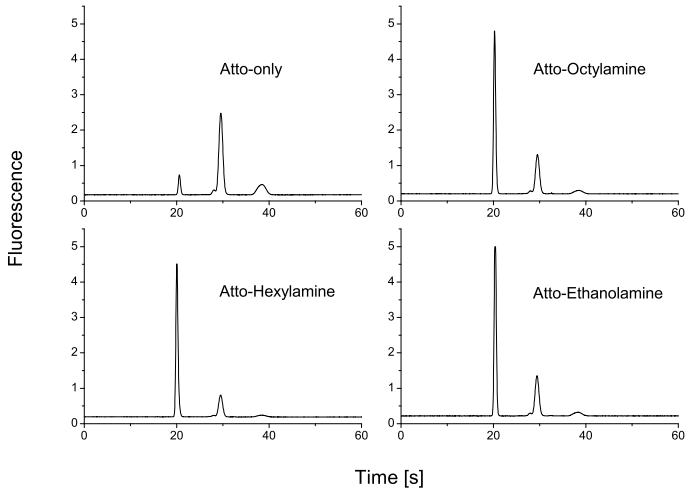

Figure 4.7: Microchip CE runs of three labeling reactions for different amines(ethanolamine, hexylamine and butylamine, 2.0 μM each) labeled with Atto-532-NHS (1:1 ratio of reagents), as well as one CE run with Atto-532-NHS only (2.0 μM). Running buffer: 10 mM tetraborate at pH 9.2. 3.0 cm separation channel. Detection point 2.0 cm downstream of injection cross. Fluorescence detection with excitation at 532 nm and detection at 568 nm. Electric field strength 633 V/cm. Gated injection with 0.2 s injection time.

and 1.0 mM Atto 532-NHS in 100 mM carbonate buffer at pH 8 and 40% dimethylformamide. The reactions were allowed to proceed overnight at room temperature. The labeled products have a maximum concentration of 1.0 mM given by the limiting concentration of the Atto-532 label.

Microchip CE and MEKC to evaluate labeling

To verify that the labeling worked, the labeled amines were injected and separated by CE on a standard glass microchip. Figure 4.7 shows four microchip CE runs, three from labeling reactions for different amines as well as one run with Atto-532-NHS only (labeling reaction with a blank) where all runs were performed at identical conditions. All of the labeled amines in Figure 4.7 have the same elution time at around 20 s. This shows that the labeled amines are not separated by capillary electrophoresis. The unreacted Atto-532-NHS elutes at around 30 s and all of the labeling reactions in Figure 4.7 had a significant peak for the unreacted label at 30 s. These labeling reactions were performed with a reagent ratio of 1:1. To get rid of the unreacted label, new labeling reactions were prepared where the reagent ratio was 2.5:1 (amine:Atto-532-NHS) and these were used in subsequent

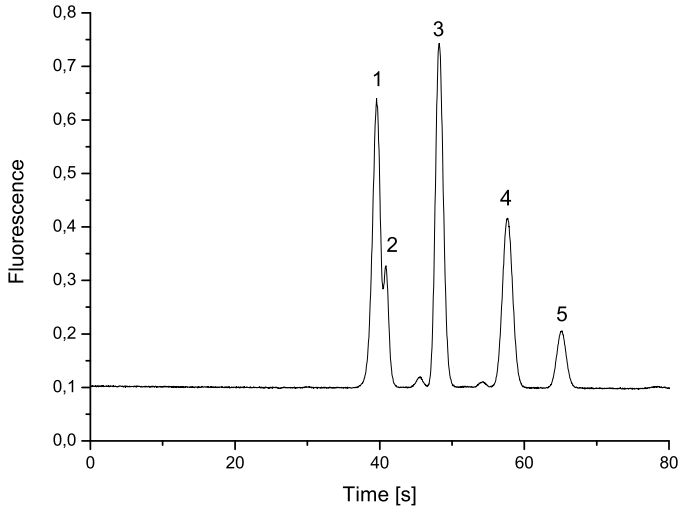

Figure 4.8: MEKC separation of four amines labeled with Atto-532. The components are 1) non-reactive Atto-532 label, 2) Atto-532-ethanolamine, 3)Atto-532-butylamine, 4) Atto-532-hexylamine, 5) Atto-532-octylamine, (1.25 μM each). Mobile phase: 10 mM tetraborate buffer at pH 9.2, 25 mM SDS and 35% acetonitrile. 3.0 cm long separation channel. Detection point 2.0 cm downstream of injection cross. Fluorescence detection with excitation at 532 nm and detection at 568 nm. Electric field strength 633 V/cm. Gated injection with 0.2 s injection time.

experiments. A small peak of non-reactive label (that is presumably Atto-532 label without an NHS group) can be seen at around 20 s in the run where only Atto-532-NHS was present. The elution time of the non-reactive peak coincided with the elution times of the labeled amines. Based on the product information, only 80% of the fluorescent dye is guaranteed to be reactive towards amines and the remaining non-reactive dye elutes together with the labeled amines.

A mixture of four labeled amines was then separated by microchip micellar electrokinetic chromatography (MEKC), using a 10 mM tetraborate buffer at pH 9.2 containing 25 mM SDS and varying amounts of acetonitrile. At a sufficiently low acetonitrile concentration the labeled amines could easily be separated based on the hydrophobicity of the respective amine, but at higher acetonitrile concentrations they all co-eluted. Figure 4.8 shows an MEKC separation of four amines in a mobile phase containing 35% acetonitrile where all four amines are baseline separated. The first peak is split and consists of both labeled ethanolamine and the non-reactive Atto-532. This analyte system has been shown to be suitable for demonstrating reversed

phase interactions, as the labeled amines are not separated by regular CE but can be separated by MEKC based on the hydrophobicity of the amines.

4.2.7 Microchip CEC measurements

To fill the microchips with a mobile phase it was necessary to start priming the microchip with a liquid that was less viscous than water as it was very hard to remove trapped air bubbles from the pillar region. 96% ethanol was used to initially fill the microchip and then vacuum was applied to the reservoirs to completely fill the chip and remove all bubbles. In some cases where much air was trapped in the separation column the whole microchip was placed in a vacuum chamber and put through a two to three cycles where vacuum was applied for a couple of minutes and then released. The air bubbles in the separation column got smaller with each cycle, eventually dissipating into the ethanol.

It proved difficult to get reliable electrokinetic injections into the polymer microchip. Therefore hydrodynamic pinched injections were utilized. This was performed by filling the two reservoirs in the side-T (see Figure 4.2) with sample and then applying vacuum to the reservoir on the other side of the injection cross to draw the sample across the injection cross. Voltage was then applied from the top reservoir down to the bottom reservoir, driving the mobile phase through the separation channel and carrying along a sample plug defined by the dimensions of the injection cross.

All samples were diluted in the same mobile phase as the one used in the separations in an attempt to keep the conductivity in the separation column constant.

4.3 Results and discussions

4.3.1 Electrochromatography in underivatized Topas capillaries

The electroosmotic mobility in an underivatized Topas capillary was measured by injecting thiourea, a neutral non-retained analyte, into the capillary and measuring the arrival time at the detection point. The electroosmotic mobility was determined for eight pH values in six commonly used buffers (from pH 3 to 10), all at 10 mM. All runs were performed at an electric field strength of 242 V/cm. Figure 4.9 shows the electroosmotic mobility in the native Topas capillary at different pH values. The magnitude of the electroosmotic mobility for Topas is similar to those reported recently for SU-8 and glass, which were measured to $4.8 \cdot 10^{-4}\ cm^2\ V^{-1}\ s^{-1}$ (SU-8) and $5.7 \cdot 10^{-4}\ cm^2\ V^{-1}\ s^{-1}$ (glass) in 20 mM sodium borate at pH 9.0 [12] compared to our measurements of $4.2 \cdot 10^{-4}\ cm^2\ V^{-1}\ s^{-1}$ in 10 mM tris at pH 8.0 and $3.6 \cdot 10^{-4}\ cm^2\ V^{-1}\ s^{-1}$ in 10 mM sodium borate at pH 9.2.

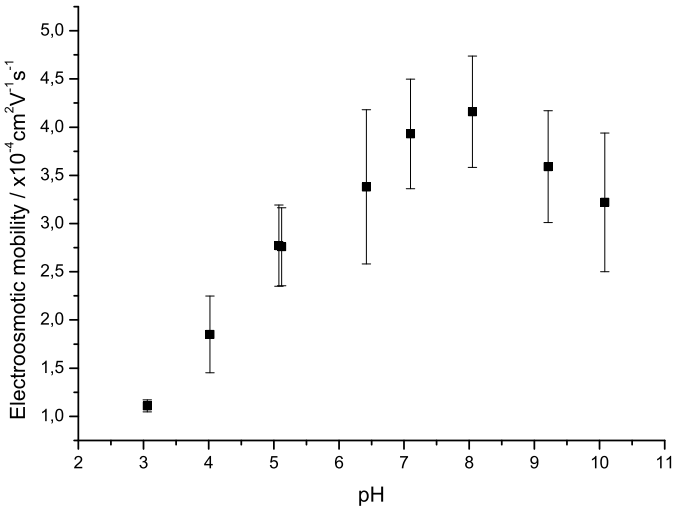

Figure 4.9: Electroosmotic mobility in Topas 8007 capillary. The buffers used are: Tetraborate at pH 10.1 and 9.2; Tris at pH 8.1; Phosphate at pH 7.1; MES at pH 6.4; Acetate at pH 5.1; Citrate at pH 5.1, 4.0 and 3.1. All buffer concentration are 10 mM.

All values correspond to a practical electroosmotic velocity for performing CE and CEC. The significant cathodic EOF measured over almost the entire pH range indicates the presence of a negative charge on the surface. The diminishing EOF with decreasing pH hints to the possibility that the charged surface groups have acid-base properties. Extrapolation of the curve in Figure 4.9 suggests that the isoelectric point (pI) of the surface, where the electroosmotic mobility is zero, lies close to pH 2. This pI value is similar to those measured for other polymers [12, 90]. However, the chemical structure of Topas, as shown in Figure 4.1, only contains saturated hydrocarbons and does not, immediately, feature chemical moieties with any acid-base properties. The source of the surface charge has been thought to come from contaminants or additives in the polymer, but recently it was suggested that enhanced autolysis of water at hydrophobic surfaces and the preferential adsorption of hydroxide ions on the surface cause the charged polymer surfaces [90]. This would account for negative surface charges on polymer materials and hence the presence of a cathodic EOF on most polymers.

To verify a reversed phase interaction between analytes and the native, underivatized Topas surface three neutral compounds were tested: acetophenone, valerophenone and hexanophenone. Figure 4.10 shows two electrochromatograms of a mixture of these three alkylphenones in the native Topas capillary. The separations were performed with 30% and 50% ace-

tonitrile in the mobile phase, respectively, in both cases using a 10 mM tetraborate buffer at pH 9.2. At 50% acetonitrile all the components co-elute. At 30% acetonitrile there are three peaks that are baseline resolved, and the elution order is established to acetophenone, valerophenone and hexanophenone, as would be expected by a reversed phase separation. The plate heights for the peaks are 5.3, 7.0 and 12.7 μm for acetophenone, valerophenone and hexanophenone, respectively. The first peak, acetophenone, is unretained by the stationary phase. The retention factors for the other components are 0.03 and 0.08 for valerophenone and hexanophenone, respectively. These retention factors are quite small compared to what is achievable with chemically bonded phases such as octyl or octadecyl chains. This is most likely due to the fact that the type of interaction with the native Topas surface is not like the partitioning type interaction normally found with bonded phases [20]. Instead, it is probably mainly based on a purely adsorptive mechanism. Also, octyl and octadecyl stationary phases are more hydrophobic than the Topas surface (as measured via the contact angle) and interact therefore more strongly with hydrophobic analytes. Finally, in the open tubular format, only very little surface per volume is available for interaction. The retention factor can be increased by using microfabricated structures in a separation microchip to increase the surface area in the separation column, as described in the following sections. Such structures would also serve to reduce the diffusion distances within the separation column making mass transfer between the mobile and the stationary phase faster. Thus, separations can be achieved at higher linear velocities without any negative impact from mass transfer, and, hence, in shorter time.

4.3.2 Microchip fabrication

Figure 4.11 shows a SEM image of the inlet structure on the fabricated imprint master. The height of the structures was measured to 5.1 μm. The angle between the structures and the wafer is slightly above 90 degrees to assure a good release of the imprinted chip. If the angle is below 90 degrees it becomes impossible to release the imprinted pillars as they get wedged in the imprint master and are ripped off as the master and the substrate are pulled apart. Figure 4.12 shows two SEM images of failed imprint, one where the pillars were completely ripped off and the other where a part of the pillars was ripped off.

Figure 4.13 shows SEM images of the pillar region in the imprinted polymer structures where the imprinting was succesful. The top image shows a region of the pillar array and the sidewall in the separation column. The pillar structures are reproducibly transferred from the imprint master into the polymer. Visual inspection of the separation column in a microscope revealed that in a 15 mm long column, which contains approximately 120,000 pillars, less than 20 pillars were ripped off due to stiction to the stamp.

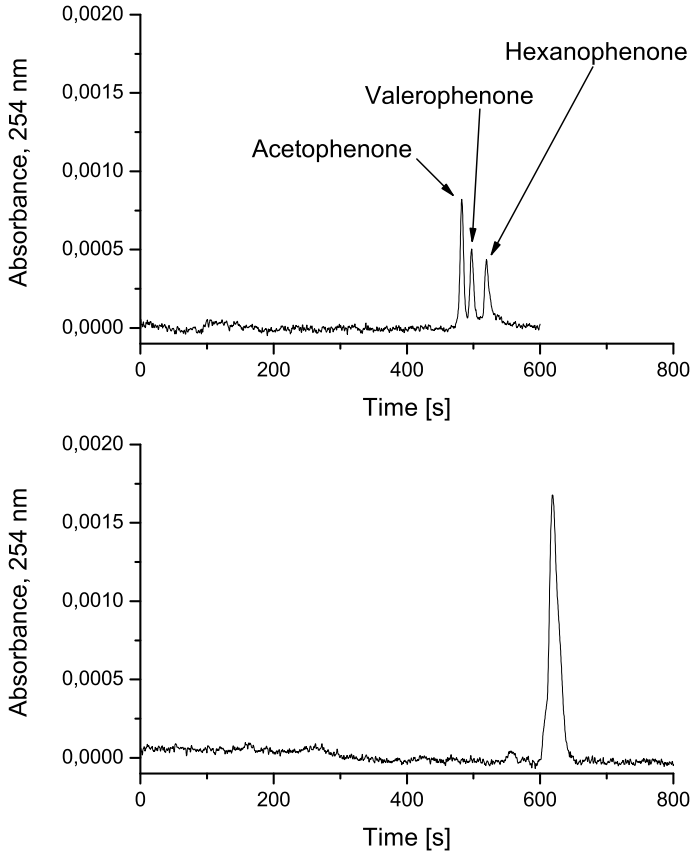

Figure 4.10: CEC separations of acetophenone, valerophenone and hexanophenone (500 $\mu g/mL$ each) in an underivatized Topas 8007 capillary with ID=25 μm. Top: 30% acetonitrile. Bottom: 50% acetonitrile. Both runs were performed at identical settings, 10 mM tetraborate buffer at pH 9.2, E=242 V/cm, injection: 4 s at 30 mbar, UV-absorbance detection at 254 nm. The baseline in both chromatograms has been adjusted to compensate for a drift in the light source.

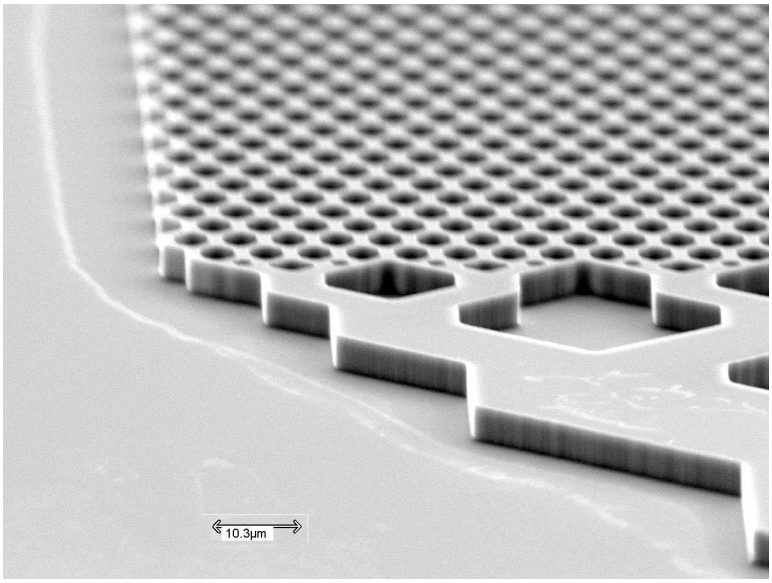

Figure 4.11: Scanning electron micrograph of the inlet and the separation column on the silicon imprint master. The structures are 5.1 μm high.

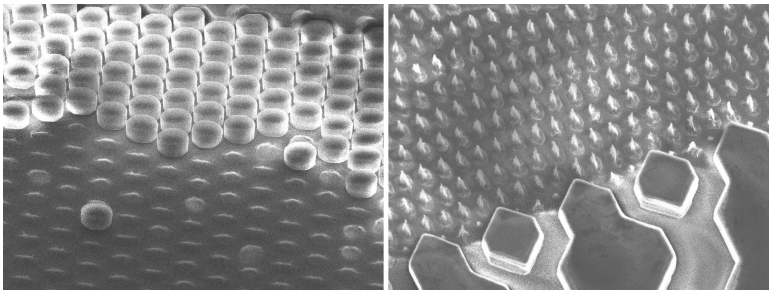

Figure 4.12: SEM image of imprinted columns where pillars have been ripped off due to stiction to the imprint master. Left image shows a partially ripped off region while the right image shows a region where the pillars have been completely ripped off.

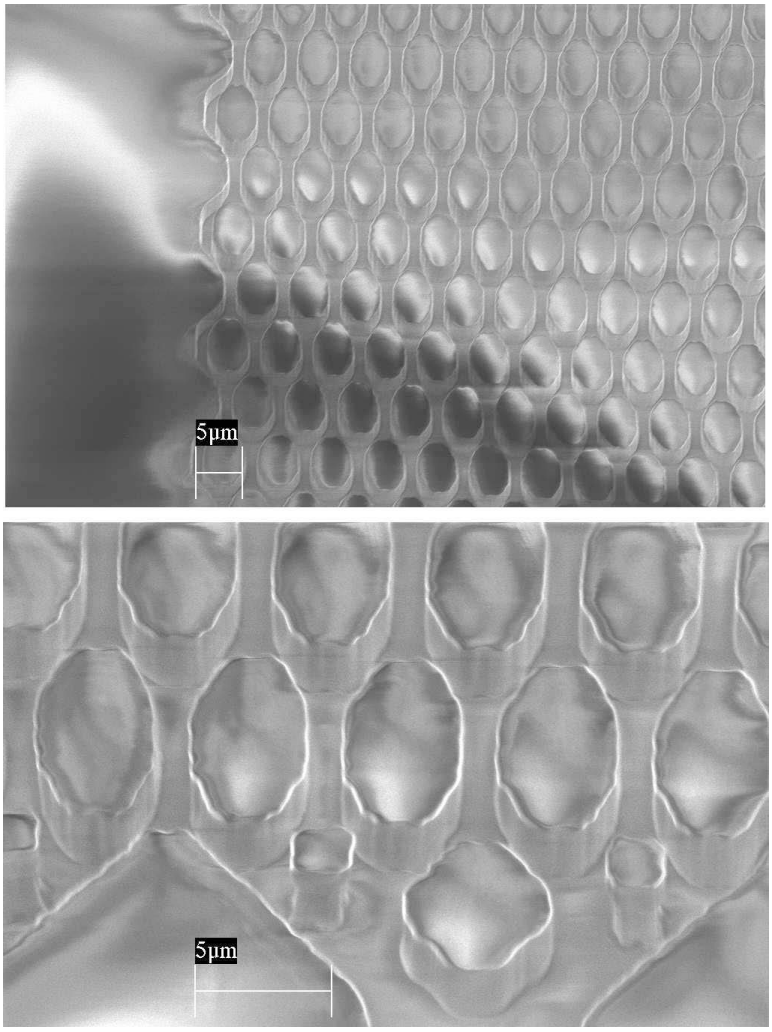

Figure 4.13: SEM images of imprinted structures in the separation column. Top: Tilted view of imprinted pillars close to the sidewall. Bottom: Tilted view of the end of the inlet splitting structure and the start of the separation column.

Figure 4.13 also shows that the pillars have lost some of the smaller features during the imprint process, as the corners of the pillars are rounded instead of being sharp. This results in pillars that look more elliptical than hexagonal. The bottom part of Figure 4.13 shows a more detailed view of the inlet structure of the separation column. The imprinted channel depth was measured to 4.9 μm using a profilometer. The pillars in the separation column measure 4.4 μm in width and the channels between the pillars measure 1.6 μm in width. The column was designed to have pillars of 4.0 μm and channels of 2.0 μm so the measurements indicate that there has been some underetching of the imprint master. This underetching also contributes to the rounding of the sharp corners. The smallest features that are imprinted are the pillars at the end of the inlet structure, right before the separation column. These small pillars measure 2.9 μm in width and are reproducibly imprinted, indicating that the dimensions of the pillars in the separation column could be reduced even further. The outlines of all the imprinted structures in Figure 4.13 do not appear perfectly straight. It is not clear where in the fabrication process these deviations from the mask design originate. However, this should not have a drastic effect on the separation performance as the dimensions of these features are much smaller than the channel dimensions.

4.3.3 Electrochromatography in an underivatized Topas microchip

Before operation, the microchip was filled with a 0.1 M sodium hydroxide solution and allowed to stand for four hours to remove any impurities in the channel and to condition the channel surface. The sample was introduced into the separation channel using a hydrodynamic pinched injection, where vacuum was used to draw the sample across the injection cross and then a potential was applied from the top reservoir, containing the mobile phase, to the bottom reservoir. The length of the sample plug using this pinched injection was defined by the injection cross geometry and therefore limited to a length of 128 μm and did not add significantly to the plate height of the peaks [41]. As the substrate is clear the detection point could be placed anywhere along the channels, either in an open region or inside the separation column. As the inlet and outlet flow distribution and collection structures always constitute a source of possible band broadening we chose to place the detection point within the separation column, 11 mm downstream from the injection cross. For detection, a 532 nm laser was used for excitation and the fluorescence intensity at 568 nm was monitored. The reaction mixtures of the labeled amines were diluted in a mobile phase containing 30% acetonitrile and 10 mM tetraborate at pH 9.2. The final concentration of the analyte mixture was 3.0 μM for Atto-532-octylamine, 2.5 μM for Atto-532-hexylamine and 1.2 μM for Atto-532-ethanolamine.

Figure 4.14 shows two chromatograms for the separations of the analyte mixture. The chromatogram in Figure 4.14a shows a separation of the three analytes in a mobile phase containing 20% acetonitrile and 10 mM tetraborate buffer at pH 9.2. The three analytes are separated and elute in the order of increasing hydrophobicity of the amines, as predicted by a reversed phase interaction between the analyte and the stationary phase. The first peak in the chromatogram of Figure 4.14a is a doublet, consisting of the peak for Atto-532-ethanolamine and the non-reactive dye. The peaks are very sharp with the peak for the non-reactive dye having a plate height of 0.14 μm and the peak for ethanolamine 0.55 μm. Such low plate heights should not be achievable, not even at very low values for the retention factor, as longitudinal diffusion alone already gives a larger contribution to the plate height. The reason for the very low observed plate heights is that there is a difference in the pH value of the sample plug and that of the mobile phase (background electrolyte, BGE). The sample has a pH of 8.0 while the BGE has a pH of 9.2. Because of the difference in pH the negatively charged dye has a slightly different charge in the BGE than in the sample plug and therefore also a different electrophoretic mobility. The charged analytes experience a stacking effect due to a dynamic pH junction, where anions in a sample plug with a lower pH value than that of the BGE focus at a front of hydroxide ions sweeping through the sample plug [91, 92]. The effect is less pronounced for ethanolamine as it is slightly retained and broadens due to interaction with the stationary phase. The remaining two peaks, enlarged on the inset of Figure 4.14a, have plate heights of 3.4 μm for Atto-532-hexylamine and 22 μm for Atto-532-octylamine. The stacking effect is not noticeable for the last two peaks as their retention causes sufficient band broadening to overshadow the stacking. Tailing is observed for both retained peaks, most probably due to non specific adsorption of the analytes to the polymer surface. The retention factors for the retained peaks are 0.38 for Atto-532-hexylamine and 1.5 for Atto-532-octylamine. These retention factors are an order of magnitude larger that those found for the Topas capillary, but these values cannot be compared directly as a different set of analytes was used in the two experiments. Figure 4.14b shows a separation of the same analyte mixture with 50% acetonitrile in the mobile phase. Only two peaks are present in this case; first, a very sharp unretained peak containing the non-reactive dye, Atto-532-ethanolamine and Atto-532-hexylamine. The second peak can be assigned to Atto-532-octylamine and is almost baseline separated from the first peak. The plate height is 0.17 μm for the stacked, unretained peak and 5.6 μm for the slightly retained Atto-532-octylamine peak. Again, tailing is observed on the retained peak. These separations clearly demonstrate the reversed phase type interaction between the analytes and the native Topas separation column. While these experiments demonstrate the feasibility of directly using a native Topas surface for reversed phase chromatographic separation, the carbon loading of the accessible surface is

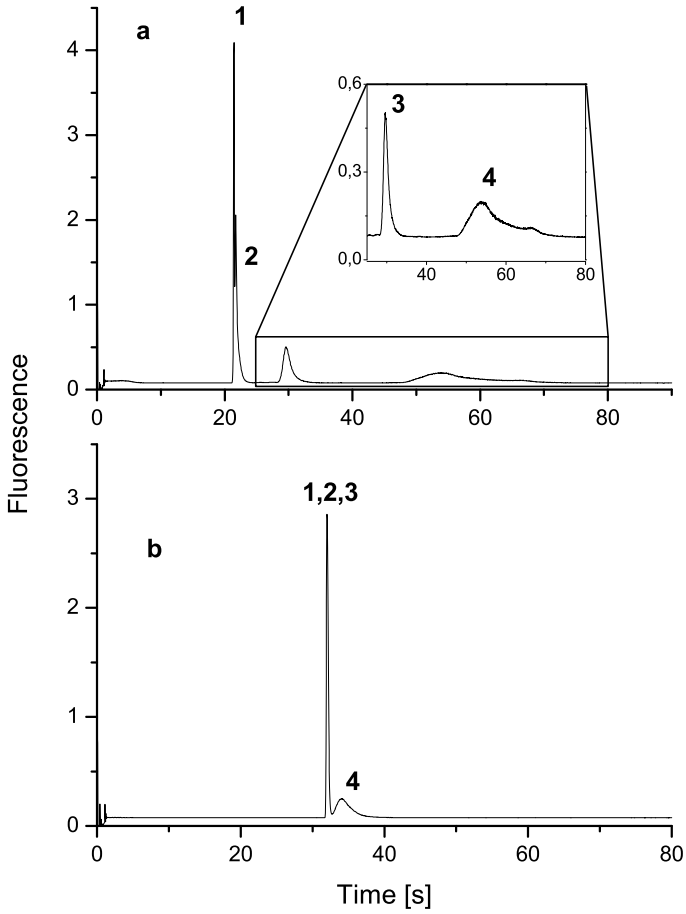

Figure 4.14: Electrochtomatography separations on an underivitized Topas microchip. Analytes: 1) non-reactive Atto-532 label, 2) Atto-532-ethanolamine (1.2 μM), 3) Atto-532-hexylamine (2.5 μM), 4) Atto-532-octylamine (3.0 μM). Mobile phase: 10 mM tetraborate buffer at pH 9.2 containing a) 20% acetonitrile and b) 50% acetonitrile. Excitation at 532 nm and detection at 568 nm. Electric field strength 172 V/cm. Pinched injection.

probably too low. It is very likely that better separations could be achieved by attaching a stationary phase layer (e.g., octyl or octadecyl functionality) to increase the volume of the stationary phase and the amount of carbon in the separation column. We performed first tests using an anthraquinone-based surface grafting approach to introduce a stationary phase layer in the Topas capillary, but the initial results gave in fact a less hydrophobic surface (as determined by the contact angle) and a worse separation than the native, underivatized Topas. This was most likely due to insufficient reaction yields and a too low coverage of stationary phase on the polymer surface. More work on a simple and reliable surface modification procedure is needed to achieve better separations and, at the same time, a more stable electroosmotic flow.

4.3.4 Additional considerations

The main problem during operation of these microchips was that the bonding did not seem to be good enough. The microchips would last for a couple of hours where they could be used but then the current between the reservoirs grew by an order of magnitude, implying that there was a short circuit between the reservoirs. After that it was impossible to achieve flow control in the microchip when using electrokinetic flow solely. It is not completely clear if the problem is the bonding between the two Topas layers or if the Topas is delaminating from the glass wafer. Either one would result in a short circuit when the regions between two reservoirs would be delaminated. Other groups at DTU Nanotech using similar microfluidic device have not experienced this problem, but they do not use solvents or high voltage for their microchip operation. The problem could thus be that either the solvents (acetonitrile) cause the delamination or that the heat generated by the current in the microchannels causes localized melting of the polymer that results in the delamination. It is therefore necessary to optimize the bonding procedure, both by exploring the adhesion between the Topas layer and the borosilicate wafer and also by improving the bonding between the two Topas layers. The bonding could possibly be optimized by using either solvent assisted bonding [93] or by plasma treating the substrate before bonding [89]. Also, if the delamination is due to localized melting at the channel surface, it might be feasible to use Topas with a higher melting point.

4.4 Conclusions and outlook

In this chapter, the use of underivatized Topas as a stationary phase for reversed phase electrochromatography separations was presented, both in a capillary and on a microchip. Topas is considered a very promising substrate for use in microfluidic systems, especially because of its optical properties and chemical compatibility. A significant cathodic electroosmotic flow above

a pH value of 3 was measured in the capillary, a clear indication of a negative surface charge. Capillary electrochromatography separation of three neutral compounds using a native Topas capillary was demonstrated, where the hydrophobic compounds are interacting with the hydrophobic polymer chains on the capillary surface causing retention. The elution order of the compounds verifies that it is a reversed phase separation. Furthermore, the fabrication of a nanoimprinted Topas microchip for electrochromatography was presented where the separation column consists of an array of hexagonal pillars that serve to increase the surface area in the column. A reversed phase electrochromatographic separation of three fluorescently labeled amines was successfully demonstrated on the microchip with plate heights for retained compounds ranging from 3.4 μm to 22 μm.

Future studies on the Topas electrochromatography microchips need first and foremost to be directed towards improving the lifetime of the microchips by optimizing the bonding procedure and preventing delamination.

Surface modifications also need to be explored further, both for getting a more reliable EOF so that injections can be performed using electrokinetic flow and also to get a stationary phase that has properties that are better defined. The underivatized polymer surface only provides a specific chromatographic interaction that is determined by the chemical structure of the polymer, while surface modifications would allow different stationary phases to be introduced, depending on the analysis that is to be performed.

It would also be interesting to add integrated waveguides to the microchips to allow for absorbance detection or simply to couple excitation light to a detection point. The waveguides can be fabricated by nanoimprint lithography in the same step as the microfluidic channels [51] so there is no added complexity in the fabrication process.

Chapter 5

Conclusion

The work performed for this thesis focused on developing microchip electrochromatography systems that can in the future be utilized for the separation and detection of proteins, peptides and biogenic amines. Three different separation microchip designs were developed and reversed phase electrochromatography separations of model analytes were demonstrated on these designs.

In Chapter 2, a silicon based electrochromatography microchip with integrated waveguides for UV-absorbance detection and a separation column with microfabricated solid support structures for a stationary phase was presented. A separation of 5 neutral chemicals was demonstrated on a microchip coated with an octadecyl stationary phase. Plate heights as low as 5.0 μm were obtained for retained analytes on a microchip with 1.5 μm spacing between the solid support pillars in the separation column.

In Chapter 3, the fabrication and operation of an oxidized silicon microchip for electrochromatography was presented. The microchip featured a separation column with microfabricated solid support structures for the stationary phase, UV-transparent waveguides for absorbance detection and integrated fiber couplers to assist with alignment of optical fibers to the waveguides. All components on the microchip were fabricated in a single etching step. A glass lid was thermally bonded to the substrate for sealing. Reversed phase electrochromatography separation using an octylsilane stationary phase was demonstrated where three neutral compounds were baseline separated and detected using UV-absorbance at 254 nm. A minimum plate height of 30 μm was achieved on the microchip, at least an order of magnitude larger than what might be expected in a microchip. The large plate heights are considered to be due to design flaws in the microchip. Optimization of the microchip design should therefore yield better separation efficiencies.

In Chapter 4, the use of underivatized Topas, a cyclic olefin copolymer, as a substrate and a stationary phase for reversed phase electrochromatog-

raphy was demonstrated both in a capillary and on a microchip. A useful cathodic electroosmotic flow was measured in the Topas capillary. Furthermore, a reversed phase capillary electrochromatography separation of three neutral compounds using the underivatized Topas surface as a stationary phase was demonstrated in approximately nine minutes with plate heights ranging from 5.3 μm to 13 μm. The fabrication of a Topas microchip with solid support structures in the separation column by nanoimprint lithography was presented. The imprinting process for the microchips is quite robust and does not require further optimization but the bonding process to seal the microchips needs to be optimized to get a more permanent sealing. A reversed phase electrochromatography separation of three fluorescently labeled amines was achieved in less than two minutes on the microchip with plate heights for retained compounds ranging from 3.4 μm to 22 μm. Future work on the Topas microchip should involve the surface modification of the polymer as well as the integration of polymer waveguides for detection.

As mentioned in the introduction, the original goal of this project was to perform microchip electrochromatography on biochemicals such as proteins and biogenic amines. That was not possible as many aspects of this project turned out to be more challenging and time consuming than originally anticipated. Technical problems, such as downtime of machinery in the cleanroom and defective polymer capillaries, delayed the projects several weeks. At times it felt as if all the paths chosen in the project would turn out to be dead ends, although they had originally sounded plausible. It was therefore a great relief for me that in the last 10 months of the project things started to turn around and my persistency paid off, resulting in two journal papers. Of the projects described here, I believe that the polymer microchips described in Chapter 4 are best suited for further studies. Even though suitable surface modifications need to be developed and some fabrication issues are still unresolved I think that this relatively inexpensive way to fabricate an ordered pillar array for a chromatography column with sub-micron features and high reproducibility could prove useful.

Bibliography

[1] S. C. Terry, J. H. Jerman, and J. B. Angell, "Gas-chromatographic air analyzer fabricated on a silicon-wafer," *IEEE Transactions on Electron Devices*, vol. 26, pp. 1880–1886, 1979.

[2] A. Manz, Y. Miyahara, J. Miura, Y. Watanabe, H. Miyagi, and K. Sato, "Design of an open-tubular column liquid chromatograph using silicon chip technology," *Sensors and Actuators B-Chemical*, vol. 1, pp. 249–255, 1990.

[3] D. R. Reyes, D. Iossifidis, P. A. Auroux, and A. Manz, "Micro total analysis systems. 1. Introduction, theory, and technology," *Analytical Chemistry*, vol. 74, pp. 2623–2636, 2002.

[4] P. A. Auroux, D. Iossifidis, D. R. Reyes, and A. Manz, "Micro total analysis systems. 2. Analytical standard operations and applications," *Analytical Chemistry*, vol. 74, pp. 2637–2652, 2002.

[5] J. P. Kutter, S. C. Jacobson, and J. M. Ramsey, "Solid phase extraction on microfluidic devices," *Journal of Microcolumn Separations*, vol. 12, pp. 93–97, 2000.

[6] J. P. Kutter, S. C. Jacobson, N. Matsubara, and J. M. Ramsey, "Solvent-programmed microchip open-channel electrochromatography," *Analytical Chemistry*, vol. 70, pp. 3291–3297, 1998.

[7] J. D. Ramsey, S. C. Jacobson, C. T. Culbertson, and J. M. Ramsey, "High-efficiency, two-dimensional separations of protein digests on microfluidic devices," *Analytical Chemistry*, vol. 75, pp. 3758–3764, 2003.

[8] B. S. Broyles, S. C. Jacobson, and J. M. Ramsey, "Sample filtration, concentration, and separation integrated on microfluidic devices," *Analytical Chemistry*, vol. 75, pp. 2761–2767, 2003.

[9] S. C. Jacobson and C. T. Culbertson, "Microfluidics: Some basics," in *Separation Methods in Microanalytical Systems* (J. P. Kutter and Y. Fintschenko, eds.), pp. 19–54, Boca Raton: CRC Press, 2006.

[10] R. Hunter, *Zeta potential in colloid science. Principles and applications.* London Academic Press, 1981.

[11] A. Brask, *Electroosmotic Micropumps.* Ph.d thesis, Technical University of Denmark (DTU), 2005.

[12] T. Sikanen, L. Heikkila, S. Tuornikoski, R. A. Ketola, R. Kostiainen, S. Franssila, and T. Kotiaho, "Performance of SU-8 microchips as separation devices and comparison with glass microchips," *Analytical Chemistry*, vol. 79, pp. 6255–6263, 2007.

[13] J. Gaudioso and H. G. Craighead, "Characterizing electroosmotic flow in microfluidic devices," *Journal of Chromatography A*, vol. 971, pp. 249–253, 2002.

[14] D. C. Harris, *Quantitative Chemical Analysis.* New York: W.H. Freeman and Company, 6 ed., 2003.

[15] G. Desmet, E. Chmela, and R. Tijssen, "Pressure-driven separation methods on a chip," in *Separation Methods in Microanalytical Systems* (J. P. Kutter and Y. Fintschenko, eds.), pp. 165–207, Boca Raton: CRC Press, 2006.

[16] C. Ericson, J. Holm, T. Ericson, and S. Hjerten, "Electroosmosis- and pressure-driven chromatography in chips using continuous beds," *Analytical Chemistry*, vol. 72, pp. 81–87, 2000.

[17] A. M. Enlund, G. Hagman, R. Isaksson, and D. Westerlund, "Capillary electrochromatography of basic compounds in pharmaceutical analysis," *Trac-Trends in Analytical Chemistry*, vol. 21, pp. 412–427, 2002.

[18] B. He and F. Regnier, "Microfabricated liquid chromatography columns based on collocated monolith support structures," *Journal of Pharmaceutical and Biomedical Analysis*, vol. 17, pp. 925–932, 1998.

[19] B. He, N. Tait, and F. Regnier, "Fabrication of nanocolumns for liquid chromatography," *Analytical Chemistry*, vol. 70, pp. 3790–3797, 1998.

[20] J. C. Giddings, *Unified Separation Science.* New York: John Wiley & Sons, 1991.

[21] M. Minarik, F. Groiss, B. Gas, D. Blaas, and E. Kenndler, "Dispersion effects accompanying pressurized zone mobilisation in capillary isoelectric focusing of proteins," *Journal of Chromatography A*, vol. 738, pp. 123–128, 1996.

[22] W. De Malsche, H. Eghbali, D. Clicq, J. Vangelooven, H. Gardeniers, and G. Desmet, "Pressure-driven reverse-phase liquid chromatography separations in ordered nonporous pillar array columns," *Analytical Chemistry*, vol. 79, pp. 5915–5926, 2007.

[23] N. F. Yin, K. Killeen, R. Brennen, D. Sobek, M. Werlich, and T. V. van de Goor, "Microfluidic chip for peptide analysis with an integrated HPLC column, sample enrichment column, and nanoelectrospray tip," *Analytical Chemistry*, vol. 77, pp. 527–533, 2005.

[24] A. Brask, J. P. Kutter, and H. Bruus, "Long-term stable electroosmotic pump with ion exchange membranes," *Lab on a Chip*, vol. 5, pp. 730–738, 2005.

[25] T. B. Stachowiak, F. Svec, and J. M. J. Frechet, "Chip electrochromatography," *Journal of Chromatography A*, vol. 1044, pp. 97–111, 2004.

[26] J. H. Knox and R. Boughtflower, "Capillary electrochromatography - the LC analogue of capillary GC," *Trac-Trends in Analytical Chemistry*, vol. 19, pp. 643–647, 2000.

[27] S. C. Jacobson, R. Hergenroder, L. B. Koutny, and J. M. Ramsey, "Open-channel electrochromatography on a microchip," *Analytical Chemistry*, vol. 66, pp. 2369–2373, 1994.

[28] K. B. Mogensen, F. Eriksson, O. Gustafsson, R. P. H. Nikolajsen, and J. P. Kutter, "Pure-silica optical waveguides, fiber couplers, and high-aspect ratio submicrometer channels for electrokinetic separation devices," *Electrophoresis*, vol. 25, pp. 3788–3795, 2004.

[29] M. De Pra, W. T. Kok, J. G. E. Gardeniers, G. Desmet, S. Eeltink, J. W. van Nieuwkasteele, and P. J. Schoenmakers, "Experimental study on band dispersion in channels structured with micropillars," *Analytical Chemistry*, vol. 78, pp. 6519–6525, 2006.

[30] B. E. Slentz, N. A. Penner, and F. Regnier, "Geometric effects of collocated monolithic support structures on separation performance in microfabricated systems," *Journal of Separation Science*, vol. 25, pp. 1011–1018, 2002.

[31] J. De Smet, P. Gzil, N. Vervoort, H. Verelst, G. V. Baron, and G. Desmet, "Influence of the pillar shape on the band broadening and the separation impedance of perfectly ordered 2-D porous chromatographic media," *Analytical Chemistry*, vol. 76, pp. 3716–3726, 2004.

[32] J. Billen and G. Desmet, "Understanding and design of existing and future chromatographic support formats," *Journal of Chromatography A*, vol. 1168, pp. 73–99, 2007.

[33] R. Costa, K. B. Mogensen, and J. P. Kutter, "Microfabricated porous glass channels for electrokinetic separation devices," *Lab on a Chip*, vol. 5, pp. 1310–1314, 2005.

[34] K. Seiler, Z. H. H. Fan, K. Fluri, and D. J. Harrison, "Electroosmotic pumping and valveless control of fluid-flow within a manifold of capillaries on a glass chip," *Analytical Chemistry*, vol. 66, pp. 3485–3491, 1994.

[35] O. Geschke, H. Klank, and P. Telleman, *Microsystem Engineering of Lab-on-a-Chip Devices*. John Wiley & Sons, 2004.

[36] S. C. Jacobson, R. Hergenroder, L. B. Koutny, R. J. Warmack, and J. M. Ramsey, "Effects of injection schemes and column geometry on the performance of microchip electrophoresis devices," *Analytical Chemistry*, vol. 66, pp. 1107–1113, 1994.

[37] K. B. Mogensen, H. Klank, and J. P. Kutter, "Recent developments in detection for microfluidic systems," *Electrophoresis*, vol. 25, pp. 3498–3512, 2004.

[38] K. Uchiyama, H. Nakajima, and T. Hobo, "Detection method for microchip separations," *Analytical and Bioanalytical Chemistry*, vol. 379, pp. 375–382, 2004.

[39] S. Gotz and U. Karst, "Recent developments in optical detection methods for microchip separations," *Analytical and Bioanalytical Chemistry*, vol. 387, pp. 183–192, 2007.

[40] R. Jindal and S. M. Cramer, "On-chip electrochromatography using sol-gel immobilized stationary phase with UV-absorbance detection," *Journal of Chromatography A*, vol. 1044, pp. 277–285, 2004.

[41] N. J. Petersen, K. B. Mogensen, and J. P. Kutter, "Performance of an in-plane detection cell with integrated waveguides for UV/Vis absorbance measurements on microfluidic separation devices," *Electrophoresis*, vol. 23, pp. 3528–3536, 2002.

[42] K. B. Mogensen, P. Friis, J. Hubner, N. Petersen, A. M. Jorgensen, P. Telleman, and J. P. Kutter, "Ultraviolet transparent silicon oxynitride waveguides for biochemical microsystems," *Optics Letters*, vol. 26, pp. 716–718, 2001.

[43] K. B. Mogensen, N. J. Petersen, J. Hubner, and J. P. Kutter, "Monolithic integration of optical waveguides for absorbance detection in microfabricated electrophoresis devices," *Electrophoresis*, vol. 22, pp. 3930–3938, 2001.

[44] L. Szekely and A. Guttman, "New advances in microchip fabrication for electrochromatography," *Electrophoresis*, vol. 26, pp. 4590–4604, 2005.

[45] K. D. Lukacs and J. W. Jorgenson, "Capillary zone electrophoresis - effect of physical parameters on separation efficiency and quantitation," *Journal of High Resolution Chromatography and Chromatography Communications*, vol. 8, pp. 407–411, 1985.

[46] A. Manz, D. J. Harrison, E. M. J. Verpoorte, J. C. Fettinger, A. Paulus, H. Ludi, and H. M. Widmer, "Planar chips technology for miniaturization and integration of separation techniques into monitoring systems - capillary electrophoresis on a chip," *Journal of Chromatography*, vol. 593, pp. 253–258, 1992.

[47] N. J. Petersen, *Electrophoretic Separations on Microchips: Performance and Possibilities*. Ph.d. thesis, DTU, Copenhagen, 2002.

[48] N. J. Petersen, R. P. H. Nikolajsen, K. B. Mogensen, and J. P. Kutter, "Effect of Joule heating on efficiency and performance for microchip-based and capillary-based electrophoretic separation systems: A closer look," *Electrophoresis*, vol. 25, pp. 253–269, 2004.

[49] H. Becker and L. E. Locascio, "Polymer microfluidic devices," *Talanta*, vol. 56, pp. 267–287, 2002.

[50] D. Snakenborg, G. Perozziello, H. Klank, O. Geschke, and J. P. Kutter, "Direct milling and casting of polymer-based optical waveguides for improved transparency in the visible range," *Journal of Micromechanics and Microengineering*, vol. 16, pp. 375–381, 2006.

[51] B. Bilenberg, M. Hansen, D. Johansen, V. Ozkapici, C. Jeppesen, P. Szabo, I. M. Obieta, O. Arroyo, J. O. Tegenfeldt, and A. Kristensen, "Topas-based lab-on-a-chip microsystems fabricated by thermal nanoimprint lithography," *Journal of Vacuum Science and Technology B*, vol. 23, pp. 2944–2949, 2005.

[52] M. Heckele and W. K. Schomburg, "Review on micro molding of thermoplastic polymers," *Journal of Micromechanics and Microengineering*, vol. 14, pp. R1–R14, 2004.

[53] A. E. Guber, M. Heckele, D. Herrmann, A. Muslija, V. Saile, L. Eichhorn, T. Gietzelt, W. Hoffmann, P. C. Hauser, J. Tanyanyiwa, A. Ger-

lach, N. Gottschlich, and G. Knebel, "Microfluidic lab-on-a-chip systems based on polymers - fabrication and application," *Chemical Engineering Journal*, vol. 101, pp. 447–453, 2004.

[54] B. E. Slentz, N. A. Penner, E. Lugowska, and F. Regnier, "Nanoliter capillary electrochromatography columns based on collocated monolithic support structures molded in poly(dimethyl siloxane)," *Electrophoresis*, vol. 22, pp. 3736–3743, 2001.

[55] B. E. Slentz, N. A. Penner, and F. E. Regnier, "Capillary electrochromatography of peptides on microfabricated poly(dimethylsiloxane) chips modified by cerium(IV)-catalyzed polymerization," *Journal of Chromatography A*, vol. 948, pp. 225–233, 2002.

[56] K. W. Ro, W. J. Chan, H. Kim, Y. M. Koo, and J. H. Hahn, "Capillary electrochromatography and preconcentration of neutral compounds on poly(dimethylsiloxane) microchips," *Electrophoresis*, vol. 24, pp. 3253–3259, 2003.

[57] J. N. Lee, C. Park, and G. M. Whitesides, "Solvent compatibility of poly(dimethylsiloxane)-based microfluidic devices," *Analytical Chemistry*, vol. 75, pp. 6544–6554, 2003.

[58] G. T. Roman, T. Hlaus, K. J. Bass, T. G. Seelhammer, and C. T. Culbertson, "Sol-gel modified poly(dimethylsiloxane) microfluidic devices with high electroosmotic mobilities and hydrophilic channel wall characteristics," *Analytical Chemistry*, vol. 77, pp. 1414–1422, 2005.

[59] G. T. Roman and C. T. Culbertson, "Surface engineering of poly(dimethylsiloxane) microfluidic devices using transition metal sol-gel chemistry," *Langmuir*, vol. 22, pp. 4445–4451, 2006.

[60] R. R. Lamonte and D. McNally, "Uses and processing of cyclic olefin copolymers," *Plastics Engineering*, vol. 56, p. 51, 2000.

[61] G. Khanarian and H. Celanese, "Optical properties of cyclic olefin copolymers," *Optical Engineering*, vol. 40, pp. 1024–1029, 2001.

[62] T. Rohr, D. F. Ogletree, F. Svec, and J. M. J. Frechet, "Surface functionalization of thermoplastic polymers for the fabrication of microfluidic devices by photoinitiated grafting," *Advanced Functional Materials*, vol. 13, pp. 264–270, 2003.

[63] T. B. Stachowiak, D. A. Mair, T. G. Holden, L. J. Lee, F. Svec, and J. M. J. Frechet, "Hydrophilic surface modification of cyclic olefin copolymer microfluidic chips using sequential photografting," *Journal of Separation Science*, vol. 30, pp. 1088–1093, 2007.

[64] K. B. Mogensen, *Integration of Planar Waveguides for Optical Detection in Microfabricated Analytical Devices*. Ph.d. thesis, Technical University of Denmark (DTU), Copenhagen, 2002.

[65] A. L. Crego, J. Martinez, and M. L. Marina, "Influence of mobile phase composition on electroosmotic flow velocity, solute retention and column efficiency in open-tubular reversed-phase capillary electrochromatography," *Journal of Chromatography A*, vol. 869, pp. 329–337, 2000.

[66] S. Y. Park, C. J. Russo, D. Branton, and H. A. Stone, "Eddies in a bottleneck: An arbitrary Debye length theory for capillary electroosmosis," *Journal of Colloid and Interface Science*, vol. 297, pp. 832–839, 2006.

[67] C. Legido-Quigley, N. D. Marlin, V. Melin, A. Manz, and N. W. Smith, "Advances in capillary electrochromatography and micro-high performance liquid chromatography monolithic columns for separation science," *Electrophoresis*, vol. 24, pp. 917–944, 2003.

[68] O. Gustafsson and J. P. Kutter, "Electrokinetic chromatography on microfluidic devices," in *Electrokinetic Chromatography: Theory, Instrumentation and Applications* (U. Pyell, ed.), pp. 337–349, Chichester: John Wiley & Sons, 2006.

[69] J. Eijkel, "Chip-based HPLC: the quest for the perfect column," *Lab on a Chip*, vol. 7, pp. 815–817, 2007.

[70] G. Ocvirk, E. Verpoorte, A. Manz, M. Grasserbauer, and H. M. Widmer, "High-performance liquid-chromatography partially integrated onto a silicon chip," *Analytical Methods and Instrumentation*, vol. 2, pp. 74–82, 1995.

[71] D. Allen and Z. El Rassi, "Silica-based monoliths for capillary electrochromatography: Methods of fabrication and their applications in analytical separations," *Electrophoresis*, vol. 24, pp. 3962–3976, 2003.

[72] I. Gusev, X. Huang, and C. Horvath, "Capillary columns with in situ formed porous monolithic packing for micro high-performance liquid chromatography and capillary electrochromatography," *Journal of Chromatography A*, vol. 855, pp. 273–290, 1999.

[73] K. Morishima, B. D. Bennett, M. T. Dulay, J. P. Quirino, and R. N. Zare, "Toward sol-gel electrochromatographic separations on a chip," *Journal of Separation Science*, vol. 25, pp. 1226–1230, 2002.

[74] J. H. Knox, "Band dispersion in chromatography - a new view of A-term dispersion," *Journal of Chromatography A*, vol. 831, pp. 3–15, 1999.

[75] P. Gzil, J. De Smet, N. Vervoort, H. Verelst, G. V. Baron, and G. Desmet, "Computational study of the band broadening in two-dimensional etched packed bed columns for on-chip high-performance liquid chromatography," *Journal of Chromatography A*, vol. 1030, pp. 53–62, 2004.

[76] S. Hu, X. Ren, M. Bachman, C. E. Sims, G. P. Li, and N. L. Allbritton, "Surface-directed, graft polymerization within microfluidic channels," *Analytical Chemistry*, vol. 76, pp. 1865 – 1870, 2004.

[77] S. J. Hawkes, "Modernization of the van-Deemter equation for chromatographic zone dispersion," *Journal of Chemical Education*, vol. 60, pp. 393–398, 1983.

[78] C. Gui, M. Elwenspoek, N. Tas, and J. G. E. Gardeniers, "The effect of surface roughness on direct wafer bonding," *Journal of Applied Physics*, vol. 85, pp. 7448–7454, 1999.

[79] S. H. Christiansen, R. Singh, and U. Gosele, "Wafer direct bonding: From advance substrate engineering to future applications in micro/nanoelectronics," *Proceedings of the IEEE*, vol. 94, pp. 2060–2106, 2006.

[80] C. Schwer and E. Kenndler, "Electrophoresis in fused-silica capillaries - the influence of organic-solvents on the electroosmotic velocity and the zeta-potential," *Analytical Chemistry*, vol. 63, pp. 1801–1807, 1991.

[81] H. J. Crabtree, E. C. S. Cheong, D. A. Tilroe, and B. C. J., "Microchip inection and separation anomalies due to pressure effects," *Analytical Chemistry*, vol. 73, pp. 4079–4086, 2001.

[82] F. Svec, E. C. Peters, D. Sykora, G. Yu, and J. M. J. Frechet, "Monolithic stationary phases for capillary electrochromatography based on synthetic polymers: Designs and applications," *Hrc-Journal of High Resolution Chromatography*, vol. 23, pp. 3–18, 2000.

[83] P. Gzil, N. Vervoort, G. V. Baron, and G. Desmet, "Advantages of perfectly ordered 2-D porous pillar arrays over packed bed columns for lc separations: A theoretical analysis," *Analytical Chemistry*, vol. 75, pp. 6244–6250, 2003.

[84] P. Mela, A. van den Berg, Y. Fintschenko, E. B. Cummings, B. A. Simmons, and B. J. Kirby, "The zeta potential of cyclo-olefin polymer mi-

crochannels and its effects on insulative (electrodeless) dielectrophoresis particle trapping devices," *Electrophoresis*, vol. 26, pp. 1792–1799, 2005.

[85] X. Q. Ren, M. Bachman, C. Sims, G. P. Li, and N. Allbritton, "Electroosmotic properties of microfluidic channels composed of poly(dimethylsiloxane)," *Journal of Chromatography B-Analytical Technologies in the Biomedical and Life Sciences*, vol. 762, pp. 117–125, 2001.

[86] R. Chen, H. Z. Guo, Y. W. Shen, Y. Z. Hu, and Y. Q. Sun, "Determination of EOF of PMMA microfluidic chip by indirect laser-induced fluorescence detection," *Sensors and Actuators B-Chemical*, vol. 114, pp. 1100–1107, 2006.

[87] D. Belder and M. Ludwig, "Surface modification in microchip electrophoresis," *Electrophoresis*, vol. 24, pp. 3595–3606, 2003.

[88] J. Shin, J. Park, C. Liu, J. He, and S. Kim, "Chemical structure and physical properties of cyclic olefin copolymers - (IUPAC technical report)," *Pure And Applied Chemistry*, vol. 77, pp. 801–814, 2005.

[89] P. Kettner, R. L. Pelzer, T. Glinsner, S. Farrens, and D. Lee, "New results on plasma activated bonding of imprinted polymer features for bio mems applications," *Journal of Physics: Conference Series*, vol. 34, pp. 65–71, 2006.

[90] J. K. Beattie, "The intrinsic charge on hydrophobic microfluidic substrates," *Lab on a Chip*, vol. 6, pp. 1409–1411, 2006.

[91] Z. Mala, L. Krivankova, P. Gebauer, and P. Bocek, "Contemporary sample stacking in CE: A sophisticated tool based on simple principles," *Electrophoresis*, vol. 28, pp. 243–253, 2007.

[92] P. Britz-McKibbin and D. Chen, "Selective focusing of catecholamines and weakly acidic compounds by capillary electrophoresis using a dynamic ph junction," *Analytical Chemistry*, vol. 72, pp. 1242–1252, 2000.

[93] H. Klank, J. P. Kutter, and O. Geschke, "CO_2-laser micromachining and back-end processing for rapid production of PMMA-based microfluidic systems.," *Lab on a Chip*, vol. 2, pp. 242–246, 2002.

Appendix A

List of Publications

A.1 Peer reviewed papers in journals

- **Ó. Gústafsson**, K.B. Mogensen and J.P. Kutter, "Underivatized cyclic olefin copolymer as substrate material and stationary phase for capillary and microchip electrochromatography". Electrophoresis, Vol 29, Issue 15, p. 3145-3152, 2008.
- **Ó. Gústafsson**, K.B. Mogensen, P.D. Ohlsson, Y. Liu, S.C. Jacobson and J.P. Kutter, "Electrochromatography chip with integrated waveguides for UV absorbance detection". Journal of Micromechanics and microengineering, Vol 18, Issue 5, April, 2008.
- K.B. Mogensens, **Ó. Gústafsson**, P. Nunes and J.P. Kutter, "Lab-on-a-chip system with integrated optics for biochemical applications". Proceedings of SPIE, Vol 6898, p. 68981A, Feb 13, 2008.

A.2 Peer reviewed abstracts in conference proceedings

Presenting author is indicated with an asterisk.

- **Ó. Gústafsson**,K.B. Mogensen* and J.P. Kutter, "Microchip Electrochromatography using Native Topas as the Stationary Phase", MSB 2008, Berlin, Germany, March 9-13, 2008. Poster presentation.
- **Ó. Gústafsson***, K.B. Mogensen and J.P. Kutter, "Nanoimprinted polymer microchips with solid support structures for capillary electrochromatography". LabAutomation 2007, Palm Springs, California, USA, Jan 28- 31. 2007. Poster presentation.
- **Ó. Gústafsson***, F. Eriksson, K.B. Mogensen and J.P. Kutter, "The effect of interpillar distances in ordered pillar arrays on separation effi-

ciency in microchip capillary electrochromatography" Gordon-Kenan Graduate Research Seminar on Analytical Chemistry, Roscoff, France, June 10-12, 2005. Oral Presentation

- K.B. Mogensen*, F. Eriksson, **Ó. Gústafsson** and J.P. Kutter, "Integrated optical sensors for micro-TAS systems", ICONO/LAT 2005, St. Petersburg, Russia, May 11-15, 2005. Oral presentation.

A.3 Book chapters

- **Ó. Gústafsson** and J.P. Kutter, "Chromatography in Microstructures" in "Microfluidic Technologies for Miniaturized Analysis Systems", Editors: S. Hardt and F. Schönfeldt , Springer, 2007.

- **Ó. Gústafsson** and J.P. Kutter, "Electrokinetic Chromatography in Microfluidic Devices" in "Electrokinetic Chromatography: Theory, Instrumentation and Applications", Editor U. Pyell , John Wiley & sons, 2006.

Appendix B

Injection calculations

These injection calculations are adapted from the Ph.D. thesis by Nickolaj J. Petersen [47]. To determine the voltages that are used for both the gated and pinched injection schemes the electrical resistance in the microchannels is determined experimentally and then the voltages can be found using some relatively simple criteria.

B.1 Experimental determination of channel resistances

In Figure B.1 a standard microchip layout is shown. The resistances of the channels connecting the reservoirs are found by applying a voltage between two reservoirs at a time and measuring the current. The current for each set of reservoirs is measured at 100, 200, 300, 400 and 500 V and the values plotted on a graph. According to Ohm's law, the slope of the line is then the resistance between the reservoirs. The resistance from each of the reservoirs

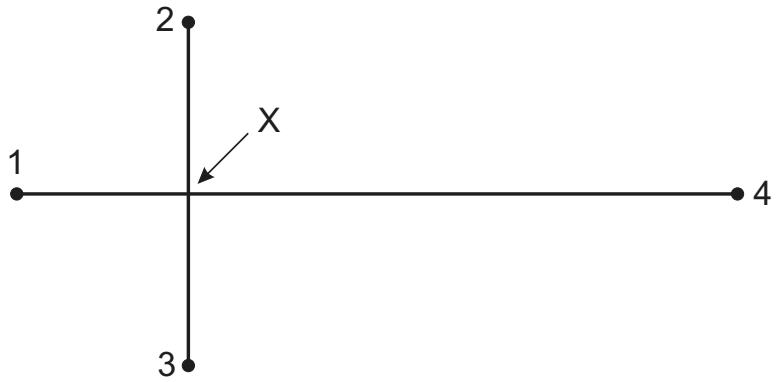

Figure B.1: Standard cross chip. 1, 2, 3, 4: Fluid reservoirs, X: injection cross, X-4: Separation channel.

towards the injection cross, X, are calculated using the equations below. The resistance for each channel segment can be estimated three different ways from the measured resistances. An average, $< R >$, is then calculated using all three measured values.

$$R_{1-X} = \frac{R_{1-2} + R_{1-4} - R_{2-4}}{2} \tag{B.1}$$

$$R_{1-X} = \frac{R_{1-2} + R_{1-3} - R_{2-3}}{2} \tag{B.2}$$

$$R_{1-X} = \frac{R_{1-3} + R_{1-4} - R_{3-4}}{2} \tag{B.3}$$

Averaging these three equations for R_{1-X} we get:

$$< R_{1-X} >= \frac{2R_{1-2} + 2R_{1-3} + 2R_{1-4} - R_{2-4} - R_{2-3} - R_{3-4}}{6} \tag{B.4}$$

Similarly for $< R_{2-X} >$, $< R_{3-X} >$ and $< R_{4-X} >$ we get:

$$< R_{2-X} >= \frac{2R_{1-2} + 2R_{2-3} + 2R_{2-4} - R_{1-3} - R_{1-4} - R_{3-4}}{6} \tag{B.5}$$

$$< R_{3-X} >= \frac{2R_{1-3} + 2R_{2-3} + 2R_{3-4} - R_{1-2} - R_{1-4} - R_{2-4}}{6} \tag{B.6}$$

$$< R_{4-X} >= \frac{2R_{1-4} + 2R_{2-4} + 2R_{3-4} - R_{1-2} - R_{1-3} - R_{2-3}}{6} \tag{B.7}$$

B.2 Voltage settings for gated injection

After the resistances of the different channel segments have been estimated the voltages that need to be applied during injection and separation can be calculated from some simple criteria. As mentioned in Section 1.1.3 there are three steps in the gated injection, pre-injection, injection and separation. The voltage settings for the pre-injection and separation are the same.

B.2.1 Injection

During injection the current from reservoir 1 should be equal to the current running towards reservoir 4:

$$I_{1-X} = I_{X-4} \tag{B.8}$$

Using Ohms law we get:

$$\frac{U_1 - U_X}{R_{1-X}} = \frac{U_X - U_4}{{}_R4 - X} \tag{B.9}$$

$$U_1 = U_X + \frac{R_{1-X}}{R_{4-X}}(U_X - U_4) \tag{B.10}$$

During the injection no flow should be from waste reservoir 2 or buffer reservoir 3 towards the injection cross. The potential at these reservoirs should therefore either be floating (with no electrical contact) or kept at the same potential as U_X during the injection.

$$U_2 = U_3 = U_X \tag{B.11}$$

U_4 is grounded during injection so the potential is zero

B.2.2 Pre injection and separation

During the separation mode the potential at the sample reservoir U_1 and the injection cross U_X is kept unchanged. That will say $I_{1-X} = I_{X-4} = I_{1-4}$ during both injection and separation mode. In order to avoid leakage of sample into the separation channel (X-4) during separation a flow of buffer from reservoir 3 is generated towards reservoir 2 in order to "cut off" the sample and prevent it from entering the separation channel. For the sample to be cut off completely this current toward reservoir 2 must at least be equal to the current running from reservoir 1 to 4. The ratio between the cut off current and the sampling current is denoted the buffer factor (bf) and is typically around 1.5.

$$I_{X-2} = bf \cdot I_{X-4} \tag{B.12}$$

Using Ohms law and isolating for U_2

$$U_2 = U_X - bf \cdot (U_X - U_4)\frac{R_{2-X}}{R_{4-X}} \tag{B.13}$$

This current must also flow from 3 to X giving

$$U_3 = U_X + bf \cdot (U_X - U_4)\frac{R_{3-X}}{R_{4-X}} \tag{B.14}$$

The potential that should be applied during injection and separations (U1, U2 and U3) can now be calculated. Reservoir 4 is grounded in all runs, so U4 is always zero. The potentials for U1, U2 and U3 are determined by choosing a value U_X and calculating all the other potentials from that value. A quick check whether the calculated potentials for the injection work or not, can be done by monitoring the current during the injection and separation. The current should be constant since U_X in the calculations is maintained constant during both the separation and the injection.

Appendix C

Glass-Oxidized silicon bonding

The protocol is adapted from a protocol by Zexi Zhuang in Dr. Stephen C. Jacobson´s group at Indiana University, Bloomington.

- Preparation of Glass lid
    1. Seal a Borofloat glass wafer in blue film.
    2. Align glass wafer with etched silicon wafer.
    3. Mark placement of access holes.
    4. Mark outline of individual chips.
    5. Use CO_2 laser to burn access holes through blue film.
    6. Use scalpel to cut small hole in the blue film on the back side of glass wafer (aligned with burnt holes on front).
    7. Cut small strips in both sides of film to mark outline of microchips.
    8. Use powder blaster (110 μm Al_2O_3 particles) to drill access holes through glass, and to saw chips apart.
- Cleaning
    1. Remove blue film and rinse thoroughly with water.
    2. Sonicate glass lids for 10 minutes in ultrapure water with 1-2% Tween.
    3. Sonicate glass lids for 10 minutes in ultrapure water.
    4. Rinse thoroughly with ultrapure water.
- Hydrolysis

1. Prepare hydrolysis solution: 1 part H_2O_2 (30%), 2 parts NH_4OH (30%) and 2 parts ultrapure water.
2. Heat solution to 70-75°C.
3. Add glass lid AND microchip substrate to heated solution. Cover and allow 15-20 minutes before removal.
4. Remove and rinse thoroughly in ultrapure water.

- Bonding

1. Place lids and substrates in ultrapure water with N_2 bubbles for 10 minutes.
2. Remove substrate and rinse with ultrapure water for 2 minutes. Repeat for glass lid.
3. Bring the substrate and lid into contact while wet, align access holes to channels and apply clamps on each side.
4. Heat at 90°C for 4 minutes.
5. Inspect for bonding success around all channels and drilled holes. If bonding unsuccessful, wet the plates, separate, rinse and try again. If bonding is successful proceed to next step.
6. Keep heating at 90°C for 2 hours, check for bonding success every 30 minutes and clamp to apply pressure where needed.
7. If the two plates appear to be bonded, permanently anneal them in a furnace.

- Permanent annealing

1. Bonded Chips placed between two pieces of quartz glass in the furnace.
2. Temperature program:
   - 90-200°C in 2 hours.
   - Hold at 200°C for 2 hours.
   - 200-550°C in 1 hour.
   - Hold at 550°C for 2 hours.
   - 550-90°C in 10 hours.
   - Hold at 90°C for 2 hours.

Appendix D

Nanoimprint lithography

Topas solutions used:

1. mrI T85-5.0 from microresist technologies.
2. 6.1% Topas 9506 in sec-butyl benzene.

Topas solutions should be prepared well beforehand, as the Topas takes a few days to dissolve.
Borosilicate wafers are available in the cleanroom.

- Cleaning of borosilicate wafers
  1. Place wafers in Pirania for 10 minutes.
  2. Rinse wafers in ultrapure water with nitrogen bubbles for 10 minutes.
  3. Dry wafers in spin drier.
  4. Place wafers in 250°C overnight.
- Spincoating Topas onto borosilicate wafers.

  Use "Speedline manual spinner" in fumehood, and have hotplates at 150°C ready.
  1. Pre bake wafers for 5 minutes on a hotplate at 150°C.
  2. Place wafer on vacuum chuck in the spinner.
  3. Add 3 mL of Topas solution onto wafer and spin.
     - Spin 1750 rpm for 60 s for mrI T85-5.0 (8 μm).
     - Spin 3000 rpm for 60 s for 6.1% 9506 (300 nm).
  4. Remove from vacuum chuck and post bake for 7 minutes on hotplate.

5. Place in container with coated side facing in same direction.

- Imprinting.

  Use EVG 25 HE Nanoimprinting machine (EVG NIL).

  1. Stack: Al film/graphite sheet/Al film/Glass wafer with Topas mrI-T85/ imprint master/Al film/graphite sheet/Al film.
  2. Place stack in bonding chuck.
  3. Place bonding chuck in imprinter.
  4. Imprint for 10 minutes at 10 kN and 190°C using program "Imprint Topas".
  5. Disassemble stack, use razor blade to remove stamp from Topas, sliding the blade carefully between the two around the rim.

- Sandblasting access holes through patterned substrate.

  1. Cover both sides of wafer with blue film, avoiding bubbles.
  2. Use CO_2-laser to burn holes in blue film at the end of each channel(0.8 mm, 200 mm/s and 10% intensity). Burn holes on the side with the polymer structures.
  3. Turn wafer around. With a scalpel cut small squares in the blue film facing each burnt hole in the blue(outlet for sandblasting stream).
  4. Use 110 μm aluminum oxide beads and maximum pressure (7 bar) to sandblast access holes through the substrate. Sandblast through the burnt holes. Sandblaster should be kept a few centimeter from wafer during drilling.

- Bonding

  1. Wash imprinted side thoroughly with water before entering cleanroom, removing as much powder as possible.
  2. In cleanroom, wash wafer in sink in access room, and carefully remove the blue film, rinsing well with water.
  3. Rinse with water, dry with nitrogen.
  4. Stack: Al film/graphite sheet/Al film/imprinted Glass wafer/Glass wafer with topas 9506/Al film/graphite sheet/Al film. Place stack in chuck and place in imprinter. Bond for 10 minutes at 70°C and 10 kN. Use program "Bonding Topas 8007 to 9506".
  5. Remove bonded microchips.